CEMENT CHANGES AND THEIR EFFECTS ON SHRINKAGE AND DURABILITY OF CONCRETE

A Dissertation
Submitted to the Graduate Faculty
of the
North Dakota State University
of Agriculture and Applied Science

By

Achintyamugdha Surendra Sharma

In Partial Fulfillment of the Requirements
for the Degree of
DOCTOR OF PHILOSOPHY

Major Department:
Civil and Environmental Engineering

March 2018

Fargo, North Dakota

North Dakota State University
Graduate School

Title

CEMENT CHANGES AND THEIR EFFECTS ON SHRINKAGE AND DURABILITY OF CONCRETE

By

Achintyamugdha Sharma

The Supervisory Committee certifies that this ***disquisition*** complies with North Dakota State University's regulations and meets the accepted standards for the degree of

DOCTOR OF PHILOSOPHY

SUPERVISORY COMMITTEE:

Dr. Todd Sirotiak
Chair

Dr. Jerry Gao

Dr. Matthew Stone

Dr. Megan Orr

Dr. Peter Taylor

Approved:

April 13, 2018
Date

Dr. Michael Chu
Department Chair

ABSTRACT

In this work, the effects of different cementitious combinations on drying shrinkage and durability of concrete are investigated. Shrinkage is caused due to loss of water from concrete due to evaporation. Cement paste is the most vulnerable part of concrete to shrinkage. As concrete consists of cement paste and aggregates, the latter pose as restraints to the shrinking paste. As a result, tensile stresses are formed thereby leading to the formation of cracks. Cracks in concrete are responsible for the ingress of deleterious chemical ions such as, Chloride and Sulfate ions, which may form expansive compounds. Chloride ions also induce corrosion of steel reinforcement bars. Prior literature has indicated that coarser cementitious systems lead to less shrinkage in concrete. Additionally, tri-calcium silicate (C_3S) and tri-calcium aluminate contents in cement also influence the extent of shrinkage in concrete. However, the extensive use of such cement in concrete as per current industry standards will be challenging. Therefore, in this study investigations are made with Type IL (10) portland limestone with or without supplementary cementitious materials (SCMs), such as fly ash, and engineered nanomaterials such as nanosilica, to develop concrete with similar shrinkage performance as compared to coarse ground portland cement, without adversely affecting other engineering properties of concrete. Key engineering properties include workability, degree of hydration, compressive and splitting tensile strengths, electrical resistivity, setting time, and bleeding. Portland limestone cement used in this study has a partial replacement level of 10% of portland cement with limestone. Although, ASTM C595 allows up to 15% replacement with limestone, current industry use is limited to ~5%. Micro-cracking tendency of selected concrete mixtures from this study is also investigated by using fluorescence microscopy and micro computed tomography (μ-CT). In this study, life cycle assessment (LCA) studies are conducted on select cementitious combinations to quantify the

benefits of such replacement of portland cement. Additionally, life cycle cost analysis (LCCA) is also performed to determine feasibility of cost. Results show that Type IL portland limestone cement can be an effective alternative for reduced shrinkage strain and enhanced durability properties.

ACKNOWLEDGEMENTS

At the outset, I would like to thank my advisor Dr. Todd Sirotiak, for his constant support and excellent guidance, without whom this work would not have been possible. I am also grateful for the exemplary mentorship that he has provided. He has a very positive influence on my career. My deepest appreciation is extended to my doctoral committee member, Dr. Peter Taylor for his constant inputs and encouragement. Dr. Taylor has been very helpful in all aspects of my graduate research, including but not limited to technical advice, laboratory facilities, presentation skills, and encouragement to be an independent researcher. I would also like to acknowledge my doctoral committee member Dr. Matthew Stone for his invaluable help and guidance in several aspects of my doctoral work. I profusely thank my doctoral committee member Dr. Jerry Gao for providing me with valuable suggestions, guidance, and support throughout my graduate career. I am also grateful to my doctoral committee member, Dr. Megan Orr for her insights into various general aspects of my dissertation and constant good will. I would also like to thank Dr. Xuhao Wang for his constant support and guidance. I would also like to acknowledge Dr. Ravi Yellavajjala for his guidance and technical support.

I am proud to acknowledge US Department of Energy for providing financial support to carry out my research, under the purview of the project titled *Cement Changes and Solutions to the Industry*.

I would also like to thank the Department of Construction Management and Engineering, and Department of Civil and Environmental Engineering for providing me with a platform to showcase my skills and also for providing financial support, Ingrid Skarski, Ann Denney, Milka Singha and Jan Lofberg for helping in administrative and financial aspects flawlessly, and all my friends and fellow graduate students who filled my journey with lots of pleasant memories.

I would like to thank my parents, brother, and sister in law for their love and affection throughout my doctoral career. Finally, I would like to acknowledge the divine inspiration of my life for helping me overcome all obstacles during this period and look forward to a beautiful tomorrow.

DEDICATION

I dedicate this dissertation to my late grandmother, Mrs. Maya Devi, who was a fighter and has been an inspiration to take challenges in all aspects of life.

TABLE OF CONTENTS

LIST OF TABLES

LIST OF FIGURES

CHAPTER 1: INTRODUCTION

Portland cement concrete is made up of cementitious materials, water, sand, coarse aggregates and chemical admixtures. Suitable changes in the binder composition can enhance durability in concrete, and thereby increase service life of structures built with it. With an increase in service life, repairs and maintenance of these structures will be reduced thereby resulting in cost savings.

Cement and concrete has also caused concern among environmentalists due to the associated carbon footprint (Singh et al. 2013). Approximately 3.8 billion tons of hydraulic cement is produced annually in the world (Miller et al. 2015), to be used in over 20 billion metric tons of concrete (Mehta and Meryman 2009) and this production of cement is contributing nearly 8% of the global carbon dioxide emission. If the service life of concrete is increased, this footprint can be reduced.

Another approach to improve sustainability of concrete is partial replacement of cement with supplementary cementitious materials (SCM) (Barrett et al. 2014). Traditionally, SCMs used in the United States for durability benefits are fly ash, ground granulated blast furnace slag, and silica fume. Ground limestone fines are also used to partially replace portland cement without negatively impacting system performance (Wiegrink, Marikunte and Shah 1996).

One of the major causes of a reduction in service life of concrete structures is cracking due to shrinkage under restrained conditions. These cracks provide pathways for ingress of external water and harmful chemicals, resulting in an acceleration of deterioration mechanisms.

A cause of cracking, particularly in large concrete elements, is the formation of stresses due to temperature gradients set up by heat of hydration in the system. The use of supplementary

cementitious materials is an effective means of reducing this amount of heat generated by the hydrating system.

Volume changes in concrete can also be caused by drying shrinkage, plastic shrinkage and chemical shrinkage (autogenous shrinkage) strains. Drying shrinkage is the strain resulting from a loss of water from the capillary pores due to evaporation in hardened concrete. Plastic shrinkage is the strain resulting in volume change, created due to drying in fresh concrete, when the rate of water evaporation at the surface exceeds that at which bleed water rises to the surface. Both drying shrinkage and plastic shrinkage can lead to cracks in concrete systems under restrained conditions. Chemical shrinkage occurs in concrete with low water-cement ratios (<0.42 w/c) (Deshpande 2007). In these cases, there is inadequate water for hydration of cement leading to self-desiccation. Chemical shrinkage is not applicable for the present work as the water-cement ratio chosen is 0.42. Coarser ground cements generate lower heat, and also reportedly shrink less than the finer materials currently available (Bentz 2010).

Portland Limestone Cement (PLC) is a binder which has been fairly recently accepted by ASTM. The limestone is interground with clinker and thus provides a homogenous mixture (Barrett et al. 2014). The maximum permissible content of limestone in the US is 15% by mass of cement (ASTM C595). However, common industry use in the Mid-West is limited to percentages of limestone replacement lower than 15% of the total cementitious materials. During typical cement manufacture, there is extensive use of carbon intensive fuels, such as coal in clinker making (Worrell et al. 2001). Therefore, this process emits CO_2. Moreover, the clinker making process emits CO_2 from the calcining process. In case of Type IL cement, there is partial replacement of portland cement with limestone. Therefore, Type IL cement has the advantage of helping in reduced emission of CO_2 into the atmosphere. Moreover, PLC is designed to perform almost the

same way as conventional portland cement (Barrett et al. 2014). This is done by grinding the PLC finer than conventional ordinary portland cement (OPC), as there is a clinker reduction in case of PLC over OPC (Barcelo et al. 2013). Prior researchers have reported that when interground PLC systems with similar strengths were evaluated, the PLC systems were shown to have similar or slightly less shrinkage than the OPC system. Also, the PLC system had no increased tendency to crack under restrained shrinkage conditions as tested by using ASTM ring test as per ASTM C1851 (Barrett et al. 2014).

Engineered nanomaterials have been used with portland cement to make use of the benefits of higher reactivity of the former on account of higher specific surface area. Of the different nanomaterials used with portland cement, such as Carbon Nanotubes, nano-TiO_2, nano-Al_2O_3, and nano-Fe_2O_3, nanosilica has been the most widely used. Portland cement concrete containing nanosilica usually exhibits a higher rate of formation of calcium silicate hydrate (C-S-H) crystals. Moreover, nanosilica can physically fill pores and the interfacial transition zone resulting in a refined microstructure of the concrete system (Singh et al. 2013). This refined microstructure can result in reduced permeability, water absorption, capillary absorption and chloride ion penetration.

Although the use of coarse ground cement can be beneficial to reduce shrinkage cracking under restrained conditions, the current industry trends would have to be altered altogether for its extensive use. Time of completion of construction would be increased from currently achievable targets. Therefore, it will be of interest to investigate the possibility of developing a cementitious mixture with presently available materials and industry standards, capable of providing similar benefits of resistance to shrinkage cracking as coarse ground cement. One of the approaches can be combining of the benefits of materials such as Type IL cement, and other SCMs, such as fly ash and nanosilica.

1.1. Literature Review

1.1.1. Types of Shrinkage

There are two identifiable phases of shrinkage: early and later ages. Early age of shrinkage refers to the first day, setting and hardening phases, and shrinkage observations beyond the first day are referred to as later age of shrinkage.

Plastic shrinkage is an early age phenomenon, which occurs in concrete while it is still in semi-fluid or plastic state. The voids between cement particles are filled by water. Water can be removed from exposed surfaces due to factors such as evaporation. At a point when the rate of removal exceeds that at which bleed water rises to the surface, menisci are formed which exert negative capillary pressures on the cementitious system. This subsequently results in volume reduction in the cement paste (Mindess, Young and Darwin 2002). However, this volume reduction only occurs at the surface which ends up creating tensile stresses that cause cracks to form at the surface.

Another form of early age shrinkage is chemical shrinkage. Chemical shrinkage is volume reduction of the hydration products and desiccation of the system if all of the water is consumed in hydration. This process is applicable low water cement ratio (<0.42) systems (Wilson and Kosmatka 2011).

Carbonation shrinkage occurs on the surface of the low-permeable concrete [16]. CO_2 reacts with hardened cement paste, specifically calcium silicate hydrate (C-S-H), thereby decreasing the calcium-silica (Ca/Si) ratio with accompanying water loss. The resulting volume change is known as carbonation shrinkage (Deshpande 2007).

Drying shrinkage is created in hardened cement paste, when there is a loss of adsorbed water from the capillary pores. Drying shrinkage occurs by several mechanisms in concrete. At

relative humidity between 45% and 95% capillary forces are formed due to formation of menisci on the adsorbed water. This reduces the overall volume of the concrete. Another mechanism associated with drying shrinkage is disjoining pressure. It is the pressure exerted by adsorbed water confined within the capillary pores on the adjacent cement surfaces. However, when the adsorbed water is lost, the disjoining pressure is reduced resulting in the cement particles being drawn together, resulting in shrinkage. The last molecular layer of water is more strongly adsorbed onto the cement particles having a high surface tension and causing a net reduction in the volume of the concrete system. This type of shrinkage due to changes in surface energy are applicable at relative humidity below 45%.

1.1.2. Role of Water in Concrete

Water plays a vital role in the strength gain and overall functionality of concrete systems. The classification of the various forms of water is done on the basis of degree of ease with which it can be removed from cement paste (Malhotra and Mehta 1996). Void systems in the form of capillaries are formed in the cement paste and are filled with unhydrated water. The water present in the larger voids (>50 nm) when removed does not result in volume change and therefore is considered to be “free water”. However, when the size of the pores is small (5 to 50 nm) large shrinkage strains may develop when the water is forced to leave the system due to capillary tension (Monteiro 2006).

The water held within the calcium silicate hydrate nano structure is known as the interlayer water which is held by Van der Waals forces (Idiart 2009). Numerous factors determine the size and volume of gel pores (a system of interconnected voids inside concrete consisting of pore fluid) including Ca/Si ratio, whether the molecules are non-ionic, anionic or cationic, concentration and pH. However, size and volume of gel pores is independent of the water-cementitious materials

ratio and the degree of hydration (Raki et al. 2010). Removal of interlayer water is possible only in very dry conditions (about 10% RH) (Idiart 2009). The resistance to water removal can be increased by increasing the Ca/Si ratio which may decrease the size and volume of gel pores (Monteiro 2006).

In case of fresh concrete structures, the volume of the mix is reduced by evaporation and by dissolution of cement in water, which in turn leads to a vertical movement of the upper surfaces (Wittmann and Beltzung 2016). With continued evaporation, the water film on the surface will be replaced by menisci between the particles near the surface. A capillary pressure will be created in the water under these menisci:

$$P_C = \frac{2\sigma Cos\theta}{r} \quad (1.1)$$

Where, P_C = capillary pressure

σ = surface energy

θ = wetting angle

r = average radius of the menisci.

The movement of water within the porous solid is one of the major driving factors for drying shrinkage along with others such as permeation due to pressure head, capillary suction due to surface tension and capillary tension, absorption phenomena including fixation and liberation of water molecules due to mass forces (Monteiro 2006). Elastic shrinkage strains are produced by the tensile stresses in the capillary water (up to about 50% Relative Humidity, RH) (Idiart 2009). Capillary shrinkage has been considered to be a significant threat as wide cracks can be formed due to capillary pressure in the first few hours after compacting fresh concrete. However, it is also

reported that by adequate curing and by keeping the surface of fresh concrete wet the problem of capillary shrinkage can be mitigated (Idiart 2009).

Considering two spherical solid particles with radii R_1 and R_2 connected by a thin water layer. We can consider the entire structure of fresh concrete to be built up by many such units in three dimensions. The capillary pressure forming on the water layer will be (Wittmann and Beltzung 2016):

$$P_C = \sigma Cos\theta \left(\frac{1}{R_1} + \frac{1}{R_2}\right) \quad (1.2)$$

Where, σ = surface energy

θ = wetting angle

R_1, R_2 = radii of the two spherical particles (Figure 1).

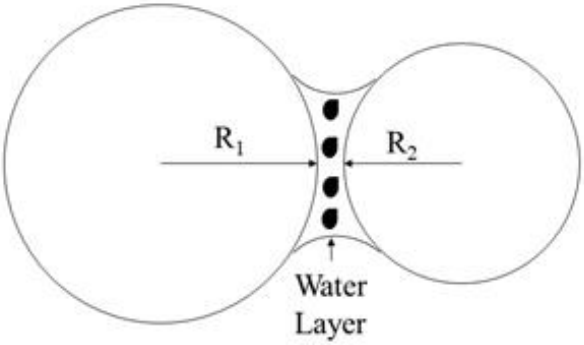

Figure 1. Water layer between two spherical particles

Now, if there is an evaporation of water from this system, then the radii R_1 and R_2 will be decreased and therefore the capillary pressure P_C will be increased. However, with this increase in capillary pressure there is also a decrease in the surface of contact between the liquid and solid particles, due to which the resultant force of attraction Fa between the two particles remains constant in all practicality (Wittmann and Beltzung 2016).

Considering the above, it is important to understand the importance of mechanisms other than capillary pressure contributing towards drying shrinkage, one of them being disjoining pressure. Disjoining pressure is created in a thin layer of water between two particles by the interaction of the neighboring solid surface. The influence of relative humidity (RH) is very important to determine the extent of disjoining pressure on materials. Prior researchers have provided for the evidence for existence of repulsive forces and for the influence of dissolved ions

on the interaction between solid surfaces and a liquid (Beltzung and Wittmann 2005). Below an RH of 40% adsorbed water reduces the surface energy of gel particles which results in the expansion of the particles. Below an RH of 50% the hygral volume changes take place mainly due to Bangham's law (Beltzung and Wittmann 2005) which describes the relationship between microscopic length change and the change of surface tension of the adsorbent. In simpler terms, there is an expansion of the particles at the nanoscale for hardened cement paste when the RH of the environment of hydration products is increased and the water molecules are gradually adsorbed resulting in a decrease of the surface tension. At higher RH the nanostructure of the material is modified due to the widening of the existing gaps by the effect of disjoining pressure. Consequently, the strength of the material is reduced (Wittmann and Beltzung 2016). This spreading or widening of gaps is further amplified when monovalent salts are added into the system and starts at RH as low as 60-70%. This amplification of disjoining pressure by dissolved ions occurs by the mechanisms of hydration of ions and/or by the electrical double layer which builds up. Prior researchers have thus observed that disjoining pressure exceeds capillary under pressure and therefore controls essentially hygral volume change as a function of RH. Moreover, repulsive forces become even more pronounced and lead to surface separation process in the presence of electrolytes (Beltzung and Wittmann 2005).

Disjoining pressure is thus affected by ions dissolved in the pore water. With an increase in the alkali content in the cement there is also an increase in the disjoining pressure and in turn the shrinkage. Alkalis are present in anhydrous cement either as impurities in C_3A and C_3S or as sulfates. An increase in KOH and NaOH concentration induces a decrease of $Ca(OH)_2$ solubility. There is a preferential adsorption Ca^{2+}, K^+ and Na^+ cations by the negatively charged surfaces of the hydration products. A hydration shell of at least two molecular layers surrounds the cations.

The gap width between two neighboring C–S–H surfaces growing into the pore solution depends on the volume of structured water which covers each surface, volume consisting of adsorbed water films and hydration shells. During desiccation when the structured water evaporates, disjoining pressure is reduced, and the surfaces come closer due to attractive forces leading to macroscopic shrinkage deformation. Therefore, it may be assumed that the alkali concentration in the pore solution influences hygral shrinkage of hardened cement paste as the relative distance of two opposite surfaces is proportional to the amount of structured water lying between them (Beltzung and Wittmann 2005).

1.1.2.1. Factors Affecting Shrinkage

There are several factors responsible for shrinkage which are usually interrelated. Some of the material characteristics which can determine the extent of shrinkage in concrete are aggregate properties such as size, gradation, content and elastic properties, water-cementitious materials ratio, water content, cement characteristics such as particle size distribution, cementitious materials content, air content, chemical admixtures and supplementary cementitious materials content in the mix. On the other hand, external conditions such as relative humidity, ambient temperature and wind velocity are also responsible for shrinkage (Taylor and Wang 2014).

The process of drying shrinkage mainly depends upon the size and configuration of the element due to the involvement of moisture loss from the surface. Thicker specimens have a lower rate of shrinkage as large members dry slower. According to American Concrete Institute (ACI) there is an inverse proportion between shrinkage and the ratio of specimen volume to its drying surface area (Wang et al. 2009) and there may be decrease in drying shrinkage if the volume to specimen surface area is increased (Wang 2011).

As mentioned before, the quantity of aggregates is a factor affecting the potential for shrinkage. For a constant water–cementitious materials ratio a higher volume of aggregates in the concrete mix leads to reduced shrinkage strain. Also, by increasing the size of aggregates and decreasing the paste content drying shrinkage can be reduced. There is reportedly a 50% reduction in shrinkage when the aggregate size is changed from 1.4 to 6 inches resulting in an aggregate volumetric change from 0.6 to 0.8 (Taylor and Wang 2014). Therefore, it may be concluded that for the same water-cementitious materials ratio a decrease in paste content and consequently an increase in the aggregate content will lead to a reduction in shrinkage strain.

There is also the risk of higher shrinkage due to high clay content in fine aggregates. Higher clay content will end up absorbing more water from the cement system so as to change the moisture content in the concrete. Clay content can be determined by methylene blue index (MBI) and higher the clay content higher is the MBI value, especially when the MBI value is greater than or equal to 1.45 because clay particles coating aggregate particles will deform significantly with changing moisture content (Wang et al. 2009).

Elastic properties such as modulus of elasticity of aggregates also affects shrinkage; lower the modulus of elasticity of aggregates higher is the shrinkage of the concrete (Tritsch, Darwin and Browning 2005).

Cement paste (i.e. water and cementitious materials) is vulnerable portions of concrete to volume changes. The water-cementitious materials ratio is an important determining factor for shrinkage behavior of concrete. Shrinkage increases with an increase in water-cementitious materials ratio, because the latter controls the evaporable water content per unit volume of paste, and the rate at which the water can reach the surface (Deshpande 2007).

Cement fineness is a vital factor in determining the shrinkage of the system. Portland cement of higher Blaine fineness have higher surface area, providing higher reactive sites for hydration reactions, and a more refined micro structure is formed. As a result of this, the pore diameter of individual pores reduces, and higher capillary stresses and increased shrinkage occur. Similar to aggregates, larger cement particles that have not undergone full hydration can pose a restraining effect. Therefore, for finer cements the shrinkage values tend to be greater. In case of finer cements, the amount of evaporable water is reduced because of an increased amount of hydrated pore water as a result of a higher surface area (Institute 2005).

From ring tests data with ASTM standard rings (ASTM C1581) experimenting on different types of Type II cements, Zayed et.al. (Zayed et al. 2014) established that coarser cement mixes cracked at longer times which was in agreement with past literature. They also reported that cements with higher amounts of tricalcium aluminate (C_3A) appeared to have cracked earlier.

1.1.2.2. Optical and Fluorescence Microscopy in Concrete Research

A scanning electron microscope (SEM) is a type of electron microscope that produces images of a sample by scanning it with a focused beam of electrons. SEM has been used by various researchers in the past to investigate some of the features such as alkali silica reaction (ASR) in concrete (Zerbino, Giaccio and Marfil 2014), morphological and topographical changes along with crystallographic changes due to nanoparticles such as nano silica (Ji 2005), carbon nanotubes (Chen et al. 2011), Ag-TiO_2-CNT nanoparticle composite (Koo et al. 2014) etc. SEM images can be very detailed and thus micro-cracks can be well documented.

Fluorescence microscopy can also be used to understand and analyze the air void system in concrete samples. Researchers in the past have used a *modified point count analysis* method to analyze air voids (Wong et al. 2011). Concrete blocks were first dried to constant weight and then

vacuum impregnated with a low viscosity epoxy containing fluorescein dye. The vacuum impregnated sample was then pressurized to ensure a deep epoxy penetration (Wong and Buenfeld 2006). This was followed by grounding and polishing of the blocks with silicon carbide and diamond abrasives in successive stages. The hardened epoxy protected the air void boundaries from crumbling during grinding and polishing, while the fluorescein dye enhanced the contrast of the air voids. The polished blocks were examined at 100× magnification using a petrographic microscope with a set up capable of analyzing air voids as small as 10 µm in diameter (Wong et al. 2011). Florescence microscopy applications for detection and quantification of micro-cracks is discussed in section 1.1.6.

1.1.2.3. Micro Computed Tomography (µ-CT)

Micro computed tomography or µ-CT is x-ray imaging in 3D, by the same method as used in CT (or "CAT") scans used in the hospital. It represents 3D microscopy, where the microstructure of objects is imaged non-destructively. Sample preparation, staining and thin slicing are not required for this method and a single scan is capable of imaging the sample's complete internal 3D structure at high resolution. Moreover, the undisturbed sample then can be reused for other purposes. Various methods of determining porosity of cement-based composites include water absorption, gas adsorption, helium inflow, Mercury Intrusion Porosimetry (MIP), alternating current impedance spectroscopy (ACIS), solvent replacement, Nuclear Magnetic Resonance Imaging (MRI), image analysis and optical microscope method (Monteiro 2006). Non-destructive methods of testing have always proven to be more effective than the destructive ones. MIP and water absorption methods are arguably destructive methods although they are two of the most effective and commonly used methods to determine the total void ratio and capillarity (Zeng et al. 2012, Lawrence et al. 2007, Ramli and Tabassi 2012, Arandigoyen and Alvarez 2007). In contrast,

X-ray Computed Tomography (CT) is a non-destructive method and more effective in determining porosity of cement based composites (Birgul 2008, Landis and Keane 2010, Tomoto et al. 2011, Nambiar and Ramamurthy 2007, Wong, Zimmerman and Buenfeld 2012). In CT method, X-rays are beamed to a material from a certain distance and a part of it is absorbed by the material and part of X-rays is also scattered while some parts of X-rays pass or transmitted through the material. Detectors catch these X-rays passed through the material and transmit them to a computer after digitalizing. Then the data in digital form are reconstructed to create an image via various algorithms. The solid, liquid and gas phases of the material can also be displayed digitally making the analysis of the material easier. Amounts of X-rays absorbed by materials can also be correlated with atomic density of substances. Higher atomic density of a material, leads to higher X-ray absorption percentage. It is also possible via CT to monitor void distribution development and void structure of the cementitious systems. Tekin et.al. investigated the development of macro voids, total macro void ratio, macro void structure in mortar and macro void distribution by making use of CT technology in a non-destructive manner (Tekin et al. 2015). They determined the porosity and void ratio of the concrete specimens followed by determination of unit weight and compressive strength. Thus, micro CT can be used as an efficient method of determining porosity and spatial air void distribution in the concrete or mortar (Landis and Keane 2010). Properties such as porosity, pore density, air void distribution, and crack detection can also be analyzed very conveniently. The downside of this technique however, is that with a larger sample size better resolution cannot be achieved and micro crack detection becomes challenging. There are non-uniform light exposure issues in case of large samples.

1.1.2.4. Qualitative and Quantitative Evaluation of Cracks

In order to assess the degree of cracking in concrete due to shrinkage under restraint and other factors such as, freeze thaw deteriorations, it is important to evaluate the micro-cracks in concrete. Some of the most widely used methods such as, resonant frequency method, ultrasonic wave velocity method etc. do not really speak much about the initiation and growth of micro-cracks in concrete (Wong and Chau 2005). One non-destructive technique to make a 3D reconstruction of micro-cracks in concrete is Computed Tomography (CT). Earlier studies have detected micro-cracks as small as 10μm in width in concrete specimens (Wakimoto et al. 2008, Promentilla and Sugiyama 2010). However, a superior technology in terms of spatial resolution and field of interest would be the use of fluorescence microscopy and digital image processing (DIP) for detection and quantification of micro-cracks in concrete (Tekin et al. 2015). These techniques are a potent tool to identify origin of these micro-cracks and strike relationships between the mechanical properties and the micro-crack density. Earlier researchers have relied on vacuum impregnation of an epoxy dye mixed with a fluorescent dye, and image reconstruction through DIP technique (Tekin et al. 2015). Investigations were made towards development of micro-crack patterns of mortar cracks, interfacial transition zone (ITZ) cracks and matrix cracks (composed of ITZ cracks and mortar cracks) in non-air-entrained and air-entrained concrete with the increase of freeze thaw cycles (Tekin et al. 2015). This process has the potential to help understand the role of air voids in freezing and thawing resistance of concrete and other durability issues (Gokce et al. 2004). Chemical behavior inside the air void zone may also be understood by performing X-ray diffraction or EDX technique (Ley, Folliard and Hover 2009, Kogbara et al. 2013).

1.2. Objectives and Dissertation Organization

This work is focused on the development of concrete with existing cementitious materials to achieve similar or lower resistance to shrinkage cracking, as compared to coarse ground cement, without adversely affecting other engineering properties of concrete. Key engineering properties include workability, degree of hydration, compressive and splitting tensile strengths, electrical resistivity, setting time, and bleeding. This dissertation is organized into six chapters. Chapter 1 contains an introduction and literature review. In Chapter 2, mechanical properties of fifteen different cementitious combinations are investigated. These mixtures are formed from four different cement types: coarse ground portland cement (CG), Type I portland cement (TI), Type I/II portland cement (TI/II), and Type IL portland limestone cement (TIL). In addition to investigating the four cement types with no partial replacement, the latter three cement types are partially replaced with 20% Class F fly ash (FF), 30% Class C fly ash (FC), and 5% nanosilica (NS). For two of the mixtures, Type I/II cement and 20% replaced with Class F fly ash, and 30% of fine aggregates replaced with light weight aggregates (TI/II-FF (LWA)), and Type I cement with no SCMs, and 30% of fine aggregates replaced with light weight aggregates (TI-P(LWA)) the effects of internal curing is investigated. In Chapter 3, five cementitious combinations are selected, based on the results of Chapter 2, and the effects of basalt fiber addition at a loading rate of 0.25% (v/v) on shrinkage and durability properties of concrete are investigated. Cementitious combinations investigated in this study include coarse ground cement with no SCMs (CG-P), Type I/II cement and 20% replaced with Class F fly ash (TI/II-FF), Type IL cement and 30% replaced with Class C fly ash (TIL-FC), Type I cement and 30% replaced with Class C fly ash (TI-FC), and Type I cement and 5% replaced with colloidal nanosilica (TI-NS). In Chapter 4, the effects of different cementitious combinations on micro-cracking due to drying shrinkage are investigated.

In Chapter 5, a life cycle assessment (LCA) and life cycle cost analysis (LCCA) have been performed on selected cementitious combinations. Chapter 6 consists of key conclusions and future work.

1.3. References

Arandigoyen, M. & J. I. Alvarez (2007) Pore structure and mechanical properties of cement–lime mortars. *Cement and concrete research,* 37**,** 767-775.

Barcelo, L., M. D. A. Thomas, K. Cail, A. Delagrave & B. Blair (2013) Portland limestone cement equivalent strength explained. *Concrete international,* 35**,** 41-47.

Barrett, T., H. Sun, C. Villani, L. Barcelo & J. Weiss (2014) Early-age shrinkage behavior of Portland limestone cement. *Concrete international,* 36.

Beltzung, F. & F. H. Wittmann (2005) Role of disjoining pressure in cement based materials. *Cement and Concrete Research,* 35**,** 2364-2370.

Bentz, D. P. (2010) Blending different fineness cements to engineer the properties of cement-based materials. *Magazine of Concrete Research,* 62**,** 327-338.

Birgul, R. (2008) Monitoring macro voids in mortar by X-ray computed tomography. *Nuclear Instruments and Methods in Physics Research Section A: Accelerators, Spectrometers, Detectors and Associated Equipment,* 596**,** 459-466.

Chen, S. J., F. G. Collins, A. J. N. Macleod, Z. Pan, W. H. Duan & C. M. Wang (2011) Carbon nanotube–cement composites: A retrospect. *The IES journal part a: Civil & structural engineering,* 4**,** 254-265.

Deshpande, S. S. (2007). *Evaluating free shrinkage of concrete for control of cracking in bridge decks*. University of Kansas.

Gokce, A., S. Nagataki, T. Saeki & M. Hisada (2004) Freezing and thawing resistance of air-entrained concrete incorporating recycled coarse aggregate: The role of air content in demolished concrete. *Cement and Concrete Research,* 34**,** 799-806.

Idiart, A. E. (2009). *Coupled analysis of degradation processes in concrete specimens at the meso-level*. Universitat Politècnica de Catalunya.

Institute, A. C. (2005). Report on factors affecting shrinkage and creep of hardened concrete. In *209*, Report ACI 209.1R-2005. Farmington Hills, MI: American Concrete Institute.

Ji, T. (2005) Preliminary study on the water permeability and microstructure of concrete incorporating nano-SiO2. *Cement and Concrete Research,* 35**,** 1943-1947.

Kogbara, R. B., S. R. Iyengar, Z. C. Grasley, E. A. Masad & D. G. Zollinger (2013) A review of concrete properties at cryogenic temperatures: Towards direct LNG containment. *Construction and Building Materials,* 47**,** 760-770.

Koo, Y., G. Littlejohn, B. Collins, Y. Yun, V. N. Shanov, M. Schulz, D. Pai & J. Sankar (2014) Synthesis and characterization of Ag–TiO2–CNT nanoparticle composites with high photocatalytic activity under artificial light. *Composites Part B: Engineering,* 57**,** 105-111.

Landis, E. N. & D. T. Keane (2010) X-ray microtomography. *Materials characterization,* 61**,** 1305-1316.

Lawrence, R. M., T. J. Mays, S. P. Rigby, P. Walker & D. D'Ayala (2007) Effects of carbonation on the pore structure of non-hydraulic lime mortars. *Cement and concrete research,* 37**,** 1059-1069.

Ley, M. T., K. J. Folliard & K. C. Hover (2009) Observations of air-bubbles escaped from fresh cement paste. *Cement and Concrete Research,* 39**,** 409-416.

Malhotra, V. M. & P. K. Mehta. (1996). *Pozzolanic and cementitious materials*. Taylor & Francis.

Mehta, P. K. & H. Meryman (2009) Tools for reducing carbon emissions due to cement consumption. *Structure,* 1**,** 11-15.

Miller, S. A., A. Horvath, P. J. M. Monteiro & C. P. Ostertag (2015) Greenhouse gas emissions from concrete can be reduced by using mix proportions, geometric aspects, and age as design factors. *Environmental Research Letters,* 10**,** 114017.

Mindess, S., J. F. Young & D. Darwin (2002) Concrete, 2nd EditionPrentice Hall. *Englewood Cliffs, NJ*.

Monteiro, P. (2006). *Concrete: microstructure, properties, and materials*. McGraw-Hill Publishing.

Nambiar, E. K. K. & K. Ramamurthy (2007) Air-void characterisation of foam concrete. *Cement and concrete research,* 37**,** 221-230.

Promentilla, M. A. B. & T. Sugiyama (2010) X-ray microtomography of mortars exposed to freezing-thawing action. *Journal of Advanced Concrete Technology,* 8**,** 97-111.

Raki, L., J. Beaudoin, R. Alizadeh, J. Makar & T. Sato (2010) Cement and concrete nanoscience and nanotechnology. *Materials,* 3**,** 918-942.

Ramli, M. & A. A. Tabassi (2012) Effects of polymer modification on the permeability of cement mortars under different curing conditions: a correlational study that includes pore distributions, water absorption and compressive strength. *Construction and Building Materials,* 28**,** 561-570.

Singh, L. P., S. R. Karade, S. K. Bhattacharyya, M. M. Yousuf & S. Ahalawat (2013) Beneficial role of nanosilica in cement based materials–A review. *Construction and Building Materials,* 47**,** 1069-1077.

Taylor, P. & X. Wang (2014) Concrete Pavement Mixture Design and Analysis (MDA): Factors Influencing Drying Shrinkage. Iowa State University

Tekin, I., R. Birgul, I. O. Yaman, O. Gencel & H. Y. Aruntas (2015) Monitoring macro voids in mortars by computerized tomography method. *Measurement,* 63**,** 299-308.

Tomoto, T., A. Moriyoshi, H. Takahashi, H. Kitagawa & M. Tsunekawa (2011) Damage to cement concrete pavements due to exposure to organic compounds in a cold region. *Construction and Building Materials,* 25**,** 267-281.

Tritsch, N., D. Darwin & J. Browning. (2005). Evaluating Shrinkage and Cracking Behavior of Concrete Using Restrained Ring and Free Shrinkage Tests. University of Kansas Center for Research, Inc.

Wakimoto, K., J. Blunt, C. Carlos, P. J. M. Monteiro, C. P. Ostertag & R. Albert (2008) Digital laminography assessment of the damage in concrete exposed to freezing temperatures. *Cement and Concrete Research,* 38**,** 1232-1245.

Wang, J., Z. Yang, K. Niu, G. Ke & M. Zhou (2009) Influence of MB-value of manufactured sand on the shrinkage and cracking of high strength concrete. *Journal of Wuhan University of Technology--Materials Science Edition,* 24**,** 321-325.

Wang, X. (2011). *Drying shrinkage of ternary blends in mortar and concrete*. Iowa State University.

Wiegrink, K., S. Marikunte & S. P. Shah (1996) Shrinkage cracking of high-strength concrete. *ACI Materials Journal,* 93**,** 409-415.

Wilson, M. L. & S. H. Kosmatka. (2011). Design and Control of Concrete Mixtures. Portland Cement Association. Skokie.

Wittmann, F. H. & F. Beltzung (2016) Fundamental aspects of the interaction between hardened cement paste and water applied to improve prediction of shrinkage and creep of concrete: A Critical Review. *Journal of Sustainable Cement-Based Materials,* 5**,** 106-116.

Wong, H. S. & N. R. Buenfeld (2006) Patch microstructure in cement-based materials: Fact or artefact? *Cement and Concrete Research,* 36**,** 990-997.

Wong, H. S., A. M. Pappas, R. W. Zimmerman & N. R. Buenfeld (2011) Effect of entrained air voids on the microstructure and mass transport properties of concrete. *Cement and Concrete Research,* 41**,** 1067-1077.

Wong, H. S., R. W. Zimmerman & N. R. Buenfeld (2012) Estimating the permeability of cement pastes and mortars using image analysis and effective medium theory. *Cement and Concrete Research,* 42**,** 476-483.

Wong, R. C. K. & K. T. Chau (2005) Estimation of air void and aggregate spatial distributions in concrete under uniaxial compression using computer tomography scanning. *Cement and concrete research,* 35**,** 1566-1576.

Worrell, E., L. Price, N. Martin, C. Hendriks & L. O. Meida (2001) Carbon dioxide emissions from the global cement industry. *Annual review of energy and the environment,* 26**,** 303-329.

Zayed, A., A. Sedaghat, A. Bien-Aime & N. Shanahan (2014) Effects of portland cement particle size on heat of hydration. Florida Department of Transportation

Zeng, Q., K. Li, T. Fen-Chong & P. Dangla (2012) Effect of porosity on thermal expansion coefficient of cement pastes and mortars. *Construction and Building Materials,* 28**,** 468-475.

Zerbino, R., G. Giaccio & S. Marfil (2014) Evaluation of alkali–silica reaction in concretes with natural rice husk ash using optical microscopy. *Construction and Building Materials,* 71**,** 132-140.

CHAPTER 2: EFFECTS OF PORTLAND LIMESTONE CEMENT ON SHRINKAGE AND DURABILITY OF CONCRETE

2.1. Abstract

In this work, different cementitious systems have been used to investigate shrinkage of concrete under plastic, and drying conditions. Emphasis has been placed on portland limestone cement (Type IL (10)) with replacement amounts of 10% of portland cement. Comparisons have been made with a cement with low Blaine fineness. Results indicate that Type IL cement has good shrinkage results, without adversely affecting other engineering properties of concrete, such as strength, resistivity, degree of hydration, and setting time.

2.2. Introduction

Concrete is perhaps an abundantly used building material. However, one of the major causes of damage in concrete is shrinkage cracking. Results of significant cracking may ultimately adversely affect the overall serviceability of concrete and lead to the ultimate failure of the structure. Out of the different types of shrinkage in concrete, plastic shrinkage and drying shrinkage are the major shrinkage mechanisms investigated in this work. Plastic shrinkage occurs within the first few hours of mixing concrete due to a higher rate of evaporation of water near the surface. Drying shrinkage occurs after the setting of concrete through days, months, or years as water is through the capillary pores.

It has been reported that concrete or mortar containing coarser cement can exhibit reduced shrinkage (Bentz 2010; Mehta and Burrows 2001). However, the concrete industry has moved towards finer cement that reacts faster (Kosmatka et al. 2002) in order to achieve faster strength gain. Researchers have also reported that cementitious systems with higher amounts of C_3S and

C_3A have a tendency to have higher shrinkage strain compared to those with lower amounts of the same (Mehta and Burrows 2001; Zayed et al. 2014).

Portland limestone cement (ASTM C595 Type IL in the United States) is a cement type that may contain up to 15% limestone interground with the clinker (Zayed et al. 2014). In addition to reducing CO_2 emissions, which is beneficial to the environment, Type IL cement has been reported to provide similar or reduced shrinkage in concrete (Barrett et al. 2014).

The use of supplementary cementitious materials (SCMs) such as fly ash and SiO_2 nanoparticles can enhance the long-term durability of concrete (Singh et al. 2013). Earlier studies have also reported that shrinkage of concrete is reduced by providing internal curing (De la Varga et al. 2012).

In this work, fresh and hardened tests have been conducted on concrete mixtures containing four types of cement: Coarse Ground cement, Type I (9% C_3A), Type II (4% C_3A) and Type IL (Portland Limestone Cement). Some of these cement types were blended with Fly Ash (Class F and Class C) and nanosilica. The primary goal of this work was to investigate plastic and drying shrinkage in concrete containing portland limestone cement. During this study, portland limestone cement was investigated with and without any SCMs, and compared to concrete containing coarse ground cement. Additionally, other engineering properties of strength, electrical resistivity, degree of hydration, and setting time were investigated. The goal was to identify concrete with cementitious systems having equal or less shrinkage strain than concrete containing coarse ground cement, without adversely affecting the engineering properties.

2.3. Background

Volume changes in concrete can occur under different conditions and at different ages. Some of these volume changes can be classified as plastic shrinkage, drying shrinkage and

chemical shrinkage (autogenous shrinkage). The emphasis of this research is on plastic and drying shrinkage.

Plastic shrinkage occurs in fresh concrete while it is still in a plastic state. When the rate of water evaporation at the surface exceeds that, at which bleed water rises to the surface, menisci are formed between particles. These menisci exert negative pressures on the system resulting in a net volume reduction in the paste. The strain is controlled by internal and external restraints leading to surface cracks (Mindess et al. 2002). Additionally, the rate of shrinkage at the surface is different from that of underlying concrete. This differential shrinkage also leads to additional tensile stresses, resulting in random shallow cracks in concrete (Deshpande 2007).

Drying shrinkage is due to the loss of water from capillary pores, normally by evaporation. At a relative humidity (RH) between 45% and 95%, free water in the pores is readily extracted from the system. When the RH in the pores drops below about 45% then water adsorbed to the walls of the pores starts to be removed, allowing pores to close and solid particles to move closer together (Idiart 2009). Some of the material characteristics that determine the extent of shrinkage in concrete are:

- Aggregate properties such as size, gradation, content and elastic properties,
- Water-cementitious materials ratio and water content,
- Cement characteristics such as particle size distribution, cementitious materials content, SCM type, and dosage
- Other ingredients such as air and chemical admixtures.

In concrete, cement paste (cementitious materials and water) is the most vulnerable to volume changes. The water to cementitious materials ratio of concrete directly influences shrinkage. An increase in the water to cementitious materials ratio increases the evaporable water

content per unit volume of paste, and the rate at which the water can reach the surface. Therefore, shrinkage is increased (Tritsch et al. 2005). Since the bulk of the shrinkage occurs in the paste, it is to be expected that shrinkage of concrete may be reduced by reducing the volume of paste. The volume and type of aggregates used in concrete influences the extent of shrinkage as aggregates restrain the shrinkage of cement paste. An increase in the volume of aggregates will lead to a decrease in the volume of paste and subsequently a decrease in shrinkage (Deshpande 2007).

External conditions such as relative humidity, ambient temperature, and wind velocity can also influence shrinkage (Taylor and Wang 2014) as well as the size and configuration of the element that affects rates of moisture loss from the surface. There is an inverse relationship between shrinkage and the ratio of specimen volume to its drying surface area (Institute 2005; Wang 2011). A summary of the factors affecting drying shrinkage of concrete has been presented in Table 1.

Table 1. Summary of factors affecting concrete shrinkage (Taylor and Wang 2014)

Categories	Factors	Specific Factors	General findings and conclusions on shrinkage
Paste quality	Cement characteristics	Chemistry	Higher sulfate and gypsum content may reduce shrinkage
		Fineness	Through change of the rate of hydration and water demand, finer cement leads to higher shrinkage
	Supplementary cementitious material	Fly ash	Class F fly ash potentially decreases shrinkage; Class C fly ash increases shrinkage with increasing dosage
		Slag cement	Conflicting results, depending on paste content; overall, comparable to ordinary PCC mixtures
		Silica fume	Conflicting results; depending on w/cm, curing period, and paste content; limited replacement may reduce long-term shrinkage
		Ternary mixtures	Normally, adverse effect can be diminished (i.e., PC + slag cement + silica fume) or even reduced (i.e., PC + slag cement + F fly ash)
	Chemical admixtures	Superplasticizers	May increase concrete shrinkage with a given w/cm ratio and cement content; dependent on admixture chemistry
	Air content		No significant effect on the magnitude of drying shrinkage if it is less than 8%
Paste quantity	w/cm		Influence is relatively small with a constant paste content for w/cm > 0.40
	Paste content		For a given w/cm ratio, shrinkage linearly increases with increasing paste content/volume
Other factors	Aggregate	Type	Influenced by mixing water demand and the stiffness of the aggregate
		Gradation	Indirect influence through the change of water demand and paste content; increased size results in decreased paste content, so decreased shrinkage
		Fines	Most fines increase shrinkage
	Curing	Duration	Increasing curing period reduces the amount of un-hydrated cement, resulting in reduced overall shrinkage
	Environment	Relative humidity	Higher relative humidity leads to lower shrinkage
		Temperature	High temperatures accelerate moisture loss leading to higher shrinkage
		Wind	Similar to temperature effect
	Construction		Improper addition of water during finishing, and poor curing will increase shrinkage
	Geometry		Increasing the volume-to-surface area ratio decreases shrinkage

Since finer cement has a higher surface area, higher reactive sites for hydration reactions are provided, and a more refined microstructure is formed. Consequently, the diameter of individual pores reduces, and higher capillary stresses are formed, resulting in higher shrinkage. Similar to aggregates, larger cement particles that have not undergone hydration can provide a restraining effect that subsequently induce cracks (Deshpande 2007).

Shrinkage in concrete is also dependent upon the chemical admixtures used, such as super plasticizers/high range water reducers, air entraining agent, and shrinkage reducing admixtures. Shrinkage reducing admixtures helps reduce shrinkage by reducing the surface tension of water and the pore fluid (Pease et al. 2005; Weiss et al. 2008). Superplasticizers are also important as they help reduce the water content of concrete which arguably may help in the reduction of shrinkage (Qi et al. 2002).

In addition, the particle size distribution of cementitious materials, and the chemistry of the system will affect early heat generation in concrete. High early heat generation can lead to thermal gradients, which may also influence concrete cracking (Zayed et al. 2014).

2.4. Experimental Program

In this study, fresh and hardened properties of concrete were investigated for select cementitious combinations. Emphasis was laid on Type IL portland limestone cement due to its potential benefits toward reduction of shrinkage strain and enhancement of durability in concrete. The cement types and tests used have been discussed in the following sub-sections.

2.4.1. Materials and Mixture Proportions

In this study, four cement types were used Coarse Ground portland cement (CG), Type I portland cement (TI), Type I/II portland cement (TI/II), and Type IL portland limestone cement (TIL). Additionally, Class C fly ash (FC), Class F fly ash (FF), and colloidal nanosilica (NS) were

used as supplementary cementitious materials (SCM). Some of the chemical and physical properties of the cement types, fly ash, and nanosilica were presented in Table 2, Table 3 and Table 4, respectively. ½" (nominal aggregate size) limestone aggregates and locally available sand were used. Lightweight aggregates were used to replace about 30% of the fine aggregate to provide internal curing. Figure 2 shows the combined gradation of the aggregates. For five selected mixtures (CG-P, TI-FC, TI/II-FF, TI-NS, and TIL-FC) ¾" (nominal aggregate size) limestone aggregates were used. An organic acid based air entraining agent, and a polycarboxylate based Type F high range water reducer were used.

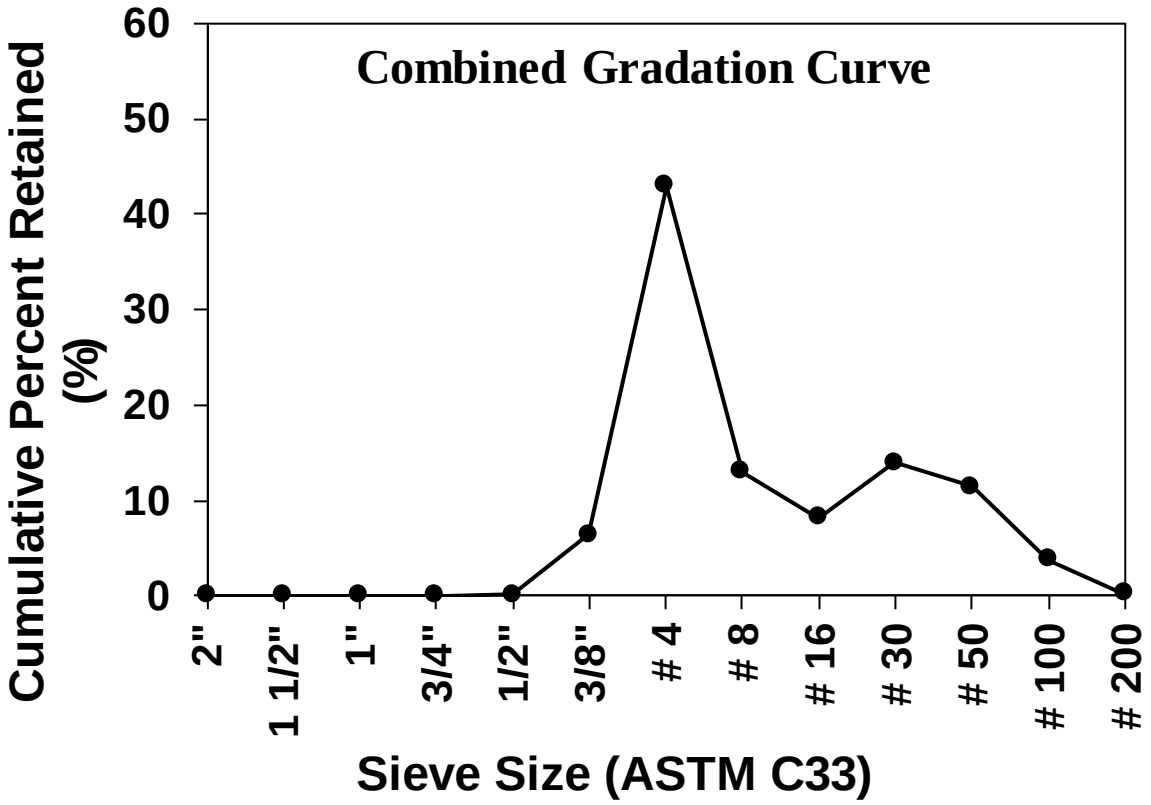

Figure 2. Combined particle size distribution curve for coarse and fine aggregates

Table 2. Chemical and physical properties of cements used

Item	Coarse Ground Cement*	Type I Cement*	Type I/II Cement*	Type IL Cement**
SiO_2 (%)	21.07	19.80	20.31	-
Al_2O_3 (%)	4.25	4.90	3.79	-
Fe_2O_3 (%)	3.13	2.40	3.22	-
CaO (%)	65.00	63.40	64.29	-
MgO (%)	0.97	2.80	3.38	0.90
SO_3 (%)	2.88	3.00	2.26	3.10
Loss on ignition (%)	0.75	2.60	2.73	4.80
Na_2O (%)	0.14	0.04	0.09	-
K_2O (%)	0.58	0.73	0.20	-
Insoluble Residue (%)	0.21	0.34	0.37	0.40
CO_2 (%)	-	1.50	1.85	-
Limestone (%)	-	3.7	4.7	10.0
$CaCO_3$ in limestone (%)	-	93.00	90.16	96.20
C_3S (%)	61.62	60.00	60.00	-
C_2S (%)	12.44	9.00	11.00	-
C_3A (%)	5.83	9.00	4.00	7.00
C_4AF (%)	9.3	7.00	10.00	-
Equivalent alkalies (%)	0.52	0.52	0.23	-
Blaine Fineness (m^2/kg)***	316.94	397.00	393.00	382.00

*Limits specified in ASTM C150

**Limits specified in ASTM C595

***Physical property

Table 3. Chemical and physical properties of fly ashes used

Item	Class C Fly Ash*	Class F Fly Ash*
SiO_2 (%)	39.01	51.65
Al_2O_3 (%)	21.23	16.29
Fe_2O_3 (%)	5.72	5.63
$SiO_2+Al_2O_3+Fe_2O_3$	65.96	73.57
SO_3 (%)	0.81	0.67
CaO (%)	24.31	13.00
MgO (%)	5.31	4.26
Na_2O (%)	1.58	3.23
K_2O (%)	0.53	2.45
Equivalent alkalies (%)	1.15	1.63
Loss on Ignition (%)	0.16	0.10
Fineness (+325 Mesh) (%)**	16.90	21.29

*Limits specified in ASTM C618

**Physical property

Table 4. Chemical and physical properties of nanosilica used

Item	Colloidal Nanosilica
SiO_2 (%)	49.0-51.0
SiO_2:Na_2O Ratio	200-250
Na_2SO_4 (%)	≤0.135
pH	8.5-9.5
Viscosity (at 25°C) (cps)*	≤55
Specific Gravity (at 60°F)*	1.388-1.407
Surface Area (m^2/g)*	110-150

*Physical properties

The mixture proportions for the concrete used are shown in Table 5. Cementitious combinations investigated in this study include coarse ground cement (CG) with no SCMs (designated as P), Type I/II cement (TI/II), Type I cement (TI), and Type IL cement (TIL), each with no SCMs (designated as P), 20% replaced with Class F fly ash (designated as FF), 30% replaced with Class C fly ash (designated as FC), and 5% replaced with colloidal nanosilica (designated as NS). Mixtures containing lightweight aggregates include Type I/II cement and 20% replaced with Class F fly ash, and 30% of fine aggregates replaced with light weight aggregates (TI/II-FF (LWA)), and Type I cement with no SCMs, and 30% of fine aggregates replaced with light weight aggregates (TI-P (LWA)). The water-to-cementitious materials ratio, binder content, and binder to coarse aggregates to fine aggregates weight ratio were fixed at 0.42, 580 lb/yd^3, and 1:3.08:2.23, respectively. The effect of the volume of aggregates on concrete shrinkage is investigated for five selected mixtures:

- Coarse ground cement with no SCMs (CG-P)
- Type I cement and 30% replaced with Class C fly ash (TI-FC)
- Type I/II cement and 20% replaced with Class F fly ash (TI/II-FF)

- Type I cement and 5% replaced with colloidal nanosilica (TI-NS)
- Type IL cement and 30% replaced with Class C fly ash (TIL-FC).

Table 5. Mixture proportions for Chapter 2

Mix Code	Cement (pcy)	Class F Fly Ash (pcy)	Class C Fly Ash (pcy)	Nano Silica (pcy)	Water (pcy)	WR (oz/cwt)	AEA (oz/cwt)	Fine Aggregates. (pcy)	Light Weight Aggregates (pcy)	Coarse Aggregates (pcy)
CG-P	580	0	0	0	244	3.96	0.2	1789	0	1295
TI/II-P	580	0	0	0	244	4.183	0.2	1789	0	1295
TI-P	580	0	0	0	244	3.2163	0.2	1789	0	1295
TIL-P	580	0	0	0	244	6.5	0.2	1789	0	1295
TI/II-FF	464	116	0	0	244	2.5	0.2	1789	0	1295
TI-FF	464	116	0	0	244	2	0.2	1789	0	1295
TIL-FF	464	116	0	0	244	2.5	0.2	1789	0	1295
TI/II-FC	406	0	174	0	244	3.23	0.2	1789	0	1295
TI-FC	406	0	174	0	244	3.845	0.2	1789	0	1295
TIL-FC	406	0	174	0	244	4.333	0.2	1789	0	1295
TI/II-NS	551	0	0	29	244	18.36	0.2	1789	0	1295
TI-NS	551	0	0	29	244	17.62	0.2	1789	0	1295
TIL-NS	551	0	0	29	244	19.09	0.2	1789	0	1295
TI-P (LWA)	580	0	0	0	244	7.65	0.2	1109	281	1295
TI/II-FF (LWA)	464	116	0	0	244	2.5	0.2	1109	281	1295

The water-to-cementitious materials ratio, binder content, and binder to coarse aggregates to fine aggregates weight ratio for these mixtures were fixed at 0.42, 564 lb/yd^3, and 1:3:2.5, respectively. The mixtures with these proportions are designated with a suffix 2.

2.4.2. Test Methods

Fresh properties such as workability (ASTM C143), air content/unit weight (ASTM C231, ASTM C138), setting time (ASTM C403), bleeding (ASTM C232), and hydration rate were measured. Semi-adiabatic calorimetry tests were used to investigate the hydration characteristics of the concrete mixtures (ASTM C1753). In this test, the evolution of temperature in concrete was measured over time for 24 hours. Isothermal calorimetry test was also used to investigate hydration trends of five critical mixtures as identified in sections 3.1 and 3.2. Cement paste was placed in a calorimeter under isothermal conditions, and changes in heat was measured over time up to 24 hours.

One of the key fresh tests of this paper is the investigation of plastic shrinkage. Concrete specimens were cast in a box having dimensions specified in ASTM C1579. A novel modified test method was followed in this study, to measure the length change within the first six hours of mixing within the panel, and thereby calculate the strain per elapsed time due to plastic shrinkage. This was achieved by introducing four markers across the long edge of the concrete panel (top view of the specimen can be seen in Figure 3). Flanged metal bolts with a distinctly marked point in each were used as the markers. These were placed firmly on the concrete surface immediately after casting. The length change over time was measured by using slide calipers of accuracy up to 0.0001 inches.

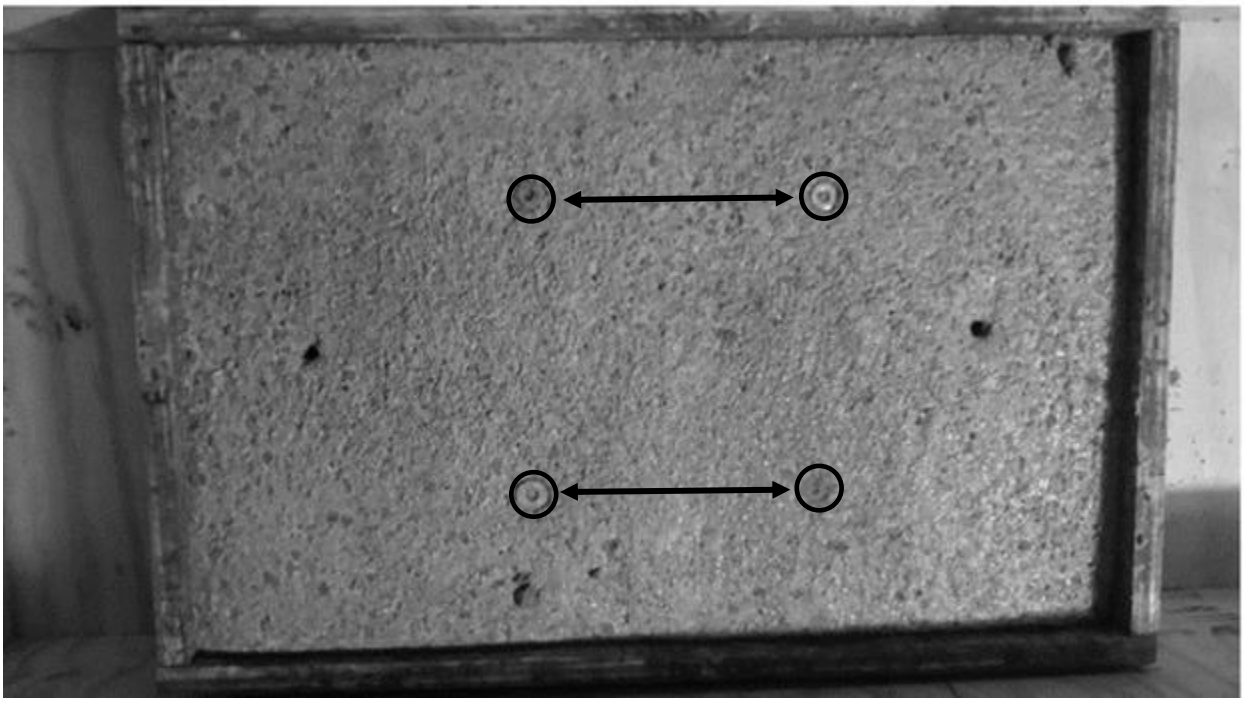

Figure 3. Plastic shrinkage experimental set up

Free shrinkage in concrete was measured in accordance with ASTM C157. Shrinkage strain in the concrete mixtures due to external restraints was measured by the standard ring test method specified in ASTM C1581 (Figure 4).

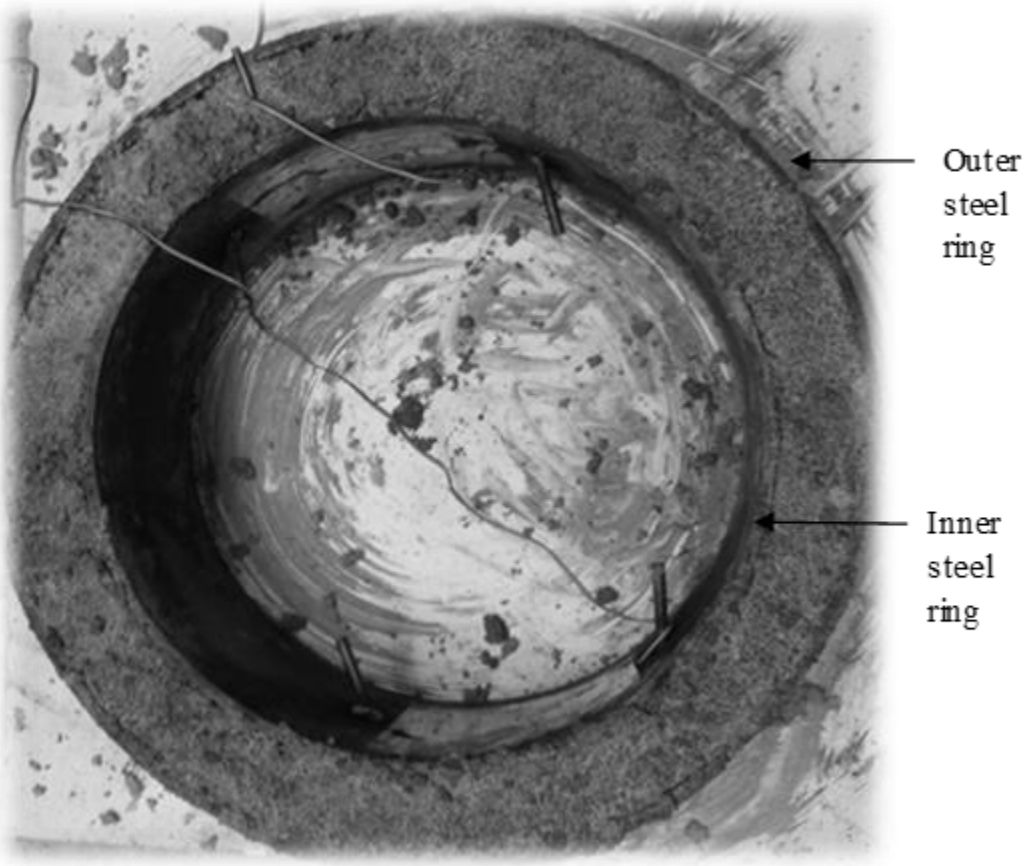

Figure 4. Restrained shrinkage test setup

Other hardened concrete tests including compressive strength (ASTM C39), splitting tensile strength (ASTM C496), and electrical resistivity (ASTM C1760) were also performed on the concrete mixtures. Electrical resistivity test was conducted in concrete to have an indirect assessment of the ability of concrete to resist the ingress of harmful chemical ions like Chloride.

2.5. Results and Discussion

2.5.1. Fresh Properties

All of the concrete mixtures were maintained with a slump ranging between 1 and 5½ inches. The air content of the mixtures ranged between 5% and 8.5% (Table 6), representing typical specifications of exposed concrete especially in the Midwest.

Table 6. Fresh properties for Chapter 2

Mix Code	Fresh Properties						
	Slump (in)	Air (%)	Unit Weight (lb/ft^3)	Bleeding (ml/cm^2)	Calorimetry Temperature Rise (°F)	Setting Time from Calorimetry (min)	
						Initial (20% of Temperature Rise)	Final (50% of Temperature Rise)
CG-P	4	6	145	0.00	30	240	380
TI/II-P	5.5	8.2	139.3	0.00	27	370	540
TI-P	4	8.3	141.4	0.00	35	220	360
TIL-P	1.5	6.3	141.5	0.01	29	220	360
TI/II-FF	4.5	8	144.6	0.00	22	240	360
TI-FF	4	8	143.6	0.01	26	240	390
TIL-FF	5.5	8.1	142.6	0.00	24	220	360
TI/II-FC	5	6.5	147.2	0.00	18	410	580
TI-FC	4.25	6.4	145.8	0.00	23	360	520
TIL-FC	4	7.2	145.5	0.02	15	310	440
TI/II-NS	1	6.6	151	0.01	33	230	360
TI-NS	1	5.4	147.7	0.00	37	220	430
TIL-NS	1.5	5.4	148.3	0.00	32	400	520
TI-P (LWA)	4	5.3	139.3	0.01	33	360	520
TI/II-FF (LWA)	1.5	6.2	133.5	0.01	22	230	370

The inclusion of nanosilica in concrete resulted in a low slump (ASTM C143). This was because of an increased specific surface area to interact with water (Khaloo et al. 2016). As a

result, high dosages of Type F high range water reducer had to be added. This can retard the process of hydration (Cheung et al. 2011). This effect is reflected in the temperature change of mixtures over time obtained from semi-adiabatic calorimetry results (Figure 5). The peak of temperature rise curve of TI-NS is slightly lower than that of its control TI-P (Figure 5c). This happened as the presence of high amounts of superplasticizers impeded the crystal formation during hydration (Flatt and Houst 2001). On the other hand, the incorporation of nanosilica in itself usually enhances the rate of hydration of cementitious materials due to an increased specific surface area (Khaloo et al. 2016). This is reflected in Figures 5b and 5d.

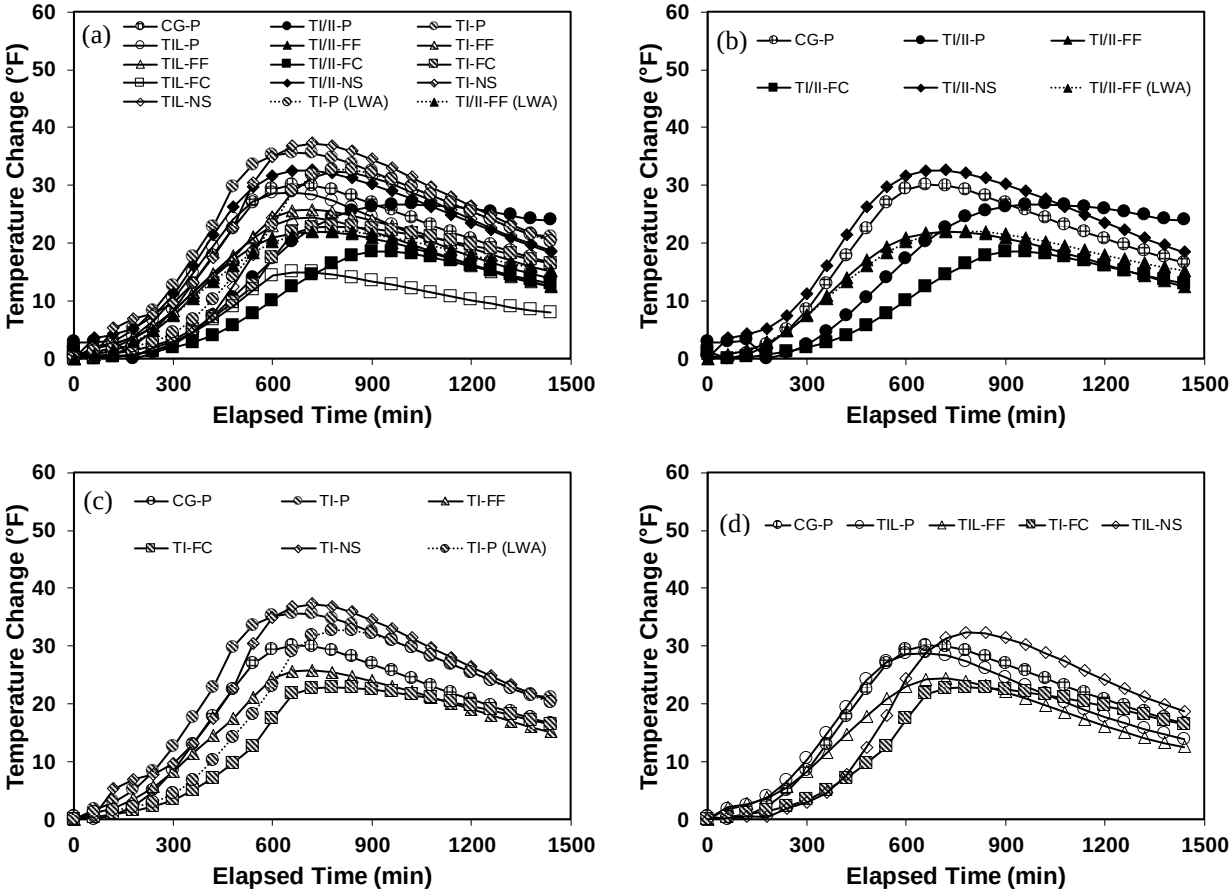

Figure 5. Temperature rise by semi-adiabatic calorimetry: (a) all mixtures, (b) mixtures containing Type I/II cement, (c) mixtures containing Type I cement, (d) mixtures containing Type IL cement

From Table 6, it can also be observed that TIL-P had a low slump. This might be due to a partial replacement of portland cement with limestone (10%) (Barcelo et al. 2013). However, it responded well to vibration. Noticeably, such low values of slump were not observed when Type IL cement was blended with fly ash (TIL-FF, TIL-FC) (Table 6). This might be due to spherical and smooth fly ash particles, which enhanced workability in concrete (Kosmatka et al. 2002). Figure 5 shows the results of initial and final setting times for the concrete mixtures as calculated from 20% and 50% of maximum temperature change through semi-adiabatic calorimetry results (Wang et al. 2016). Concrete mixtures containing fly ash, in general, had equal or slightly longer setting times than their plain cement concrete counterparts. This delayed effect was more pronounced in case of Class C fly ash than Class F fly ash (Roberts and Taylor 2007). This might be due to an interaction of sulfates in cement with fly ash (Sandberg and Roberts 2005). The Class C fly ash used in this study contained high levels of certain aluminate compounds, including C_3A. This in addition to C_3A present in the cement might result in a depletion of sulfate contained in the cement, otherwise present to control flash set. Therefore, there was an abnormal retardation in the mixtures containing Class C fly ash (Cost and Knight 2007).

Among the mixtures containing nanosilica, TI/II-NS had shorter setting time than TI/II-P, consistent with trends reported in the literature (Khaloo et al. 2016). However, use of Type F high range water reducers may sometimes retard the setting of concrete (Zakka and Carrasquillo 1989). This was evident in case of TI-NS and TIL-NS (Figure 6).

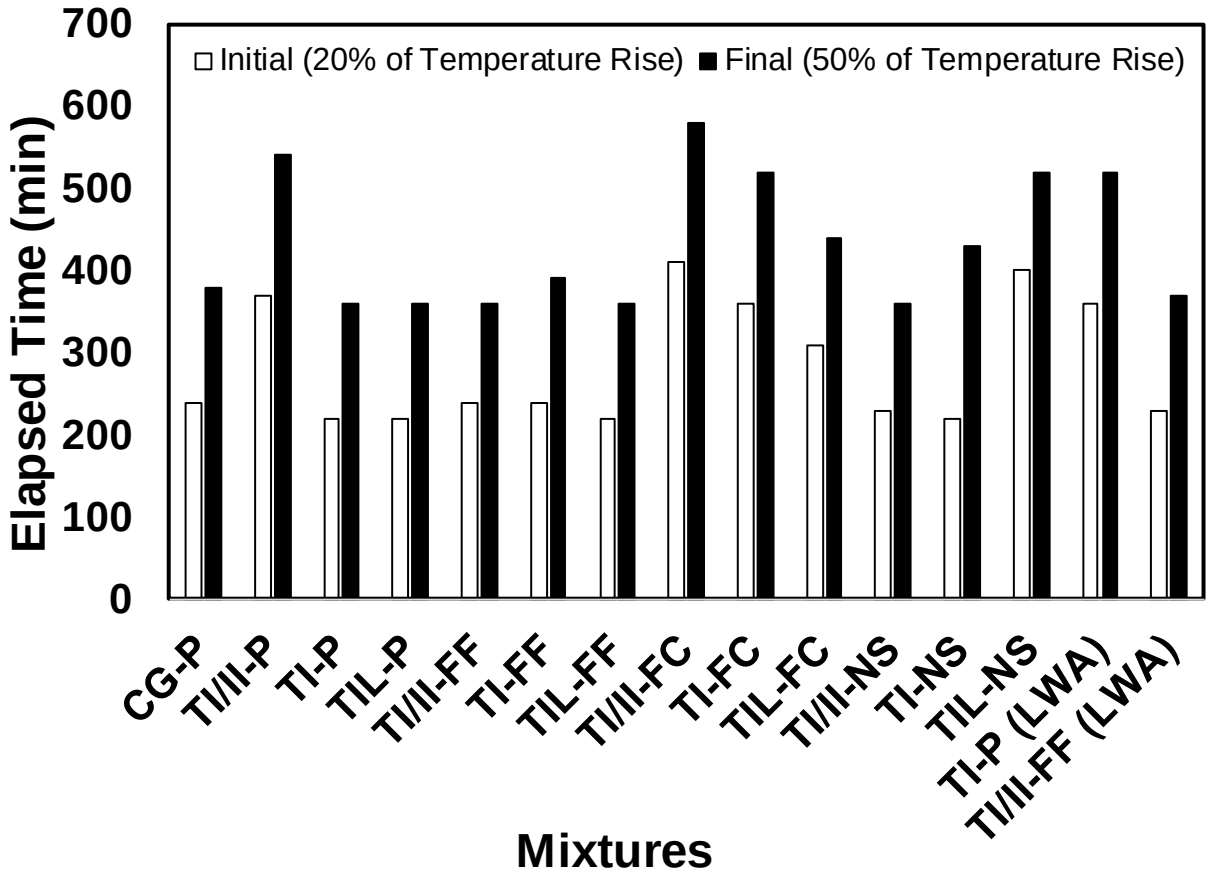

Figure 6. Initial and final setting times through semi-adiabatic calorimetry

Figure 7 shows the plastic shrinkage strain results. Out of the fifteen concrete mixtures, seven had measurable (>0.15 mm wide) surface cracks. TI/II-FF exhibited a slight crack, narrower than 0.15" confirmed by an abrupt change in the negative strain.

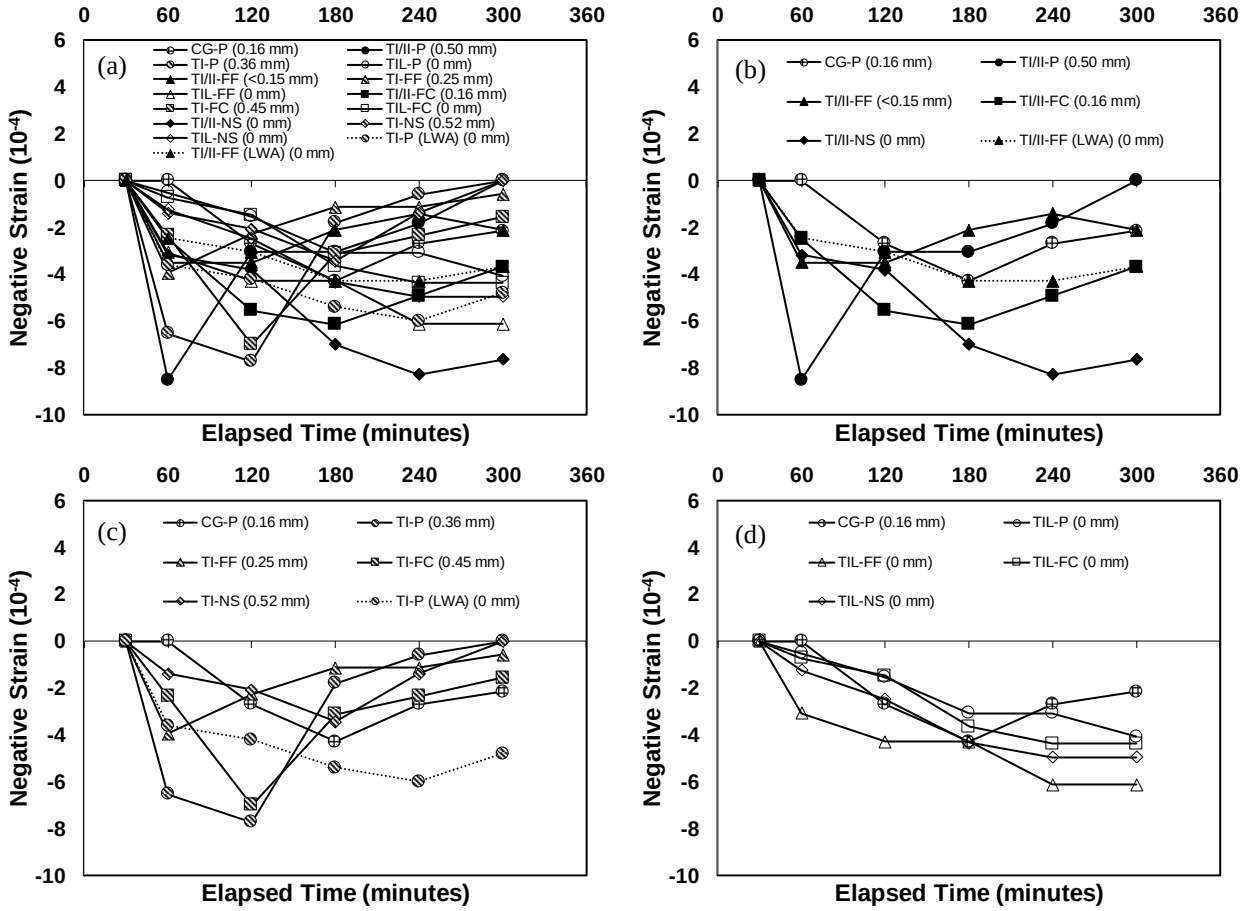

Figure 7. Plastic shrinkage (Numbers within brackets indicate crack width after 24 hours): (a) all mixtures, (b) mixtures containing Type I/II cement, (c) mixtures containing Type I cement, (d) mixtures containing Type IL cement

Noticeably, surface cracks were not observed for any of the concrete mixtures containing Type IL cement after 24 hours. This resistance to plastic shrinkage cracking might be due to a better particle size distribution (Barrett et al. 2014). The mixtures containing lightweight aggregates were also seen to have no surface cracks. This resistant behavior of these two mixtures was likely due to a supply of water inside the cementitious system through internal curing thus reducing drying strains (Bentz and Weiss 2011).

2.5.2. Hardened Properties

2.5.2.1. Compressive Strength and Splitting Tensile Strength

Figure 8 shows the compressive strength of the concrete mixtures. CG-P exhibited the lowest strength values among the plain cement concrete mixtures, to be expected with low fineness and a slower rate of hydration (Figure 8a). TIL-P had the highest compressive strength results at 28 days, among the normal cured mixtures (Figure 8a). This was likely due to a combined effect of an improved particle packing (Sprung and Siebel 1991), increased rate of cement hydration (Bonavetti et al. 2003; Vuk et al. 2001) and an early production of calcium carbo-aluminate hydrates (Ramezanianpour and Hooton 2014; Voglis et al. 2005). As expected, all the mixtures containing nanosilica had higher compressive strength and rate of strength gain than their plain cement concrete counterparts (Figure 8b, 8c, and 8d). The mixtures containing fly ash had lower strength values and a slower rate of strength gain compared to their plain cement concrete counterparts (Figures 8b, 8c, and 8d). This was because of a slower rate of hydration (Ayub et al. 2014; Juenger and Siddique 2015). Over longer periods of time, it might be anticipated that fly ash would enhance compressive strength of concrete (Shehata and Thomas 2002). The mixtures containing lightweight aggregates [TI-P (LWA) and TI/II-FF (LWA)] exhibited improved compressive strength results compared to their corresponding concrete mixtures due to improved hydration (Figures 8a, 8b, 8c) (Bentz and Weiss 2011).

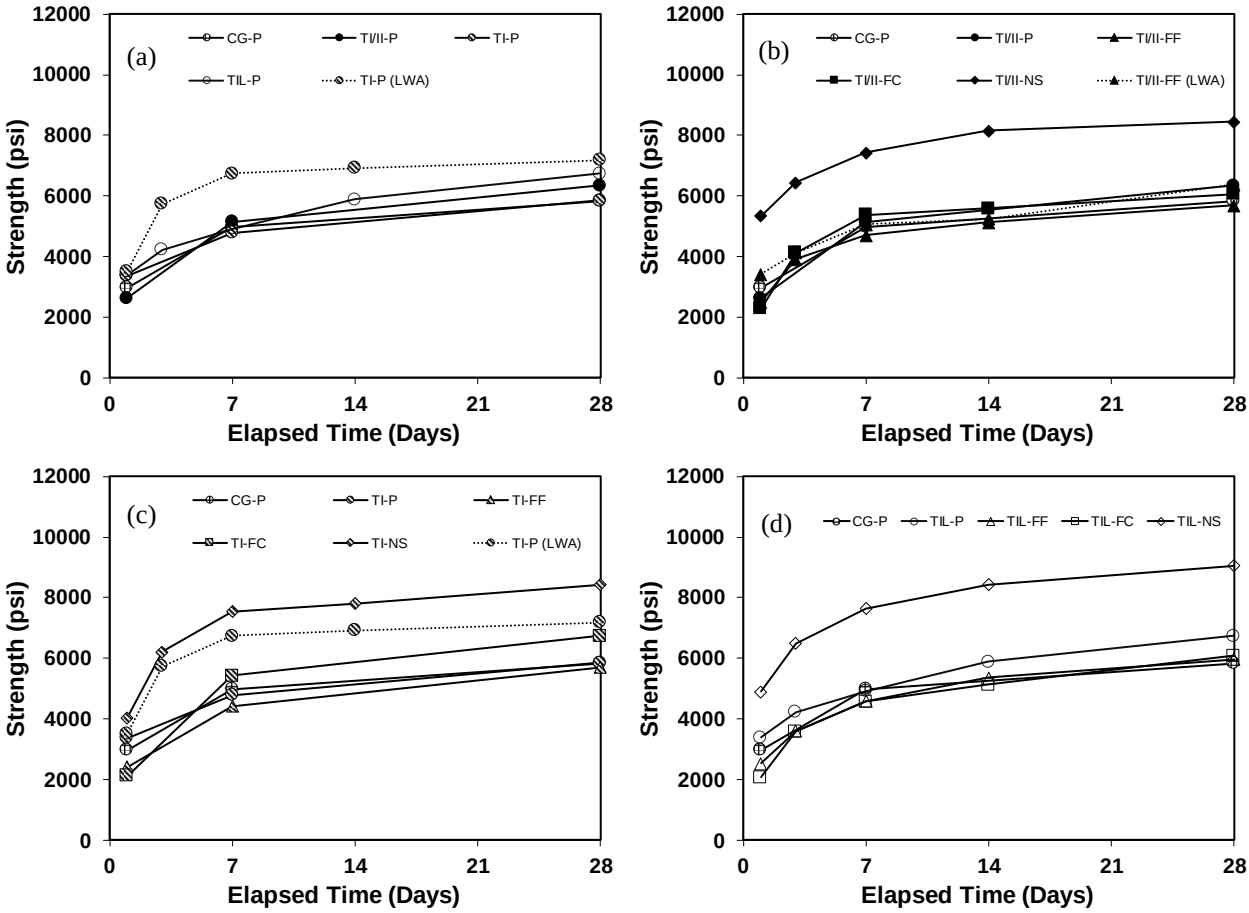

Figure 8. Compressive strength: (a) mixtures containing no SCMs, (b) mixtures containing Type I/II cement, (c) mixtures containing Type I cement, (d) mixtures containing Type IL cement

Figure 9 shows the 28-day splitting tensile strength results of the concrete mixtures showing similar trends.

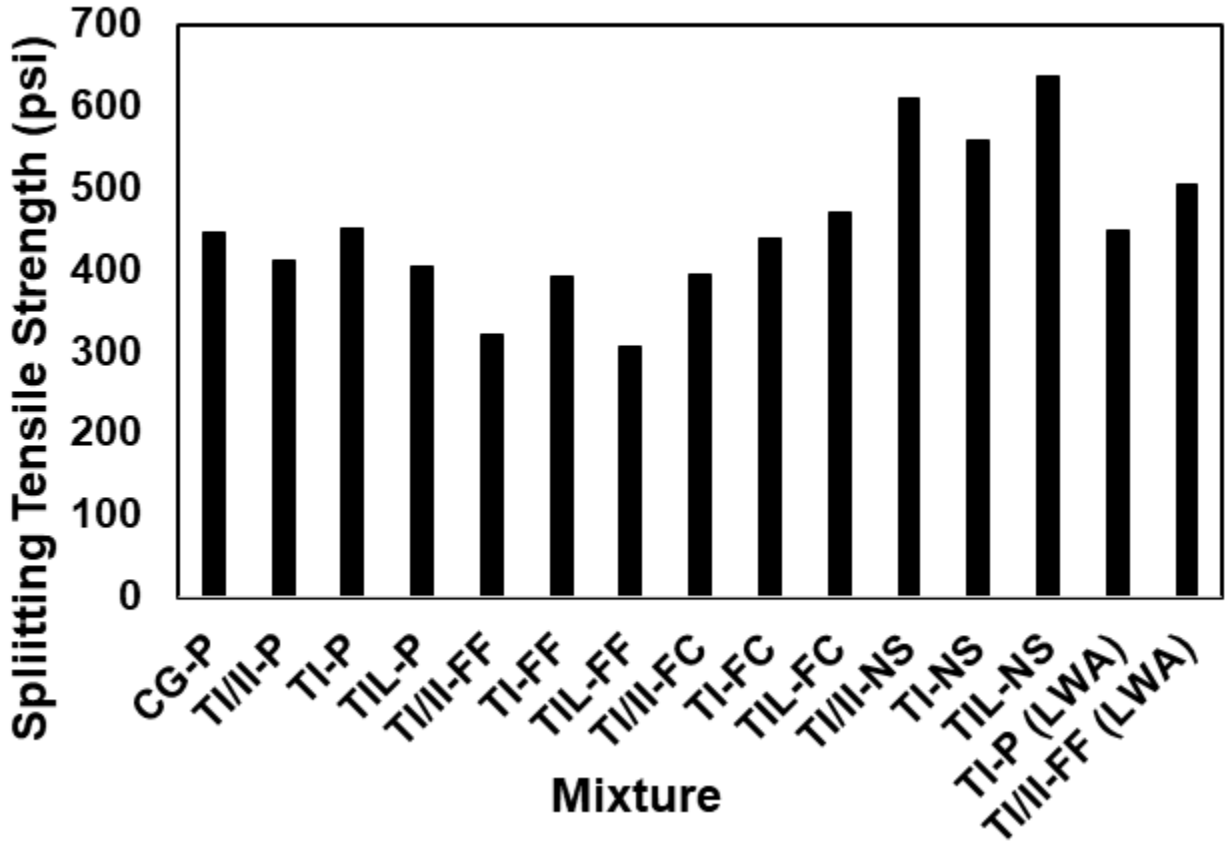

Figure 9. Splitting tensile strength

2.5.2.2. Resistivity

Figure 10 shows the results for electrical resistivity of the concrete mixtures. Some of the mixtures exhibited higher 28-day resistivity values than others. In general, the improvement in resistivity was likely due to a refinement in the microstructure of the concrete system and a reduction in the volume of fluid filled pores. Resistivity is a useful measure because it is an indirect indication of the ability of a material to resist the passage of fluids and hence the potential durability.

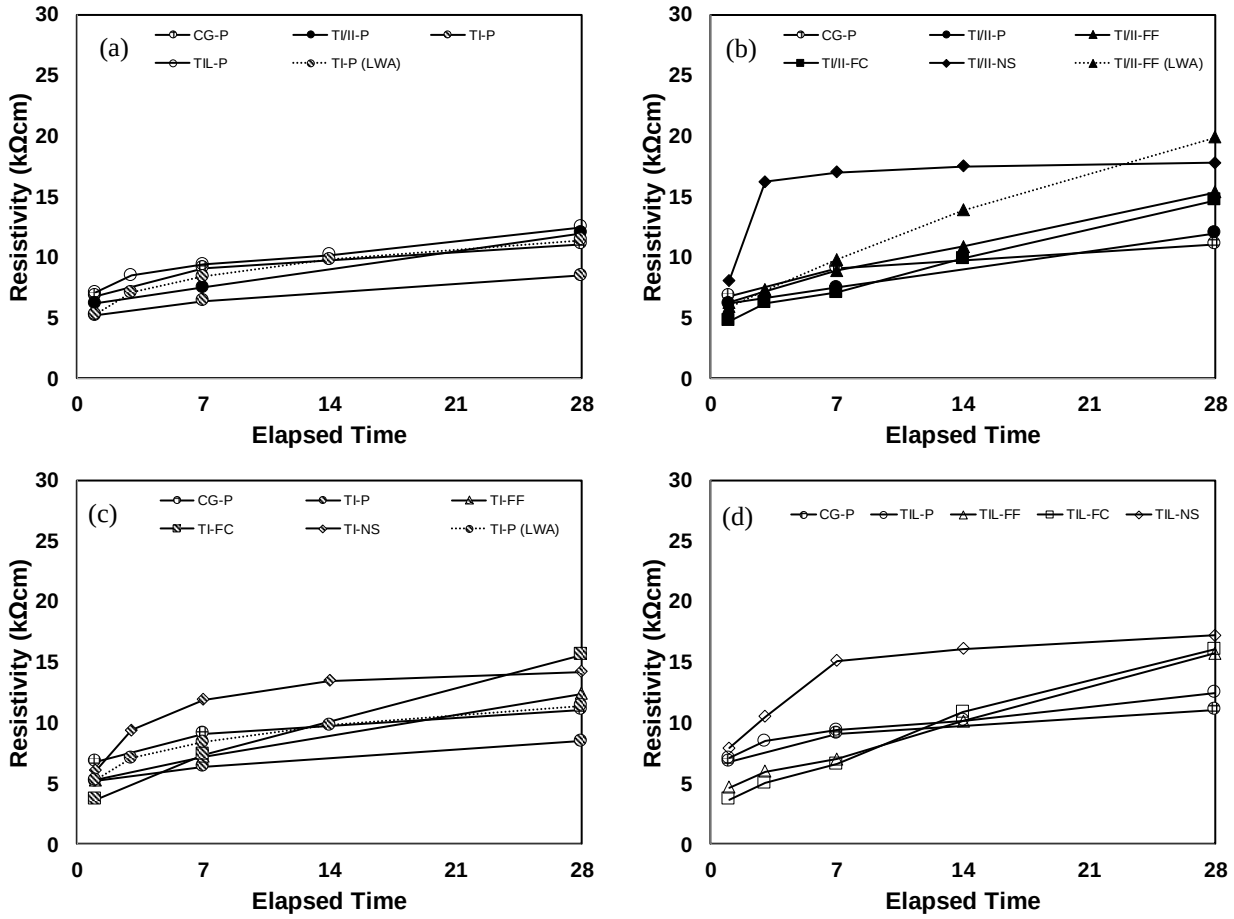

Figure 10. Electrical resistivity: (a) mixtures containing no SCMs, (b) mixtures containing Type I/II cement, (c) mixtures containing Type I cement, (d) mixtures containing Type IL cement

The systems containing limestone exhibited higher resistivity than the others, likely as a result of a refined microstructure and a superior particle packing.

Internal curing had also improved resistivity of concrete (Figure 10b, 10c). This was due to an improved microstructure from extended hydration (Bentz and Weiss 2011).

The early age resistivity results for TI/II-NS were much higher than the rest of the concrete mixtures containing Type I/II cement (Figure 10b). At 28 days, TI/II-FF (LWA) had the highest resistivity value among all the mixtures. The concrete mixtures containing nanosilica had improved resistivity results compared to their control mixtures (Figures 10b, 10c, and 10d). This is consistent with prior literature (Singh et al. 2013).

It was also evident that the mixtures containing fly ash exhibited improvements in resistivity over their control mixtures, especially towards the later ages (Figures 10b, 10c, and 10d). This was due to a refinement in microstructure from higher pozzolanicity over longer periods of time (Ayub et al. 2014).

Coarse ground cement results in a slower formation of microstructure, and thus resistivity results were inferior as compared to most other mixtures.

2.5.2.3. Drying Shrinkage

Figure 11 shows plots of free shrinkage strain of the mixtures used in this study. Coarse ground cement had exhibited the lowest free shrinkage strain beyond 28 days (Figures 11a, 11b, 11c, 11d). This is consistent with the literature (Mehta and Burrows 2001). Internal curing resulted in the reduction of strain from drying shrinkage (Figure 11c). Type IL portland limestone cement had lower strain due to drying shrinkage due to a better microstructure formation (Figure 11a). In case of restrained shrinkage tests Figure 12, coarse ground cement has the lowest recorded strain among the mixtures containing no SCMs (Figure 12a). Rings for two of the concrete mixtures have cracked: TI-NS and TI/II-FC (Figures 12b and 12c). This is apparent from a sudden reduction in recorded strains as energy due to stress is dissipated through cracks (Figures 12b, 12c). Noticeably, some of the mixtures containing fly ash showed higher free and drying shrinkage strain results over their corresponding plain cement concrete mixtures (Figures 11b, 11c, 11d, 12b, 12c, 12d). Higher drying shrinkage strain due to fly ash is reported in prior literature (Munday et al.). Higher drying shrinkage strain is recorded in case of concrete containing fly ash with an unaltered water-binder ratio as compared to control mixture containing portland cement with no SCMs (Nath and Sarker 2013). This is because of a higher availability of free water in concrete containing fly ash,

as it requires less water to achieve a consistency similar to that of concrete without fly ash (Jiang and Malhotra 2000).

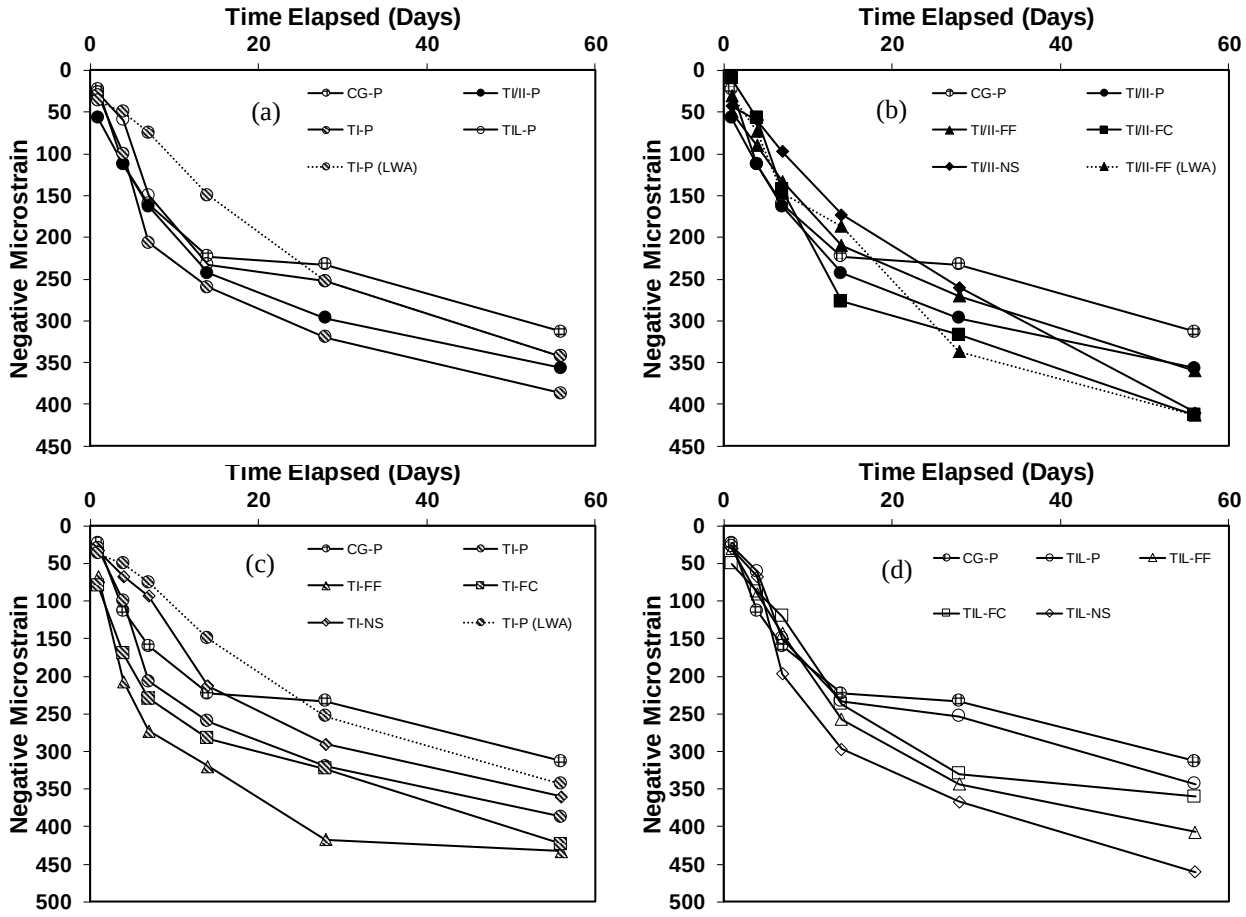

Figure 11. Free shrinkage: (a) mixtures containing no SCMs, (b) mixtures containing Type I/II cement, (c) mixtures containing Type I cement, (d) mixtures containing Type IL cement

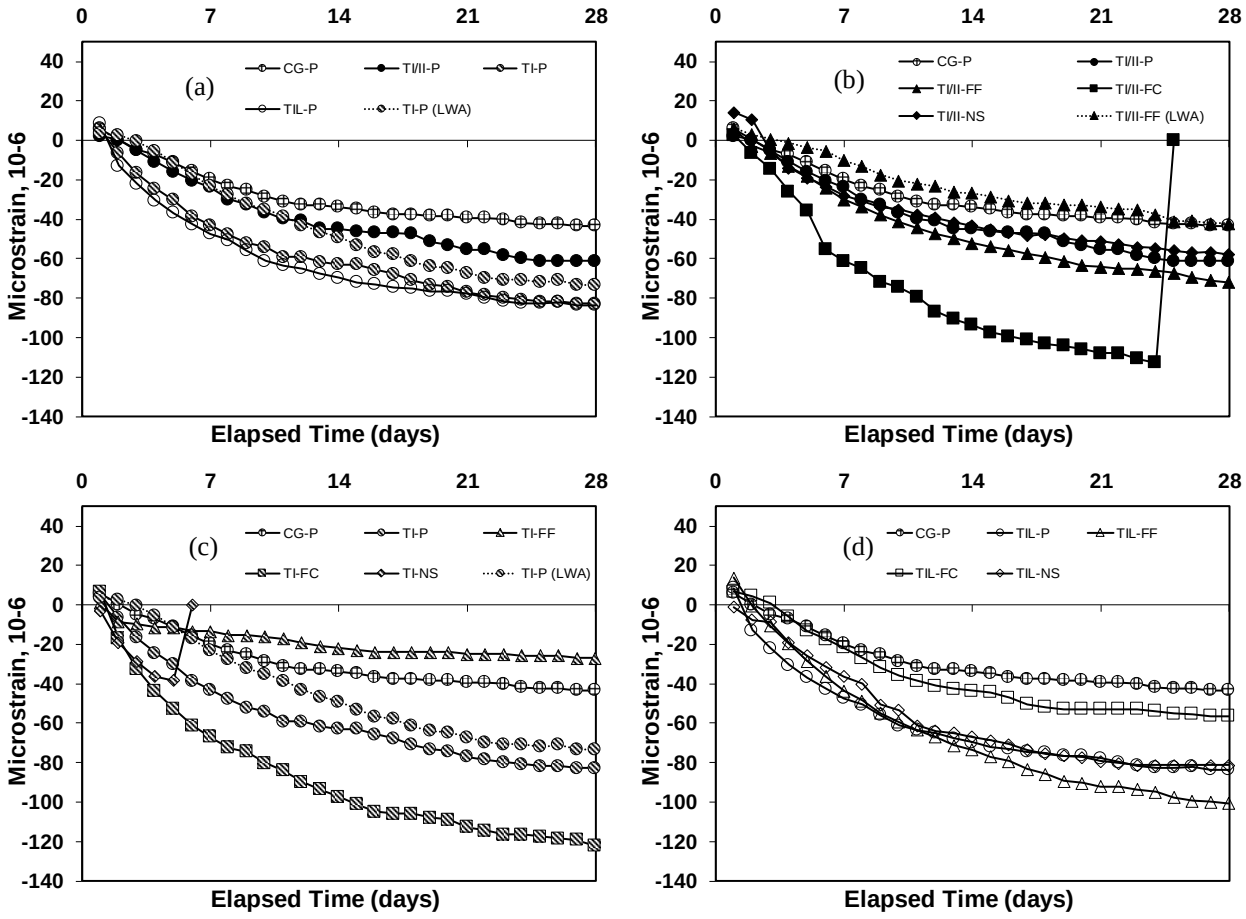

Figure 12. Restrained shrinkage: (a) mixtures containing no SCMs, (b) mixtures containing Type I/II cement, (c) mixtures containing Type I cement, (d) mixtures containing Type IL cement

The cracking potential of the mixtures has been presented in Table 7.

Table 7. Potential for Cracking (ASTM C1581)

Mix	α (in/in)/day$^{1/2}$	S (psi/day)	Cracking Potential
CG-P	-11.492	11	Low
TI/II-P	-15.892	16	Moderate Low
TI-P	-19.903	20	Moderate Low
TIL-P	-19.321	19	Moderate Low
TI/II-FF	-18.214	18	Moderate Low
TI-FF	-5.705	6	Low
TIL-FF	-26.518	26	Moderate High
TI/II-FC	-30.477	32	Moderate High
TI-FC	-27.538	27	Moderate High
TIL-FC	-16.112	16	Moderate Low
TI/II-NS	-15.833	16	Moderate Low
TI-NS	-28.535	67	High
TIL-NS	-20.720	20	Moderate Low
TI-P (LWA)	-20.898	21	Moderate Low
TI/II-FF (LWA)	-12.057	12	Low

2.5.3. Performance Matrix

Based on the results of fresh and hardened properties, five concrete mixtures with improved results than the other mixtures are selected. Some of the key properties of these five mixtures (CG-P. TI-FC, TI/II-FF, TI-NS, and TIL-FC) are presented in Table 8. Further investigations were conducted on these five mixtures.

Table 8. Selected mixtures with key results for Chapter 2

Mix	Parameters and Performance Limits	28 Day Compressive Strength (psi)	% Improvement of 28 Day Resistivity of Mix over CG-P (%)	56 Day Free Shrinkage (μ-Strain)	Cracking Potential
		>4000 psi	20%	> -400 μ-Strain	
CG-P		5845	0.00	-313	Low
TI/II-FF		5695	38.74	-360	Moderate Low
TI-FC		6738	40.54	-423	Moderate High
TIL-FC		6084	45.04	-360	Moderate Low
TI-NS		8432	27.93	-360	Moderate High

2.5.4. Effect of Aggregate Volume

The effect of a higher volume of aggregates, with larger coarse aggregates on free shrinkage, can be assessed from Figure 13. For comparison with the mixtures with ½" aggregates, trends have been plotted up to 56 days. It may be observed that TIL-FC2 and TI-NS2 had lower free shrinkage than TIL-FC and TI-NS, respectively. From prior literature, it is found that higher volume of aggregates can reduce the drying shrinkage of concrete, as the volume of cement paste consequently reduces (Zhu et al. 2016).

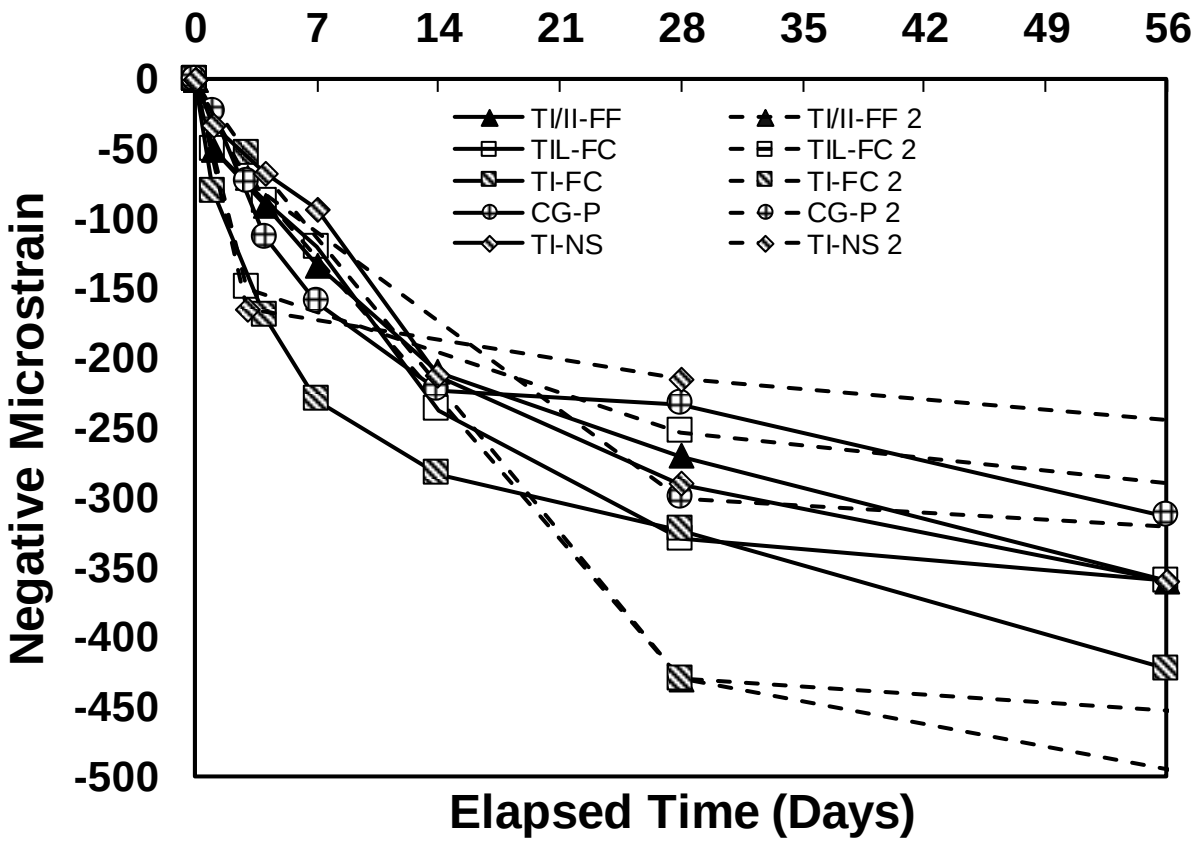

Figure 13. Effect of aggregate volume on free shrinkage

2.5.5. Isothermal Calorimetry

Figure 14 shows the isothermal calorimetry results of paste samples for the five mixtures. It may be observed that the two mixtures containing Class C fly ash (TI-FC and TIL-FC) may have a sulfate depletion point (Figure 14). This may explain the abnormally long setting times for these two concrete mixtures (Table 6). This is explained in greater detail in section 2.5.1.

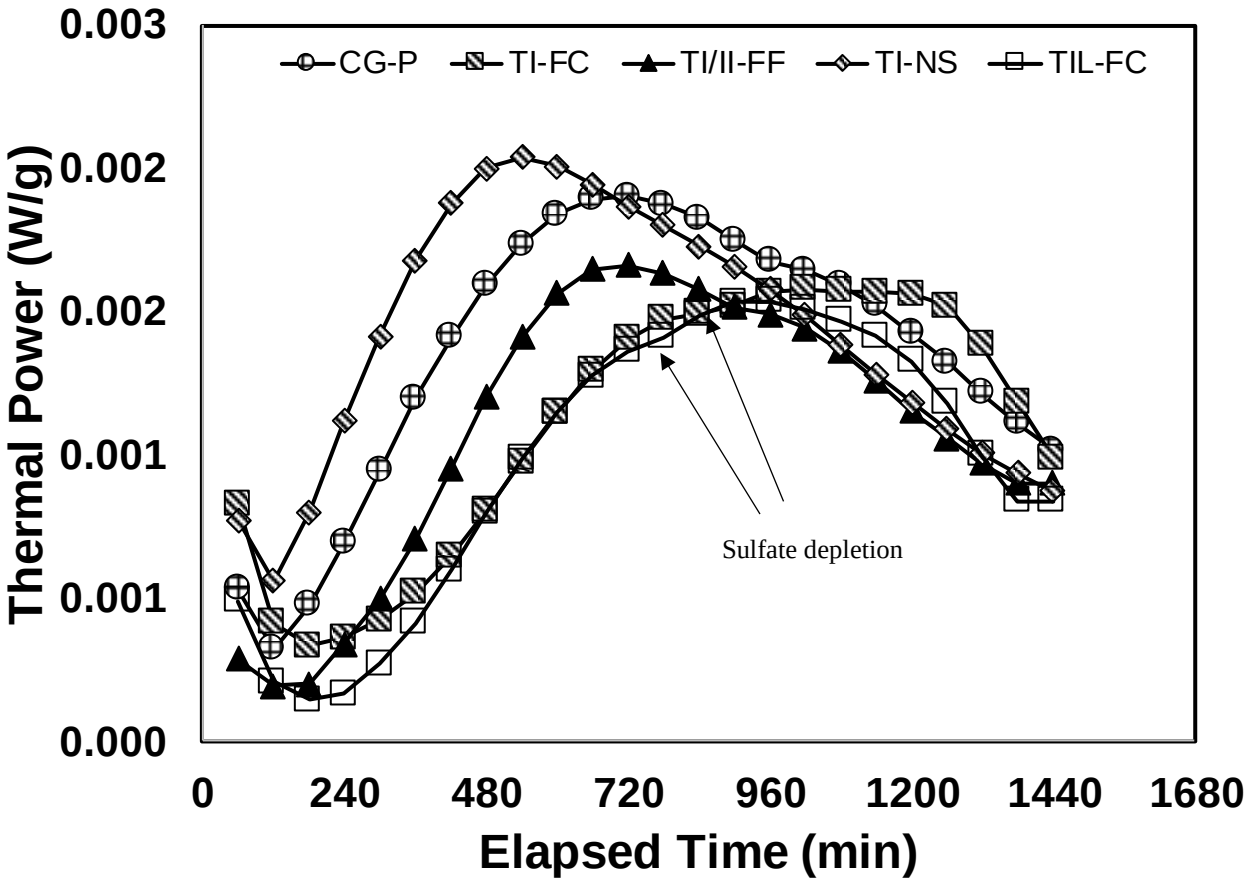

Figure 14. Isothermal calorimetry curves of key mixtures

2.6. Conclusions

The following are the key conclusions of this study:

- Concrete containing Type IL cement had low slump; slump was improved when fly ash was included;
- Concrete mixtures containing nanosilica had faster rates of hydration, higher temperature change peaks, and faster setting times as compared to their corresponding control mixtures;
- Mixtures of this study containing Class C fly ash had very long setting times likely due to sulfate depletion;
- Mixtures containing Type IL cement had improved compressive strength and resistivity due to better particle size distribution, more nucleation sites for precipitation of hydration

products, and physical filling of interfacial transition zone (ITZ) by carboaluminate hydrates;

- Type IL cement can be used to develop concrete having similar or slightly higher shrinkage strain than that with coarse ground cement;
- Rings of two of the concrete mixtures had cracked due to restrained shrinkage: TI-NS and TI/II-FC ;
- Drying shrinkage strain was higher for mixtures containing fly ash likely due to an unaltered water-binder ratio, allowing more available free water;
- Incorporation of larger agggregates and higher volume of aggregates led to a reduction of drying shrinkage strain of two mixtures: TIL-FC and TI-NS;
- Internal curing can be beneficial for shrinkage and other engineering properties due to continued hydration;

Based on this study, the use of Type IL cement and/or fly ash (in addition to conventional Type I/II cement) is recommended for further investigation, at a replacement level of 10%.

2.7. Acknowledgment

This paper is based upon work supported by the U. S. Department of Energy under Award No.DE-EE0007246. The authors also acknowledge Mr. Robert Steffes for his constant support and insight.

2.8. Disclaimer

Any findings, opinions, and conclusions or recommendations expressed in this report are those of the author(s) and do not necessarily reflect the views of the Department of Energy.

2.9. References

ASTM. (2015). “Standard Specification for Blended Hydraulic Cements.” C595/C595M-15, West Conshohocken, PA

ASTM. (2016). “Standard Specification for Portland Cement.” C150/C150M-16e1, West Conshohocken, PA.

ASTM. (2009). “Standard Test Method for Determining Age at Cracking and Induced Tensile Stress Characteristics of Mortar and Concrete under Restrained Shrinkage.” C1581/C1581M-09a, West Conshohocken, PA.

ASTM. (2016). “Standard Practice for Making and Curing Concrete Test Specimens in the Laboratory.” C192/C192M-16a, West Conshohocken, PA.

ASTM. (2015). “Standard Test Method for Slump of Hydraulic-Cement Concrete.” C143/C143M-16a, West Conshohocken, PA.

ASTM. (2014). “Standard Test Method for Air Content of Freshly Mixed Concrete by the Pressure Method.” C231/C231M-14, West Conshohocken, PA.

ASTM. (2014). “Standard Test Method for Bleeding of Concrete.” C232/C232M-14, West Conshohocken, PA.

ASTM. (2008). “Standard Test Method for Time of Setting of Concrete Mixtures by Penetration Resistance.” C403/C403M-08, West Conshohocken, PA.

ASTM. (2015). “Standard Practice for Evaluating Early Hydration of Hydraulic Cementitious Mixtures Using Thermal Measurements.” C1753/C1753M-15e1, West Conshohocken, PA.

ASTM. (2016). “Standard Test Method for Compressive Strength of Cylindrical Concrete Specimens.” C39/C39M-16b, West Conshohocken, PA.

ASTM. (2011). “Standard Test Method for Splitting Tensile Strength of Cylindrical Concrete Specimens.” C496/C496M-11, West Conshohocken, PA.

ASTM. (2012). “Standard Test Method for Bulk Electrical Conductivity of Hardened Concrete.” C1760-12, West Conshohocken, PA.

ASTM. (2014). “Standard Test Method for Length Change of Hardened Hydraulic-Cement Mortar and Concrete.” C157/C157M-08, West Conshohocken, PA.

ASTM. (2013). “Standard Test Method for Evaluating Plastic Shrinkage Cracking of Restrained Fiber Reinforced Concrete (Using a Steel Form Insert).” C1579-13, West Conshohocken, PA

ASTM. (2018). “Standard Test Method for Determining Age at Cracking and Induced Tensile Stress Characteristics of Mortar and Concrete under Restrained Shrinkage.” C1581/C1581M-18, West Conshohocken, PA.

Ayub, T., Khan, S. U., and Memon, F. A. (2014). "Mechanical characteristics of hardened concrete with different mineral admixtures: a review." *The Scientific World Journal*, 2014.

Barcelo, L., Thomas, M. D. A., Cail, K., Delagrave, A., and Blair, B. (2013). "Portland limestone cement equivalent strength explained." *Concrete international*, 35(11), 41-47.

Barrett, T., Sun, H., Villani, C., Barcelo, L., and Weiss, J. (2014). "Early-age shrinkage behavior of Portland limestone cement." *Concrete international*, 36(2).

Bentz, D. P. (2010). "Blending different fineness cements to engineer the properties of cement-based materials." *Magazine of Concrete Research*, 62(5), 327-338.

Bentz, D. P., and Weiss, W. J. (2011). *Internal curing: a 2010 state-of-the-art review*, US Department of Commerce, National Institute of Standards and Technology Gaithersburg, Maryland.

Bonavetti, V., Donza, H., Menendez, G., Cabrera, O., and Irassar, E. F. (2003). "Limestone filler cement in low w/c concrete: a rational use of energy." *Cement and Concrete Research*, 33(6), 865-871.

Cheung, J., Jeknavorian, A., Roberts, L., and Silva, D. (2011). "Impact of admixtures on the hydration kinetics of Portland cement." *Cement and concrete research*, 41(12), 1289-1309.

Cost, V. T., and Knight, G. (2007). "Use of thermal measurements to detect potential incompatibilities of common concrete materials." *Special Publication*, 241, 39-58.

De la Varga, I., Castro, J., Bentz, D., and Weiss, J. (2012). "Application of internal curing for mixtures containing high volumes of fly ash." *Cement and Concrete Composites*, 34(9), 1001-1008.

Deshpande, S. S. (2007). *Evaluating free shrinkage of concrete for control of cracking in bridge decks*, University of Kansas.

Flatt, R. J., and Houst, Y. F. (2001). "A simplified view on chemical effects perturbing the action of superplasticizers." *Cement and concrete research*, 31(8), 1169-1176.

Hooton, R. D., Nokken, M., and Thomas, M. D. A. (2007). "Portland-limestone cement: state-of-the-art report and gap analysis for CSA A 3000." *report prepared for St. Lawrence Cement*.

Idiart, A. E. (2009). *Coupled analysis of degradation processes in concrete specimens at the meso-level*, Universitat Politècnica de Catalunya.

Institute, A. C. (2005). "Report on factors affecting shrinkage and creep of hardened concrete." *209*, American Concrete Institute, Farmington Hills, MI, Report ACI 209.201R-2005.

Jiang, L. H., and Malhotra, V. M. (2000). "Reduction in water demand of non-air-entrained concrete incorporating large volumes of fly ash." *Cement and Concrete Research*, 30(11), 1785-1789.

Juenger, M. C. G., and Siddique, R. (2015). "Recent advances in understanding the role of supplementary cementitious materials in concrete." *Cement and Concrete Research*, 78, 71-80.

Khaloo, A., Mobini, M. H., and Hosseini, P. (2016). "Influence of different types of nano-SiO 2 particles on properties of high-performance concrete." *Construction and Building Materials*, 113, 188-201.

Kosmatka, S. H., Panarese, W. C., and Kerkhoff, B. (2002). *Design and control of concrete mixtures*, Portland Cement Association Skokie, IL.

Ma, H. (2013). "Multi-scale modeling of the microstructure and transport properties of contemporary concrete." Doctoral Dissertation

Mehta, P. K., and Burrows, R. W. (2001). "Building durable structures in the 21 st century." *Indian Concrete Journal*, 75(7), 437-443.

Mindess, S., Young, J. F., and Darwin, D. (2002). "Concrete, 2nd EditionPrentice Hall." *Englewood Cliffs, NJ*.

Munday, J. G. L., Ong, L. T., Wong, L. B., and Dhir, R. K. (1982). "Load independent movements in opc/pfa concrete." 243-246.

Nath, P., and Sarker, P. K. (2013). "Effect of mixture proportions on the drying shrinkage and permeation properties of high strength concrete containing class F fly ash." *KSCE Journal of Civil Engineering*, 17(6), 1437-1445.

Pease, B. J., Shah, H. R., and Weiss, W. J. (2005). "Shrinkage behavior and residual stress development in mortar containing shrinkage reducing admixtures (SRAs)." *ACI SP-227, Shrinkage Creep Concr*.

Qi, M., Li, Z., and Ma, B. (2002). "Shrinkage and cracking behavior of high performance concrete containing chemical admixtures." *Journal of Zhejinag University: Science*, 3(2), 188.

Quercia, G., Spiesz, P., Hüsken, G., and Brouwers, H. J. H. (2014). "SCC modification by use of amorphous nano-silica." *Cement and Concrete Composites*, 45, 69-81.

Ramezanianpour, A. M., and Hooton, R. D. (2014). "A study on hydration, compressive strength, and porosity of Portland-limestone cement mixes containing SCMs." *Cement and Concrete Composites*, 51, 1-13.

Roberts, L. R., and Taylor, P. C. (2007). "Understanding cement-SCM-admixture interaction issues." *Concrete international*, 29(01), 33-41.

Sandberg, P. J., and Roberts, L. R. (2005). "Cement-admixture interactions related to aluminate control." *Journal of ASTM International*, 2(6), 1-14.

Shehata, M. H., and Thomas, M. D. A. (2002). "Use of ternary blends containing silica fume and fly ash to suppress expansion due to alkali–silica reaction in concrete." *Cement and Concrete Research*, 32(3), 341-349.

Singh, L. P., Karade, S. R., Bhattacharyya, S. K., Yousuf, M. M., and Ahalawat, S. (2013). "Beneficial role of nanosilica in cement based materials–A review." *Construction and Building Materials*, 47, 1069-1077.

Sprung, S., and Siebel, E. (1991). "Assessment of the suitability of limestone for producing Portland limestone cement." *ZKG International, Edition B*, 44(1), 1-11.

Taylor, P., and Wang, X. (2014). "Concrete Pavement Mixture Design and Analysis (MDA): Factors Influencing Drying Shrinkage." Iowa State University.

Tritsch, N., Darwin, D., and Browning, J. (2005). "Evaluating Shrinkage and Cracking Behavior of Concrete Using Restrained Ring and Free Shrinkage Tests." University of Kansas Center for Research, Inc.

Tsivilis, S., Chaniotakis, E., Batis, G., Meletiou, C., Kasselouri, V., Kakali, G., Sakellariou, A., Pavlakis, G., and Psimadas, C. (1999). "The effect of clinker and limestone quality on the gas permeability, water absorption and pore structure of limestone cement concrete." *Cement and Concrete Composites*, 21(2), 139-146.

Voglis, N., Kakali, G., Chaniotakis, E., and Tsivilis, S. (2005). "Portland-limestone cements. Their properties and hydration compared to those of other composite cements." *Cement and Concrete Composites*, 27(2), 191-196.

Vuk, T., Tinta, V., Gabrovšek, R., and Kaučič, V. (2001). "The effects of limestone addition, clinker type and fineness on properties of Portland cement." *Cement and Concrete Research*, 31(1), 135-139.

Wang, X. (2011). *Drying shrinkage of ternary blends in mortar and concrete*, Iowa State University.

Wang, X., Taylor, P., Wang, K., and Lim, M. (2016). "Monitoring of setting time of self-consolidating concrete using ultrasonic wave propagation method and other tools." *Magazine of Concrete Research*, 68(3), 151-162.

Weiss, J., Lura, P., Rajabipour, F., and Sant, G. (2008). "Performance of shrinkage-reducing admixtures at different humidities and at early ages." *Materials Journal*, 105(5), 478-486.

Wilson, M. L., and Kosmatka, S. H. (2011). "Design and Control of Concrete Mixtures. Portland Cement Association." Skokie.

Zakka, Z. A., and Carrasquillo, R. L. (1989). "Effects of high-range water reducers on the properties of fresh and hardened concrete."

Zayed, A., Sedaghat, A., Bien-Aime, A., and Shanahan, N. (2014). "Effects of portland cement particle size on heat of hydration." Florida Department of Transportation

Zhu, W., Wei, J., Li, F., Zhang, T., Chen, Y., Hu, J., and Yu, Q. (2016). "Understanding restraint effect of coarse aggregate on the drying shrinkage of self-compacting concrete." *Construction and Building Materials*, 114, 458-463.

CHAPTER 3: CHOPPED BASALT FIBERS FOR REDUCTION OF SHRINKAGE CRACKING IN CONCRETE

3.1. Abstract

In this study, chopped basalt fibers have been used with multiple cementitious material systems containing portland limestone cement (PLC), coarse ground cement, fly ash and nanosilica to develop concrete resistant towards shrinkage cracking. Basalt micro-fibers have been used to investigate the impeding of macro-cracks from shrinkage, particularly plastic shrinkage, free and restrained drying shrinkage behaviors. Durability indicators, such as electrical resistivity, and other properties such as, strength, degree of hydration (as measured through semi-adiabatic calorimetry), and setting time, have been investigated as well. Results indicate that chopped basalt micro-fibers can reduce the cracking tendency of concrete under plastic and drying shrinkage conditions. This may be due to a reduction of propagation of micro-cracks to form macro-cracks and ultimate loss of serviceability.

3.2. Introduction

Drying in concrete induces stress from differential shrinkage, and formation of micro-cracks on the surface (de Sa et al. 2008). The propagation of these micro-cracks can lead to larger cracks. The presence of cracks allows for the ingress of deleterious chemicals such as chloride and sulfate ions, resulting in the loss of durability of concrete (Bisschop and van Mier 2008; Peterson et al. 2013; Tosun-Felekoğlu 2012). Shrinkage predominantly occurs in the cementitious paste (cementitious materials and water) part of the concrete. During this time, aggregates can act as restraints to the resultant volume change of the paste, causing de-bonding at the interface between paste and aggregates and subsequent cracks (Bisschop and Van Mier 2002). Additionally, self-restraint due to tensile stresses parallel to drying surface from moisture gradient can result in

perpendicular cracks (Bisschop and Van Mier 2002). Both these types of restraints are internal restraints. Concrete is also restrained externally in structures such as bridge decks, and culverts. However, internal restraints are still at play even in externally restrained concrete (Bisschop and Van Mier 2002).

Shrinkage may be defined as the volume changes resulting from loss of water from capillary pores within the concrete system. This can be due to various environmental factors and desiccation due to hydration (Taylor and Wang 2014). Shrinkage may also be as a result of differential heat due to hydration between the surface and interior of massive concrete structures. When concrete is restrained, volume changes are restricted, therefore, tensile stresses are developed. As concrete has low tensile strength, fracture or cracks may be formed (Deshpande 2007). These cracks may originate and propagate along the weaker interfacial transition zones (ITZ) between paste and aggregates (Bisschop and van Mier 2008). Out of the different types of shrinkage in concrete, plastic shrinkage and drying shrinkage are the major shrinkage mechanisms investigated in this work. Plastic shrinkage occurs within the first few hours of mixing concrete due to a higher rate of evaporation of water near the surface. Drying shrinkage occurs after the setting of concrete through days, months, or years as water is evaporated through the capillary pores.

Fibers are incorporated in concrete to make it more ductile. The addition of fibers helps dissipating tensile energies by transferring load through the fiber-matrix interfacial bond (Abbas and Khan 2016). According to ACI 544.1R, fiber reinforced concrete (FRC) can be defined as a composite primarily consisting of portland cement, aggregates, and discrete reinforcing fibers. This combination possess improved mechanical properties over unreinforced brittle concrete materials (Lee et al. 2010). Fibers can be composed of steel, glass, synthetic polymers, or naturally

occurring materials. Application of fibers in concrete may be aimed at improving bulk behavior, such as flexural strength of concrete (Lee et al. 2010), or reduction of micro-cracking due to shrinkage (Branston et al. 2016; Yousefieh et al. 2017). One of the recent and more environment-friendly fibers exhibiting good mechanical properties is chopped basalt. Prior literature has indicated that basalt fibers can prevent cracking by reducing shrinkage, and can restrict the propagation of micro-cracks (Branston et al. 2016). These fibers act as a bridge between the two surfaces across a micro-crack and transfers applied load, dissipating energy. However, basalt fibers do not enhance post-cracking response of concrete (High et al. 2015; Jiang et al. 2014).

Portland limestone cement (PLC) provides superior mechanical strength to concrete by multiple mechanisms: improved particle size distribution (Barrett et al. 2014), more nucleation sites in limestone for precipitation of hydration products (Barcelo et al. 2013), increase in the rate of silicate hydration (Stark et al.), and physical infilling of interfacial transition zone (ITZ) between cement paste and aggregates by calcium carboaluminate hydrates formed by reaction with tri-calcium aluminate (C_3A) (Ramezanianpour and Hooton 2014).

It is hypothesized that the filling of ITZ due to Portland limestone cement, and benefits of basalt fibers in reducing cracking in concrete, will help reduce adverse effects of plastic and drying shrinkage. In this study, chopped basalt microfibers are used in concrete containing portland limestone cement to investigate the potential post-cracking behavior of cracking due to plastic and drying shrinkage under restrained conditions. Additionally, other cement types, such as coarse ground cement, Type I cement and Type I/II cement, and supplementary cementitious materials such as, fly ash, and nanosilica are used in this study.

3.3. Background

Shrinkage in concrete can be broadly classified as early age shrinkage (within 24 hours after casting) and later age shrinkage (after 24 hours of casting) (Wang 2011). Types of shrinkage mechanisms in concrete include plastic shrinkage, autogenous/chemical shrinkage, carbonation shrinkage, thermal shrinkage, and drying shrinkage. (Tritsch et al. 2005). Typically, concrete used in pavements and bridge decks have water to cementitious materials ratios higher than 0.40. The predominant shrinkage mechanisms affecting concrete with water-cementitious materials ratio higher than 0.40 are drying and plastic shrinkage (Kosmatka et al. 2002). Therefore, the emphasis of this research is on plastic and drying shrinkage. These volume changes are results of loss of water from the system.

3.3.1. Types of Shrinkage

Plastic shrinkage is an early age shrinkage phenomenon, and it occurs in fresh concrete, i.e. when the concrete is still in its plastic state. In this semi-fluid state, water fills the voids between cement particles. In outdoor structures (e.g. roads, exterior surfaces of retaining walls) the exposed surfaces are subject evaporation due to high temperature and wind. These harsh environmental conditions lead to a loss of moisture from the exposed surfaces. When the rate of removal of water from surfaces exceeds that at which it is replenished in the form of bleeding water, menisci are formed (Tritsch et al. 2005). These menisci exert negative capillary pressures on the cementitious system, resulting in a net volume reduction in the paste (Mindess et al. 2002). Since evaporation of water occurs at the surface, its rate of volume change is different than the underlying cementitious layers. Therefore, tensile stresses are produced in the concrete, which easily exceeds the tensile strength of the weak plastic concrete. As a result, random, shallow cracks appear on the surface (Deshpande 2007).

Drying shrinkage occurs in hardened cement paste, when there is a loss of water from the capillary pores. According to American Concrete Institute (ACI) Committee 209, drying shrinkage is defined as "Shrinkage occurring in a specimen that is exposed to the environment and allowed to dry" (Institute 2005). Drying shrinkage occurs by several mechanisms in concrete. At relative humidity between 45% and 95%, capillary forces are formed due to the formation of menisci on the pore water (Wang 2011). This reduces the overall volume of the concrete. Another mechanism associated with drying shrinkage is disjoining pressure. It is the pressure exerted by adsorbed water confined within the capillary pores on the adjacent cement surfaces. However, when the adsorbed water is lost, the disjoining pressure is reduced resulting in the cement particles being drawn together and resulting in subsequent shrinkage. The last molecular layer of water is more strongly adsorbed onto the cement particles having a high surface tension and causing a net reduction in the volume of the cementitious system. This type of shrinkage caused due to changes in surface energy are applicable at relative humidity below 45-40% (Idiart 2009). When relative humidity drops below 10%, interlayer water, i.e. water existing in the layered structure of calcium silicate hydrate (C-S-H) crystals, may migrate out of these crystals causing considerable shrinkage (Idiart 2009).

3.3.2. Factors Affecting Shrinkage

There are several factors responsible for shrinkage which are usually interrelated. Some of the material characteristics which can determine the extent of shrinkage in concrete are aggregate properties. Aggregate items like size, gradation, content and elastic properties can change concrete properties. Other items like water-cementitious ratio, cement size distribution, cementitious materials content, air content, chemical admixtures, and supplementary cementitious materials can also change the concrete properties (Bentz 2010; Deshpande 2007; Tritsch et al. 2005). These

factors, in addition to external conditions such as relative humidity, ambient temperature, and wind velocity can adversely affect shrinkage (Malhotra and Mehta 1996). A summary of these factors has been presented in Table 1 (Taylor and Wang 2014).

Cement paste (i.e. water and cementitious materials) is the part of concrete which is most vulnerable to volume changes. In cement paste, cement fineness significantly affects the shrinkage of concrete (Mehta and Burrows 2001). Portland cements of high Blaine fineness have high surface area, resulting in a refined microstructure formation. As a result of this, the pore diameters of individual pores are reduced, and higher capillary stresses are formed, resulting in increased shrinkage. Finer cementitious systems also require more water for maintaining workability compared to coarse-ground cement (Bennett and Loat 1970). Higher water content results in a higher availability of evaporable water, and the rate at which it reaches the surface (Deshpande 2007). Therefore, for finer cements the shrinkage values tend to be greater.

Cement chemistry also influences concrete shrinkage. Higher C_3A and alkali contents may increase shrinkage (Roper 1974; Zayed et al. 2014). Moreover, lower sulfate content may also increase shrinkage (Taylor and Wang 2014). Therefore, drying shrinkage can be potentially reduced by increasing the gypsum content (Tsuruta et al. 2004), and by limiting C_3A and alkali contents.

In portland limestone cement (PLC), limestone is interground with clinker to provides a homogenous mixture (Zayed et al. 2014). According to ASTM C595, the maximum permissible content of limestone is 15% by mass of cement (Astm 2000). Ordinary portland cement (OPC) may typically contain up ~5% limestone (The Concrete Producer). According to prior sources, the standard manufacturing process of cement manufacture contributes to approximately 5-8% of the global carbon dioxide (CO_2) (Kosmatka et al. 2002; Mikulčić et al. 2016; Worrell et al. 2001).

However, in case of the newer Type IL cement, there is partial replacement of portland cement with limestone. Therefore, Type IL cement has the advantage of helping in reduced emission of CO_2. Moreover, PLC is designed to perform almost the same way as conventional portland cement (Barrett et al. 2014). This is done by grinding the PLC finer than conventional ordinary portland cement (OPC), as there is a reduction of clinker in case of PLC as compared to OPC (Barcelo et al. 2013). Prior researchers have reported that when interground PLC systems with similar strengths were evaluated, the PLC systems were shown to have similar or slightly less shrinkage than the OPC system (Barcelo et al. 2013; Barrett et al. 2014). Also, the PLC system had no increased tendency to crack under restrained shrinkage conditions. This could be due to a better particle size distribution of cementitious particles as a result of differential grinding of the two components of clinker.

Fly ash is one of the most common supplementary cementitious materials used in the United States (Kosmatka et al. 2002). It is a by-product of coal combustion and when added to concrete helps in secondary hydration reactions. Fly ash can be classified as Class F or Class C based on the chemical composition (ASTM C618). Fly ash particles are smooth and spherical, which may enhance the workability of concrete. Class F fly ash when used as a partial replacement of portland cement in binary mixtures may reduce drying shrinkage (Taylor and Wang 2014). However, this reduction of shrinkage is more pronounced at higher replacement levels (>40%) (Gesoğlu et al. 2009). Class C fly ash, on the other hand, may increase shrinkage of concrete (Deshpande 2007).

Nanomaterials have been used with portland cement to improve hardened properties due to their high specific surface area and consequent reactivity. Of the different nanomaterials used with portland cement, nanosilica has been the most widely used. Nanosilica can help refine the

interfacial transition zone between cement paste and aggregates in concrete by a physical filling effect (Singh et al. 2013). This refined microstructure can result in reduced permeability, water absorption, capillary absorption, and chloride ion penetration.

Due to shrinkage of cement paste and consequent formation of tensile stresses, micro-cracks may be formed which may propagate into bigger cracks. This may be mitigated by using fibers in concrete (Branston et al. 2016). Common examples of commercially available fibers, which are used to provide ductility to concrete, are steel fibers, glass fibers, polypropylene fibers, and carbon fibers (Ramakrishnan et al. 1998). The use of randomly dispersed fibers may help bridge cracks (Iyer et al. 2016). ACI 544.3R has classified synthetic fibers into two size classifications: micro-synthetic fibers, having a diameter equivalent or less than 0.012 in (0.3 mm) and macro-synthetic fibers, having a diameter greater than 0.012 in (0.3 mm).

Basalt is an igneous rock. Basalt fibers are very stable and have several advantages over glass fibers, including density, elastic modulus, and tensile strength (Fiore et al. 2015). The manufacturing process of basalt fibers is also argued as more environment friendly (Branston et al. 2016). Most research endeavors in the past have attempted to utilize basalt fibers for enhancing mechanical properties of concrete. Most of the studies pertaining to enhancement of flexural strength by basalt fiber reinforcement have utilized basalt macro fibers (Patnaik et al.). However, very few studies have attempted to reduce shrinkage cracking in concrete (Branston et al. 2016; Suksawang et al. 2014).The reduction in shrinkage strain and shrinkage induced cracking may be due to friction interactions at the fiber-matrix interface (Mangat and Azari 1990).

3.4. Experimental Program

3.4.1. Materials

In this study, four cement types were used:

- Coarse Ground portland cement (CG)
- Type I portland cement (TI)
- Type I/II portland cement (TI/II), and
- Type IL portland limestone cement (TIL).

Additionally, the following supplementary cementitious materials were used:

- Class C fly ash (FC)
- Class F fly ash (FF), and
- Colloidal nanosilica (NS).

The chemical and physical properties of the cement types, fly ash, and nanosilica are presented in Table 2, Table 3 and Table 4, respectively. Chopped basalt fibers 13μm in diameter, and 24 mm in length, treated with a silane-based coating (0.25% w/w) were used per manufacturers recommendations. The silane based coating is provided to protect the fibers in an alkaline environment. ½" (nominal aggregate size) limestone aggregates and locally available sand were used. Figure 15 shows the combined gradation of the aggregates. An organic acid based air entraining agent, and a polycarboxylate based Type F high range water reducing agent (WRA) were used.

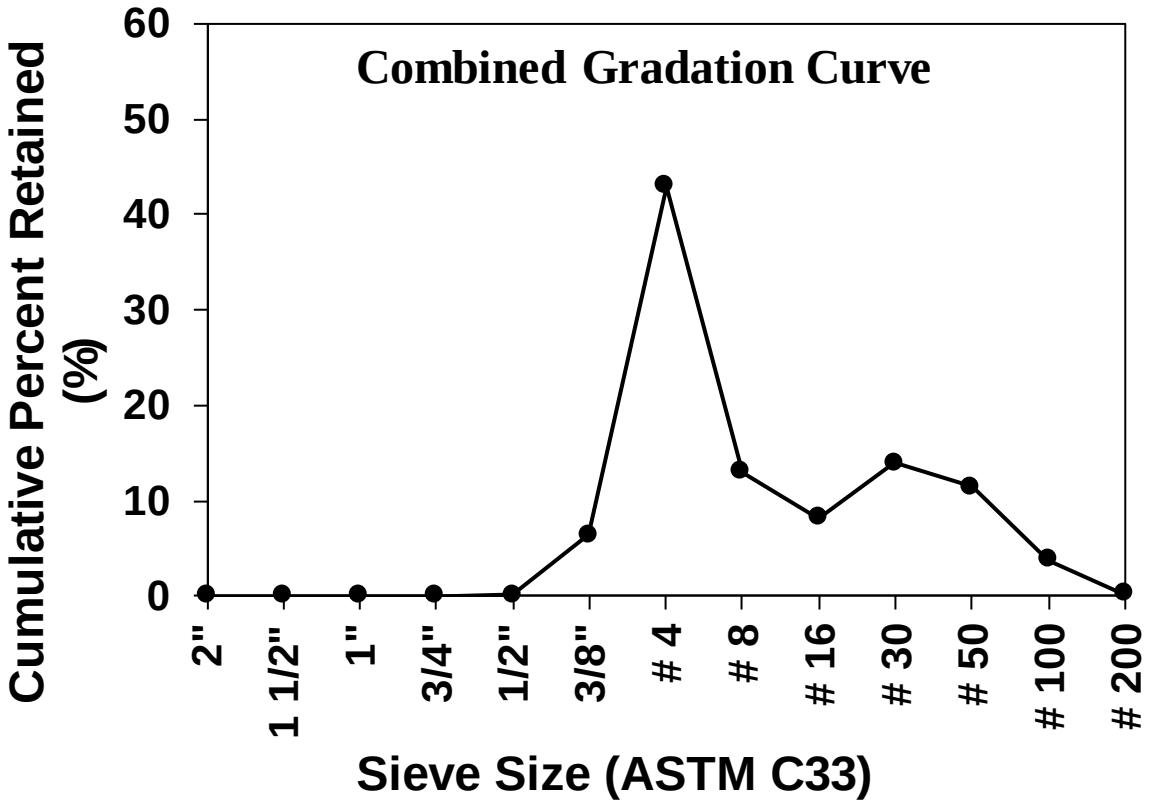

Figure 15. Combined particle size distribution curve for coarse and fine aggregates

3.4.2. Mixture Proportions

The mixture proportions for the concrete used are shown in Table 9. Cementitious combinations investigated in this study include coarse ground cement with no SCMs (CG-P), Type I/II cement and 20% replaced with Class F fly ash (TI/II-FF), Type IL cement and 30% replaced with Class C fly ash (TIL-FC), Type I cement and 30% replaced with Class C fly ash (TI-FC), and Type I cement, and 5% replaced with colloidal nanosilica (TI-NS). Chopped basalt fibers were dosed at 0.25% (v/v). The mixtures containing fibers are designated with the suffix "(B)". The water-to-cementitious materials ratio, and binder content were fixed at 0.42, 580 lb/yd^3, respectively.

Table 9. Mixture proportions for Chapter 3

Mixture Code	w/cm	Cement (pcy)	Class F Fly Ash (pcy)	Class C Fly Ash (pcy)	Nano Silica (pcy)	Chopped Basalt Fiber Addition (% v/v)	Water (pcy)	Fine Aggregates (pcy)	Coarse Aggregates (pcy)	High Range Water Reducers (oz/cwt)	Air Entraining Agent (oz/cwt)
TI/II-FF	0.42	464	116	-	-	-	244	1,789	1,295	2.5	0.2
TIL-FC	0.42	406	-	174	-	-	244	1,789	1,295	4.3	0.2
TI-FC	0.42	406	-	174	-	-	244	1,789	1,295	3.8	0.2
CG-P	0.42	580	-	0	-	-	244	1,789	1,295	4.0	0.2
TI-NS	0.42	551	-	0	29	-	244	1,789	1,295	17.6	0.2
TI/II-FF (B)	0.42	464	116	0	-	0.25	244	1,789	1,295	6.5	0.2
TIL-FC (B)	0.42	406	-	174	-	0.25	244	1,789	1,295	6.5	0.2
TI-FC (B)	0.42	406	-	174	-	0.25	244	1,789	1,295	7.5	0.1
CG-P (B)	0.42	580	-	-	-	0.25	244	1,789	1,295	8.5	0.1
TI-NS (B)	0.42	551	-	-	29	0.25	244	1,789	1,295	10.0	0.1

Based on the contract, mixtures were required to maintain similar workability while keeping the mixture proportions unchanged. Due to the low workability of concrete containing basalt fibers, WRAs had to be added at rates higher than those recommended by their manufacturers.

3.4.3. Test Methods

Fresh properties such as workability (ASTM C143), air content/unit weight (ASTM C231, ASTM C138), setting time (ASTM C403), bleeding (ASTM C232), and hydration rate were measured. Semi-adiabatic calorimetry tests were used to investigate the hydration characteristics of the concrete mixtures (ASTM C1753 for 24 hours. Isothermal calorimetry test was also used to investigate hydration trends of five selected mixtures identified in sections 3.1 and 3.2. Cement paste was placed in a calorimeter under isothermal conditions, and changes in heat were measured for up to 24 hours.

One of the key fresh tests of this work was the investigation of plastic shrinkage. In addition to following the ASTM C1579 procedure, a novel modified test method was followed in this study. This modification was used to measure the length change within the first six hours of mixing within the panel. Through this change the plastic strain per elapsed time was calculated. This was achieved by introducing four markers across the long edge of the concrete panel (top view of the specimen can be seen in Figure 16). Flanged metal bolts with a distinctly marked point in each were used as the markers. These were placed on the concrete surface immediately after casting. The length change over time was measured by using slide calipers of accuracy up to 0.0001 inches.

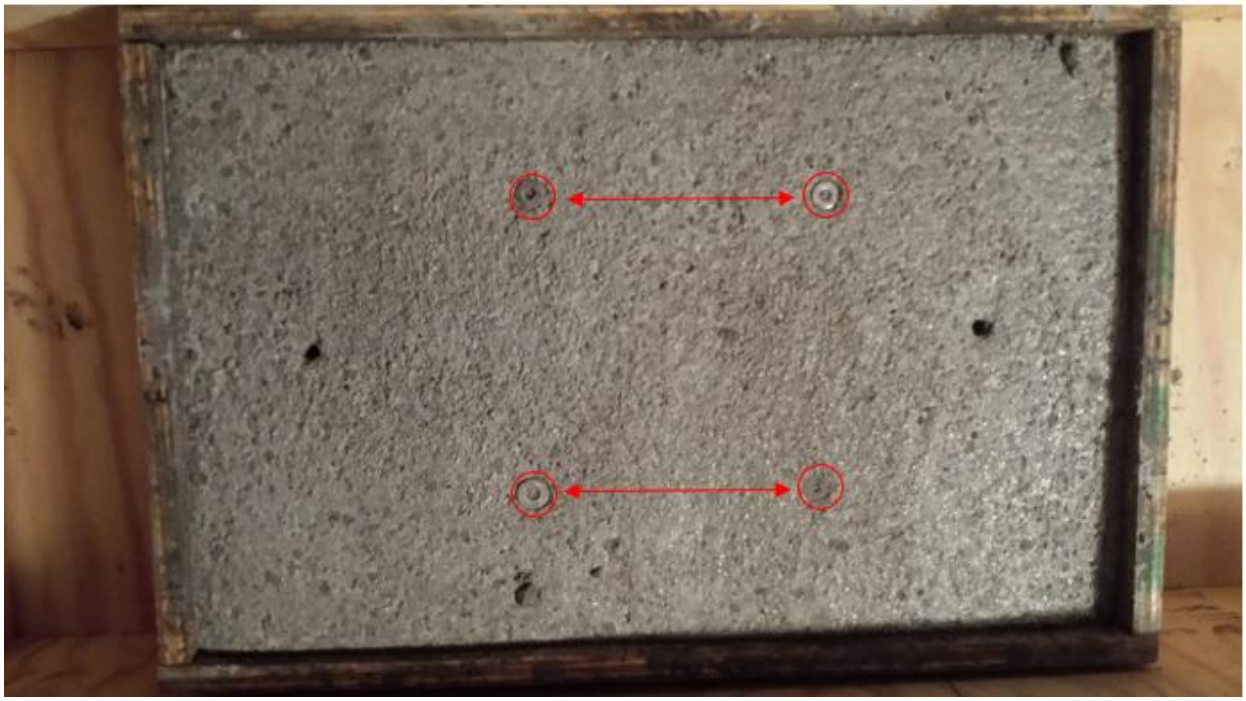

Figure 16. Plastic shrinkage experimental set up

Free shrinkage in concrete was measured in accordance with ASTM C157. Shrinkage strain in the concrete mixtures due to external restraints was measured by the standard ring test method specified in ASTM C1581 (Figure 17).

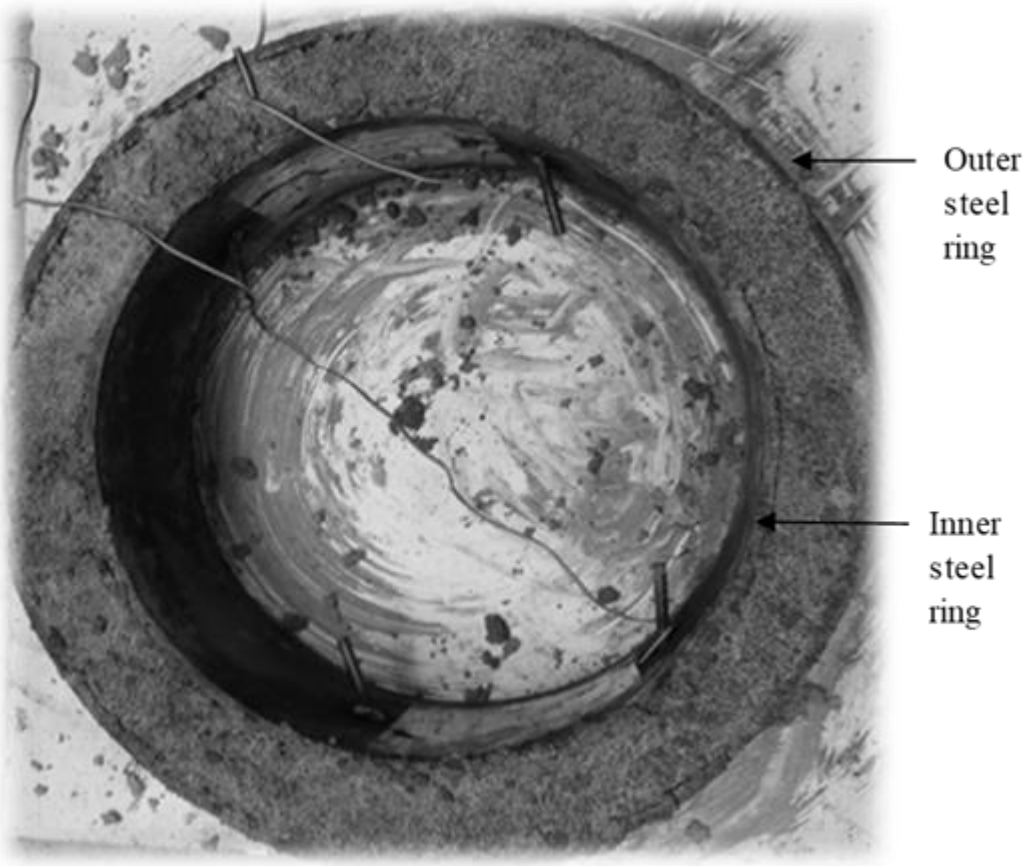

Figure 17. Restrained shrinkage test setup

Other hardened concrete tests including compressive strength (ASTM C39), splitting tensile strength (ASTM C496), and electrical resistivity (ASTM C1760) were also performed on the concrete mixtures. Electrical resistivity test was conducted in concrete to investigate an indirect assessment of concrete's ability to resist the access of harmful chemical ions related to salting like Chloride.

3.5. Results and Discussions

3.5.1. Fresh Properties

The fresh properties are summarized in Table 6. Due to the incorporation of basalt fibers, workability is reduced (Branston et al. 2016). In order to work with the concrete, high range water reducing admixtures (WRA) were added at a higher dosage rate than the control mixes. The basalt

fibers seemed to increase the entrapped air when compared to the control mixes. This behavior is consistent with prior literature (Soudki et al. 2013).

Table 10. Fresh properties for Chapter 3

Mixture Code	Fresh Properties									
	Slump (in)	Air content (%)	Unit Weight (lb/ft^3)	Set time (min)		Bleeding (ml/cm^2)	Average Cracks from Plastic Shrinkage (mm)	Calorimetry Temperature Rise (°F)	Setting Time from Calorimetry (min)	
				Initial	Final				Initial (20% of Temperature Rise)	Final (50% of Temperature Rise)
TI/II-FF (B)	5.00	8.0	135.1	225	350	0.05	0.00	22	400	620
TI/II-FF	4.50	8.0	144.6	220	355	0.02	Too slight to measure	22	240	360
TIL-FC (B)	1.50	8.1	138.9	330	450	0.01	0.00	22	370	600
TIL-FC	4.20	7.2	145.5	335	460	0.02	0.00	15	300	440
TI-FC (B)	1.50	5.5	141.1	390	480	0.04	0.00	19	380	640
TI-FC	4.25	6.4	145.8	325	450	0.01	0.45	23	340	540
CG-P (B)	1.00	7.4	138.7	300	420	0.00	0.00	26	460	690
CG-P	4.00	6.0	145.0	190	325	0.04	0.16	30	260	380
TI-NS (B)	1.50	5.2	141.6	285	475	0.00	0.00	32	300	450
TI-NS	1.00	5.4	147.7	200	375	0.00	0.52	37	200	430

The use of Type F high range water reducing admixtures may retard the setting of concrete (Cheung et al. 2011). In the hydration curves measured using semi-adiabatic calorimetry (Figure 18), concrete mixes containing basalt fibers showed delayed and reduced hydration. Table 6 also shows mixed results for bleeding. In general, bleeding reduces due to the presence of chopped fibers (Soudki et al. 2013), however the increased bleeding reported here might be due to the high water reducing agent (WRA) dosages applied in an attempt to maintain workability.

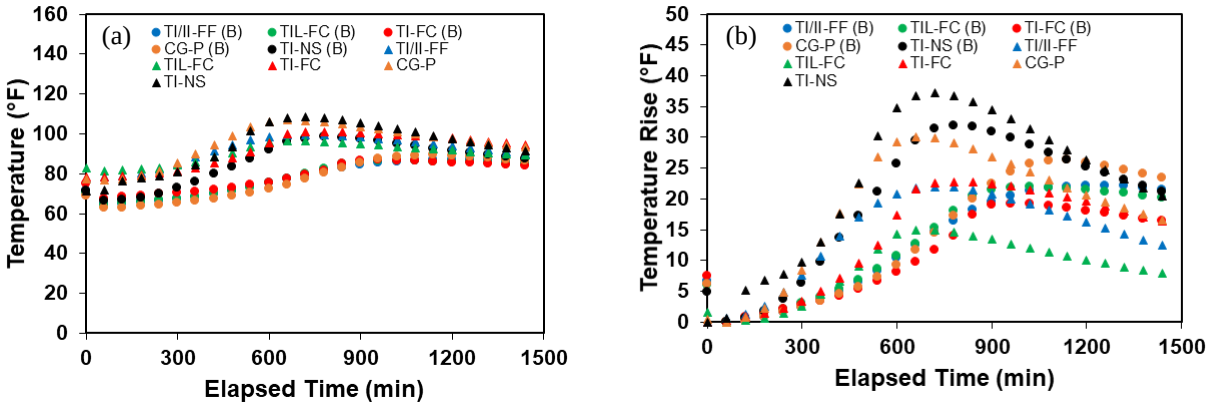

Figure 18. Semi-adiabatic calorimetry: (a) Temperature over time (b) Temperature rise over time

Figure 19 shows the plastic shrinkage results for all the mixes. It appeared that the concrete mixtures containing micro basalt fibers had provided some degree of restraint against plastic shrinkage. However, plastic shrinkage strain seemed to have increased in the basalt mixtures compared to the control mixtures, again likely due to an over-dosage of superplasticizers (Kosmatka et al. 2002; Taylor and Wang 2014). Notably, there were no visible cracks due to plastic shrinkage within 24 hours after mixing for all five concrete mixtures containing the micro basalt fibers. This positive attribute might have potential applications in controlling plastic shrinkage cracking in pavements, bridge decks and other structures exposed to harsh environmental conditions.

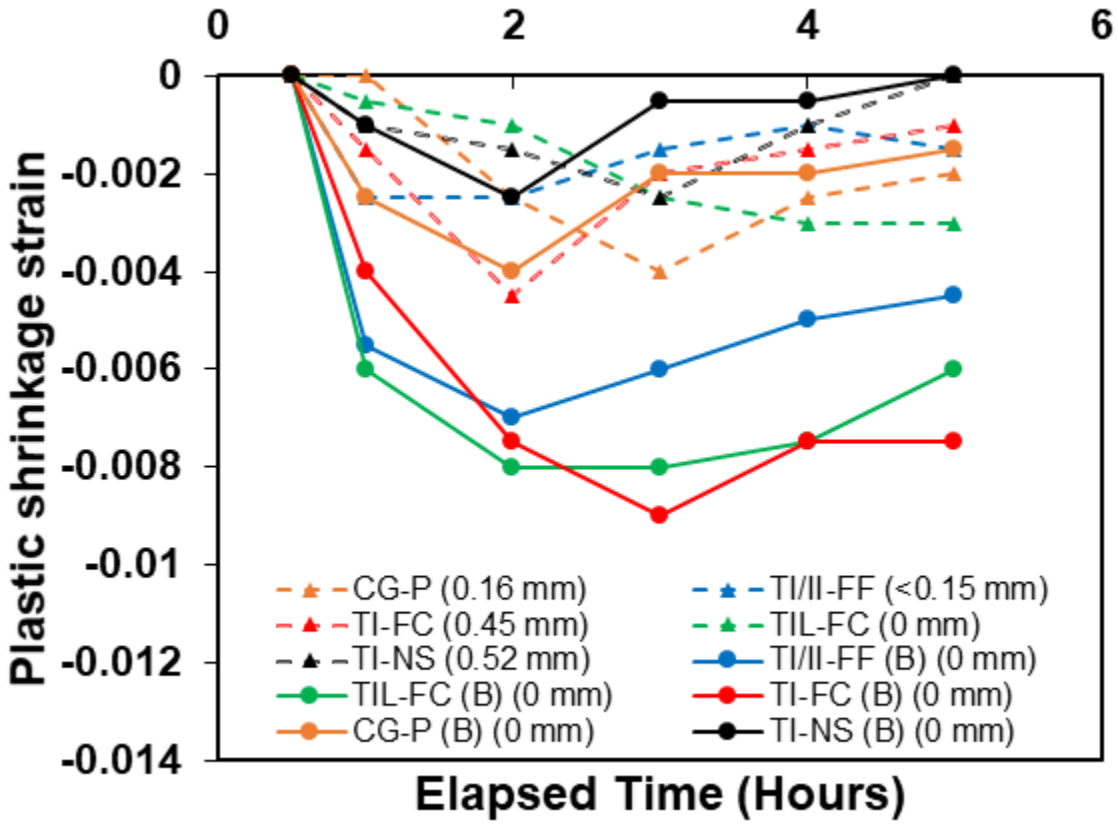

Figure 19. Plastic shrinkage (Numbers within brackets indicate crack width after 24 hours)

3.5.2. Hardened Properties

3.5.2.1. Compressive Strength and Splitting Tensile Strength

Figure 20 and Figure 21 show the compressive strength and splitting tensile strength respectively, over time for the mixtures used for this study. The mixtures containing basalt fibers, in general, exhibited a reduction in compressive and split-tensile strength. This is consistent with prior literature (Soudki et al. 2013). Moreover, over-dosage of polycarboxylate based superplasticizers could possibly have an adverse effect on compressive strength and splitting tensile strength (Yang et al. 2015). TI-NS (Type I portland cement with 5% nanosilica) had the highest compressive strength and splitting tensile strength likely due to the reactivity of the nanosilica.

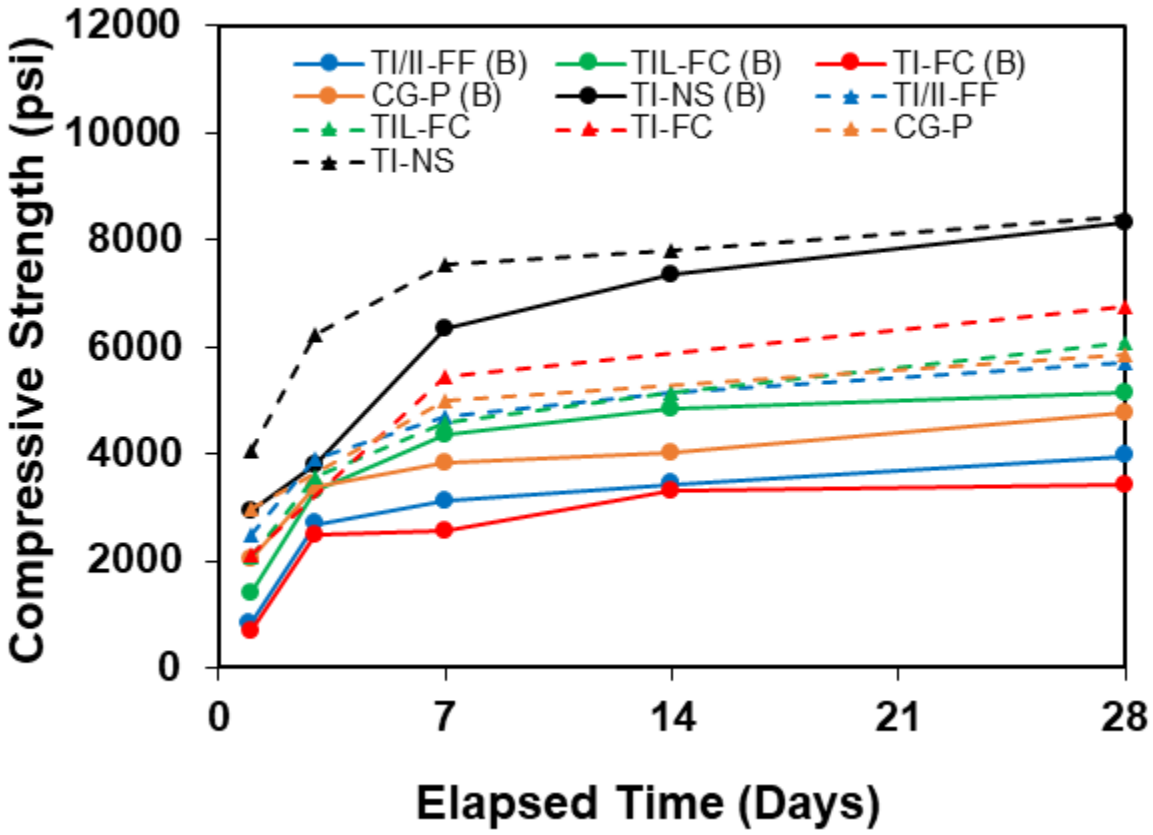

Figure 20. Compressive strength

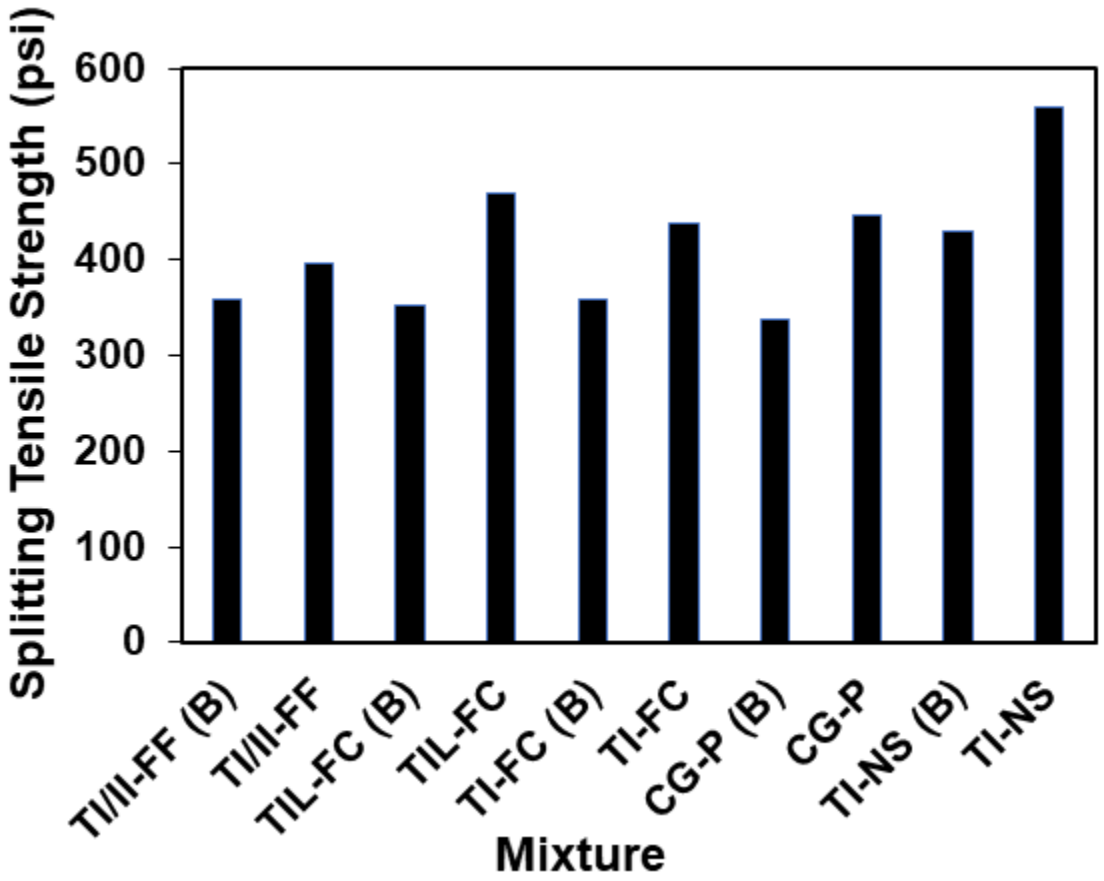

Figure 21. Splitting tensile strength

3.5.2.2. Resistivity

Electrical resistivity of a concrete sample is an indirect indicator of permeability. (Quercia et al. 2014). Nanosilica in concrete typically results in a refined microstructure, which in turn results in a disconnected system of pores, thus reducing conductivity. Therefore, resistivity for TI-NS was the highest, as shown in Figure 22. However, mixtures containing basalt microfibers are low in resistivity. This may be partly due to an increased porosity in the fiber-matrix interface (Banthia et al. 2014; Liu et al. 2006). Over-dosage of polycarboxylate superplasticizers may also lead to higher porosity (Yang et al. 2015) and in turn lower resistivity results.

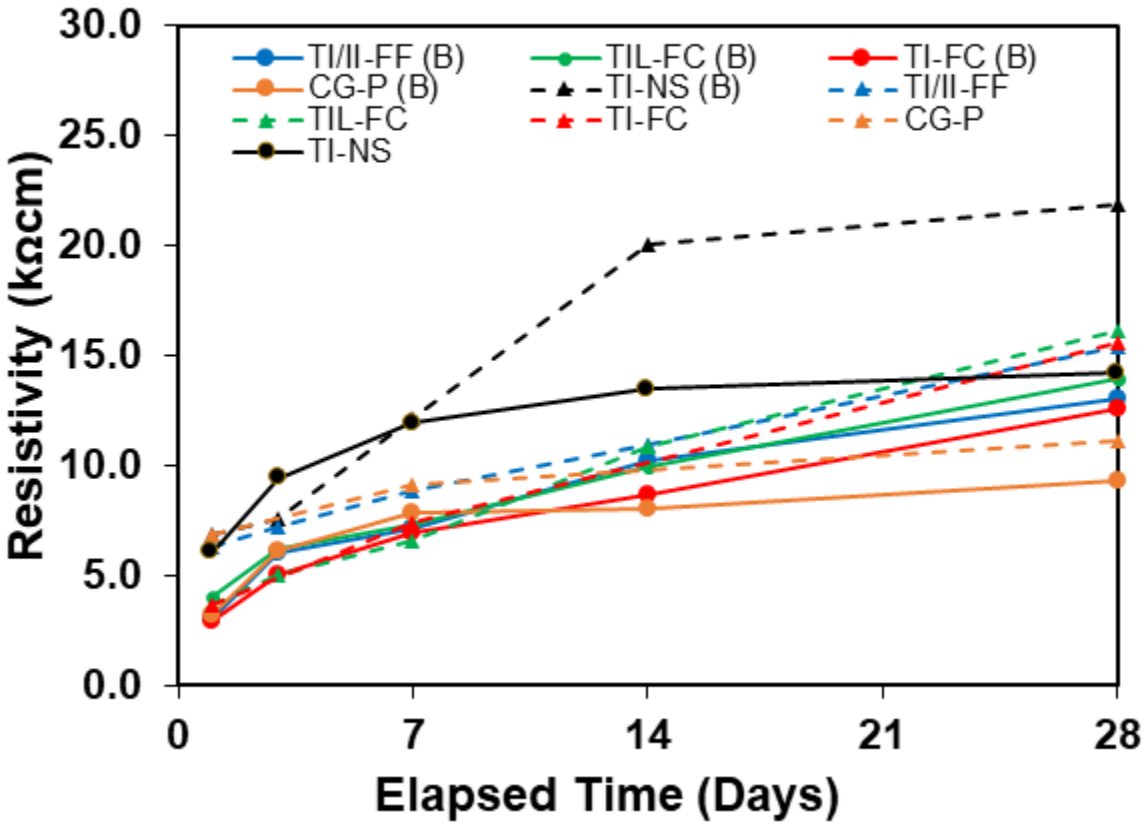

Figure 22. Electrical resistivity

3.5.2.3. Drying Shrinkage

Figure 23 and Figure 24 show the drying shrinkage strain of all the concrete mixtures under free and restrained conditions, respectively. In general, there was an increase in maximum strain in case of mixtures containing basalt fibers. This increase in strain may again be due to an over-dosage of superplasticizers (Kosmatka et al. 2002; Taylor and Wang 2014). However, unlike their control counterparts, the concrete mixtures containing basalt fibers did not have a drastic shift/jump in the shrinkage strain curve (Figure 24). Such a jump usually indicates crack formation in the concrete ring, as may be observed in case of TI-NS in Figure 24. This may be due to a physical bridging of micro-cracks by basalt fibers that will limit the development of macro-cracks.

The over dosage of superplasticizers may be avoided by appropriate changes in the mix design such as increasing the paste content or use of shrinkage reducing admixtures.

As expected, CG-P and CG-P (B) had low free shrinkage (Figure 23). Class F fly ash reduced the shrinkage strain of concrete.

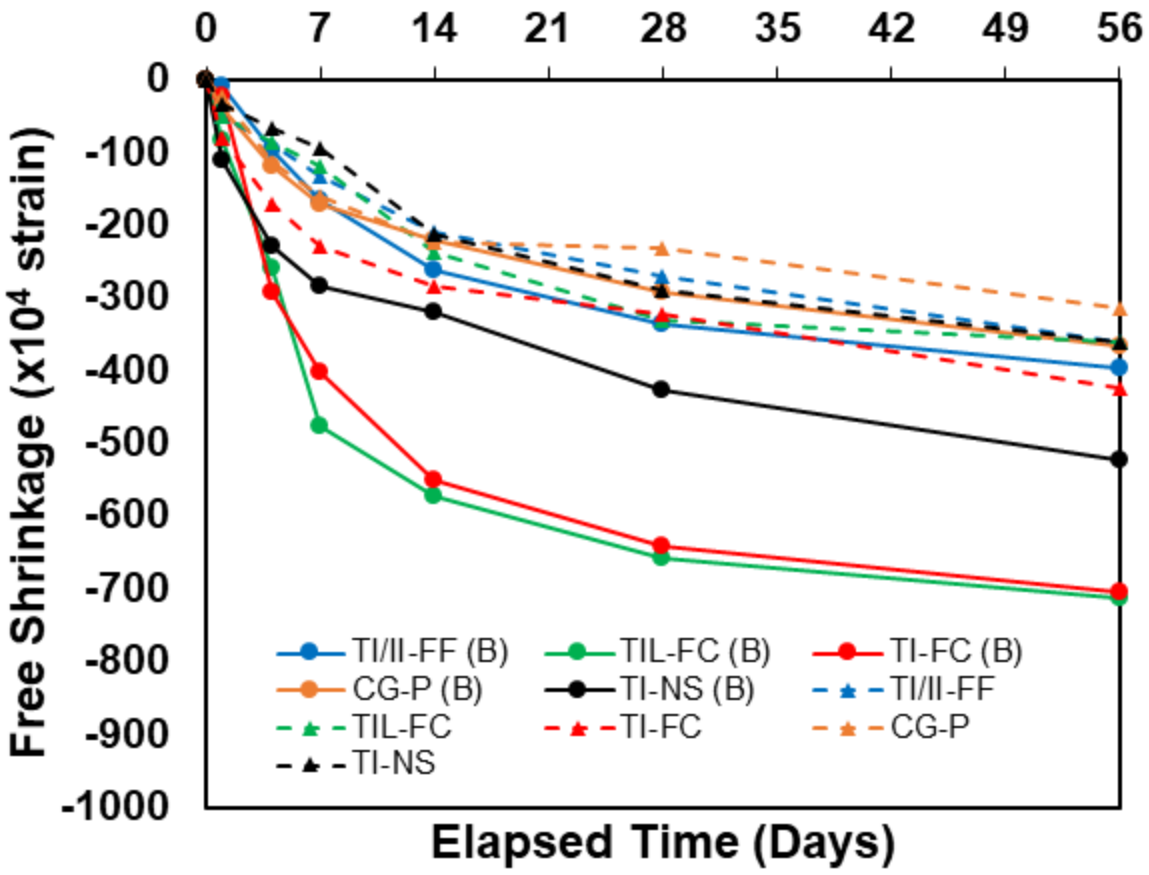

Figure 23. Free shrinkage

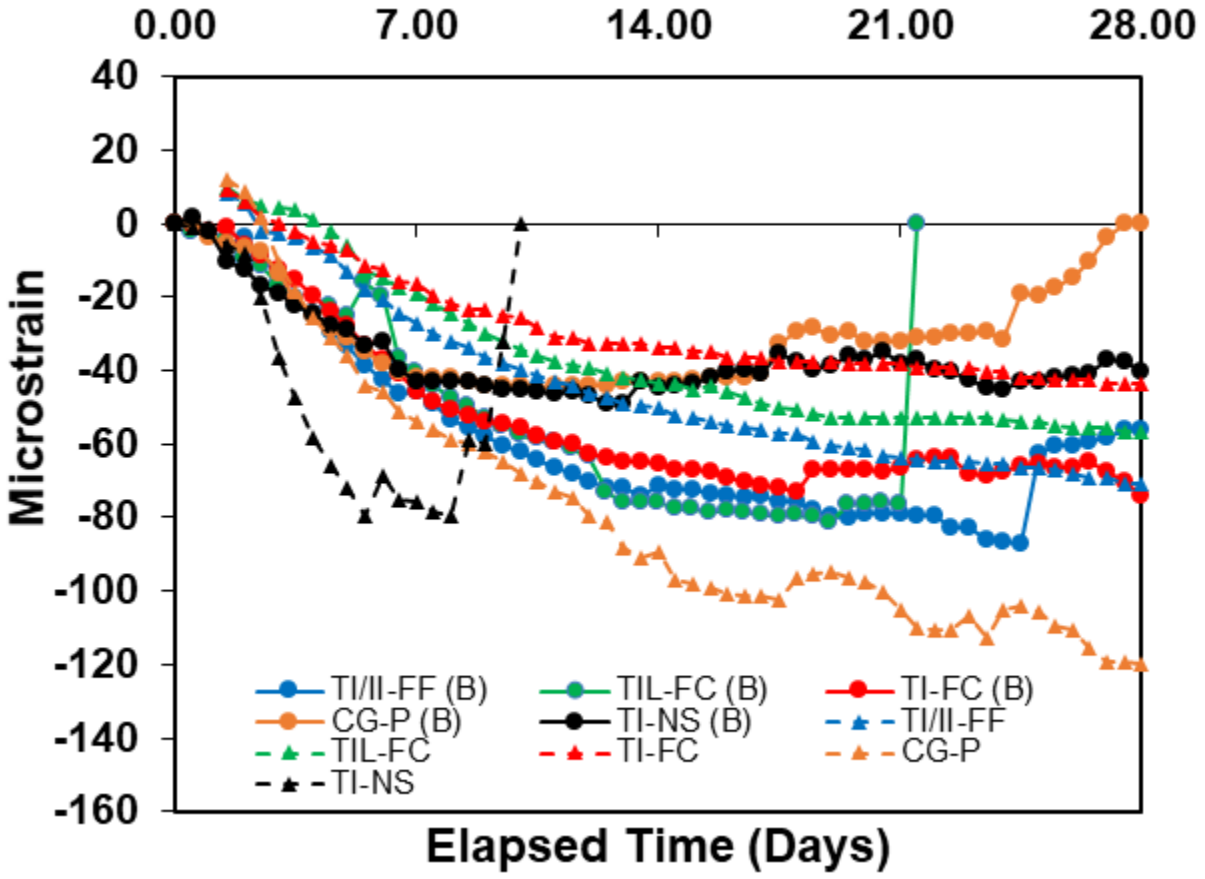

Figure 24. Restrained shrinkage

3.5.3. Performance Matrix

Table 11 shows the results for some of the parameters of the five mixtures containing basalt fibers. Some limits were set on the values of compressive strength, percentage improvement of 28-day resistivity over CG-P (B), 28-day free shrinkage, and cracking age under restrained conditions based on prevalent industry standards and internal discussions. Based on the performance matrix with an emphasis on shrinkage, TI/II-FF (B) is fulfilling most of the criteria and therefore will be recommended for further development and field implementations.

Table 11. Performance matrix for Chapter 3

Mix	Parameters and Performance Limits	28 Day Compressive Strength (psi)	% Improvement of 28 Day Resistivity of Mix over CG-P (B) (%)	28 Day Free Shrinkage (μ-Strain)	Cracking Age (Days)
		>4000 psi	20%	> -400 μ-Strain	
CG-P (B)		4763	0.00	-293	No cracks
TI/II-FF (B)		3956	58.06	-337	No cracks
TI-FC (B)		3430	35.48	-640	No cracks
TIL-FC (B)		5149	49.46	-657	21
TI-NS (B)		8322	135.48	-427	No cracks

3.6. Conclusions

The following are the key conclusions:

- Addition of basalt fibers in concrete reduced workability, resulting in slump loss. Type F high range water reducers are added in high dosages to enhance the workability.
- High superplasticizer dosage had retarded the hydration of concrete as observed through semi-adiabatic calorimetry. Moreover, the peak temperature indicating hydration of the silicates also reduced.
- Basalt fibers lowered the setting time of concrete. On the other hand, superplasticizers had a tendency to increase the setting time.

- Air content was increased because the addition of basalt fibers increased the amount of entrapped air. In order to control the total air content, the dosage of air entraining agent had to be controlled.
- There was not much improvement in compressive strength and splitting tensile strength due to fiber addition.
- Resistivity was also lower for the mixtures containing basalt fibers, due to a high dosage of high range water reducers and resulting increase in porosity.
- Plastic shrinkage and drying shrinkage strain was higher on account of high dosage of superplasticizers. However, cracks were not observed in case of mixtures containing basalt fibers, likely due to physical merging of cracks by basalt fibers.
- Based on a performance matrix, TI/II-FF is selected as the best mixture among those containing basalt fibers and recommended for further studies and field implementations. Mix proportions can be appropriately modified to prevent the use of high dosages of high range water reducers.

3.7. Acknowledgement

This paper is based upon work supported by the U. S. Department of Energy under Award No.DE-EE0007246. The authors also acknowledge Mr. Robert Steffes for his constant support.

3.8. Disclaimer

Any findings, opinions, and conclusions or recommendations expressed in this report are those of the author(s) and do not necessarily reflect the views of the Department of Energy.

3.9. References

ASTM. (2015). “Standard Specification for Blended Hydraulic Cements.” C595/C595M-15, West Conshohocken, PA

ASTM. (2016). “Standard Specification for Portland Cement.” C150/C150M-16e1, West Conshohocken, PA.

ASTM. (2009). “Standard Test Method for Determining Age at Cracking and Induced Tensile Stress Characteristics of Mortar and Concrete under Restrained Shrinkage.” C1581/C1581M-09a, West Conshohocken, PA.

ASTM. (2016). “Standard Practice for Making and Curing Concrete Test Specimens in the Laboratory.” C192/C192M-16a, West Conshohocken, PA.

ASTM. (2015). “Standard Test Method for Slump of Hydraulic-Cement Concrete.” C143/C143M-16a, West Conshohocken, PA.

ASTM. (2014). “Standard Test Method for Air Content of Freshly Mixed Concrete by the Pressure Method.” C231/C231M-14, West Conshohocken, PA.

ASTM. (2014). “Standard Test Method for Bleeding of Concrete.” C232/C232M-14, West Conshohocken, PA.

ASTM. (2008). “Standard Test Method for Time of Setting of Concrete Mixtures by Penetration Resistance.” C403/C403M-08, West Conshohocken, PA.

ASTM. (2015). “Standard Practice for Evaluating Early Hydration of Hydraulic Cementitious Mixtures Using Thermal Measurements.” C1753/C1753M-15e1, West Conshohocken, PA.

ASTM. (2016). “Standard Test Method for Compressive Strength of Cylindrical Concrete Specimens.” C39/C39M-16b, West Conshohocken, PA.

ASTM. (2011). “Standard Test Method for Splitting Tensile Strength of Cylindrical Concrete Specimens.” C496/C496M-11, West Conshohocken, PA.

ASTM. (2012). “Standard Test Method for Bulk Electrical Conductivity of Hardened Concrete.” C1760-12, West Conshohocken, PA.

ASTM. (2014). “Standard Test Method for Length Change of Hardened Hydraulic-Cement Mortar and Concrete.” C157/C157M-08, West Conshohocken, PA.

ASTM. (2013). “Standard Test Method for Evaluating Plastic Shrinkage Cracking of Restrained Fiber Reinforced Concrete (Using a Steel Form Insert).” C1579-13, West Conshohocken, PA

ASTM. (2018). “Standard Test Method for Determining Age at Cracking and Induced Tensile Stress Characteristics of Mortar and Concrete under Restrained Shrinkage.” C1581/C1581M-18, West Conshohocken, PA.

Abbas, M. Y., and Khan, M. I. (2016). "Fiber-Matrix Interfacial Behavior of Hooked-End Steel Fiber-Reinforced Concrete." *Journal of Materials in Civil Engineering*, 28(11), 04016115.

Astm, C. (2000). "595. Standard Specification for Blended Hydraulic Cements." *Annual book of ASTM standards*, 4.

Barcelo, L., Thomas, M. D. A., Cail, K., Delagrave, A., and Blair, B. (2013). "Portland limestone cement equivalent strength explained." *Concrete international*, 35(11), 41-47.

Barrett, T., Sun, H., Villani, C., Barcelo, L., and Weiss, J. (2014). "Early-age shrinkage behavior of Portland limestone cement." *Concrete international*, 36(2).

Bennett, E. W., and Loat, D. R. (1970). "Shrinkage and creep of concrete as affected by the fineness of Portland cement." *Magazine of concrete research*, 22(71), 69-78.

Bentz, D. P. (2010). "Blending different fineness cements to engineer the properties of cement-based materials." *Magazine of Concrete Research*, 62(5), 327-338.

Bisschop, J., and Van Mier, J. G. M. (2002). "Drying shrinkage microcracking in cement-based materials." *Heron, 47 (3), 2002*.

Bisschop, J., and Van Mier, J. G. M. (2002). "How to study drying shrinkage microcracking in cement-based materials using optical and scanning electron microscopy?" *Cement and concrete research*, 32(2), 279-287.

Bisschop, J., and van Mier, J. G. M. (2008). "Effect of aggregates and microcracks on the drying rate of cementitious composites." *Cement and Concrete Research*, 38(10), 1190-1196.

Branston, J., Das, S., Kenno, S. Y., and Taylor, C. (2016). "Influence of basalt fibres on free and restrained plastic shrinkage." *Cement and Concrete Composites*, 74, 182-190.

de Sa, C., Benboudjema, F., Thiery, M., and Sicard, J. (2008). "Analysis of microcracking induced by differential drying shrinkage." *Cement and Concrete Composites*, 30(10), 947-956.

Deshpande, S. S. (2007). *Evaluating free shrinkage of concrete for control of cracking in bridge decks*, University of Kansas.

Fiore, V., Scalici, T., Di Bella, G., and Valenza, A. (2015). "A review on basalt fibre and its composites." *Composites Part B: Engineering*, 74, 74-94.

Gesoğlu, M., Güneyisi, E., and Özbay, E. (2009). "Properties of self-compacting concretes made with binary, ternary, and quaternary cementitious blends of fly ash, blast furnace slag, and silica fume." *Construction and Building Materials*, 23(5), 1847-1854.

High, C., Seliem, H. M., El-Safty, A., and Rizkalla, S. H. (2015). "Use of basalt fibers for concrete structures." *Construction and Building Materials*, 96, 37-46.

Idiart, A. E. (2009). *Coupled analysis of degradation processes in concrete specimens at the meso-level*, Universitat Politècnica de Catalunya.

Institute, A. C. (2005). "Report on factors affecting shrinkage and creep of hardened concrete." *209*, American Concrete Institute, Farmington Hills, MI, Report ACI 209.201R-2005.

Iyer, P., Kenno, S. Y., and Das, S. (2016). "Performance of Fiber-Reinforced Concrete Made With Basalt-Bundled Fibers." *Advances in Civil Engineering Materials*, 5(1), 107-123.

Jiang, C., Fan, K., Wu, F., and Chen, D. (2014). "Experimental study on the mechanical properties and microstructure of chopped basalt fibre reinforced concrete." *Materials & Design*, 58, 187-193.

Kosmatka, S. H., Panarese, W. C., and Kerkhoff, B. (2002). *Design and control of concrete mixtures*, Portland Cement Association Skokie, IL.

Lee, Y., Kang, S.-T., and Kim, J.-K. (2010). "Pullout behavior of inclined steel fiber in an ultra-high strength cementitious matrix." *Construction and Building Materials*, 24(10), 2030-2041.

Lomboy, G., Wang, K., and Ouyang, C. (2010). "Shrinkage and fracture properties of semiflowable self-consolidating concrete." *Journal of Materials in Civil Engineering*, 23(11), 1514-1524.

Malhotra, V. M., and Mehta, P. K. (1996). *Pozzolanic and cementitious materials*, Taylor & Francis.

Mangat, P. S., and Azari, M. M. (1990). "Plastic shrinkage of steel fibre reinforced concrete." *Materials and structures*, 23(3), 186-195.

Mehta, P. K., and Burrows, R. W. (2001). "Building durable structures in the 21 st century." *Indian Concrete Journal*, 75(7), 437-443.

Mikulčić, H., Klemeš, J. J., Vujanović, M., Urbaniec, K., and Duić, N. (2016). "Reducing greenhouse gasses emissions by fostering the deployment of alternative raw materials and

energy sources in the cleaner cement manufacturing process." *Journal of cleaner production*, 136, 119-132.

Mindess, S., Young, J. F., and Darwin, D. (2002). "Concrete, 2nd EditionPrentice Hall." *Englewood Cliffs, NJ*.

Patnaik, A., Miller, L., and Standal, P. C. (2014) "Fiber Reinforced Concrete Made from Basalt FRP Minibar." 11-13.

Peterson, K., Julio-Betancourt, G., Sutter, L., Hooton, R. D., and Johnston, D. (2013). "Observations of chloride ingress and calcium oxychloride formation in laboratory concrete and mortar at 5 C." *Cement and Concrete Research*, 45, 79-90.

Quercia, G., Spiesz, P., Hüsken, G., and Brouwers, H. J. H. (2014). "SCC modification by use of amorphous nano-silica." *Cement and Concrete Composites*, 45, 69-81.

Ramakrishnan, V., Tolmare, N. S., and Brik, V. B. (1998). "NCHRP-IDEA Project 45: Performance evaluation of basalt fibers and composite rebars as concrete reinforcement." *Transportation Research Board, National Research Council, Washington, DC*, 1-10.

Ramezanianpour, A. M., and Hooton, R. D. (2014). "A study on hydration, compressive strength, and porosity of Portland-limestone cement mixes containing SCMs." *Cement and Concrete Composites*, 51, 1-13.

Roper, H. (1974). "Shrinkage, tensile creep and cracking tendency of concretes." *Australian Road Research*, 5(6).

Singh, L. P., Karade, S. R., Bhattacharyya, S. K., Yousuf, M. M., and Ahalawat, S. (2013). "Beneficial role of nanosilica in cement based materials–A review." *Construction and Building Materials*, 47, 1069-1077.

Stark, J., Freyburg, E., and Lohmer, K. (1999). "Investigations into the influence of limestone additions to portland cement clinker phases on the early phase of hydration." Thomas Telford, 69.

Suksawang, N., Mirmiran, A., and Yohannes, D. (2014). "Use of Fiber Reinforced Concrete for Concrete Pavement Slab Replacement."

Taylor, P., and Wang, X. (2014). "Concrete Pavement Mixture Design and Analysis (MDA): Factors Influencing Drying Shrinkage." Iowa State University.

Tosun-Felekoğlu, K. (2012). "The effect of C3A content on sulfate durability of Portland limestone cement mortars." *Construction and Building Materials*, 36, 437-447.

Tritsch, N., Darwin, D., and Browning, J. (2005). "Evaluating Shrinkage and Cracking Behavior of Concrete Using Restrained Ring and Free Shrinkage Tests." University of Kansas Center for Research, Inc.

Tsuruta, H., Matsushita, H., Harada, K., and Goto, T. (2004). "Effect of gypsum content in cement on autogenous shrinkage of portland blast-furnace slag cement concrete." *Special Publication*, 221, 683-702.

Wang, X. (2011). *Drying shrinkage of ternary blends in mortar and concrete*, Iowa State University.

Wang, X., Taylor, P., Wang, K., and Lim, M. (2016). "Monitoring of setting time of self-consolidating concrete using ultrasonic wave propagation method and other tools." *Magazine of Concrete Research*, 68(3), 151-162.

Worrell, E., Price, L., Martin, N., Hendriks, C., and Meida, L. O. (2001). "Carbon dioxide emissions from the global cement industry." *Annual review of energy and the environment*, 26(1), 303-329.

Yang, Z., Zhao, H., and Sun, W. (2015). "Effect of the Types of Superplasticizers on the Fresh, Mechanical, and Durability Properties of the High-Performance Concrete." *Journal of Testing and Evaluation*, 44(1), 699-709.

Yousefieh, N., Joshaghani, A., Hajibandeh, E., and Shekarchi, M. (2017). "Influence of fibers on drying shrinkage in restrained concrete." *Construction and Building Materials*, 148, 833-845.

Zakka, Z. A., and Carrasquillo, R. L. (1989). "Effects of high-range water reducers on the properties of fresh and hardened concrete."

Zayed, A., Sedaghat, A., Bien-Aime, A., and Shanahan, N. (2014). "Effects of portland cement particle size on heat of hydration." Florida Department of Transportation

CHAPTER 4: EFFECT OF CEMENT CHANGES ON MICRO-CRACKING TENDENCY DUE TO DRYING SHRINKAGE

4.1. Abstract

In this work, the effects of different cementitious combinations on micro-cracking due to drying shrinkage were investigated. Microstructure investigations were conducted by using Micro Computed Tomography (μ-CT) and fluorescence microscopy. This work was conducted in two parts. In Experimental Program I, three cementitious combinations were subjected to restrained drying shrinkage and the subsequent micro-cracking was investigated. Porosity distribution of these mixtures was also investigated. A protocol for microstructure analysis of cement paste samples was developed and optimized in this phase to be used for further experimentation. In Experimental Program II, eight cementitious combinations were investigated for micro-cracks and properties such as, electrical resistivity, drying shrinkage strain and Ca/Si ratio. Relationships between microstructure properties and bulk properties of concrete are discussed.

4.2. Introduction

Concrete is one of the most abundantly used building materials, due to its durability and ability to be cast into different shapes in its plastic state. Portland cement with or without supplementary cementitious materials, reacts with water to form a glue that binds aggregates together to form concrete. Unreacted water may be removed from the system due to evaporation leaving voids. If the size of such voids is less than 50 nm, the removal of water causes the paste to shrink (Taylor and Wang 2014).

Due to a difference in the degree of drying across an element, a moisture gradient may be set up, leading to tensile stress parallel to the drying surface (de Sa et al. 2008, Bisschop and Van Mier 2002a). As concrete is weak in tension, micro-cracks are produced perpendicular to the

drying surface. Additionally, since cement paste will shrink more than aggregates, a restraining effect is imposed leading to the development of internal tensile stresses. As a result, the paste/aggregate interfaces de-bond creating circumferential cracks and radial micro-cracks (0.25-50μ) (Bisschop and Van Mier 2002b). These cracks may lead to the ingress of deleterious chemical ions like chloride and sulfate ions, which in turn may react with hydration products to produce expansive compounds, leading to a loss of serviceability of the structure. Therefore, it is important to assess the extent of micro-cracking in concrete. As micro-cracks are mostly formed in paste, it may be of interest to investigate paste samples.

The outer layers of a concrete sample will lose water faster than the interior. As a result, free shrinkage is more significant near the exposed surface compared to the core, while adjacent layers impose restraint which leads to the formation of tensile stresses and discontinuous micro-cracks (Samouh, Rozière and Loukili 2017). There is reportedly a critical depth from the surface considered to be the most vulnerable to the formation of micro-cracks (de Sa et al. 2008). The porosity and permeability of concrete generally decreases with depth as a result of improved hydration (Samouh et al. 2016). As the same region may have high porosity and a high vulnerability to micro-cracking, it may be of interest to investigate if there is any relationship between the two parameters.

The strain generated due to drying shrinkage under restrained conditions is typically measured by the ring test (ASTM C1581). Although there are standards specifying petrographic analysis of concrete samples (ASTM C856), standard methods are not available for detection and quantification of micro-cracks due to drying shrinkage. Optical microscopy and scanning electron microscopy (SEM) techniques have been used by prior researchers to characterize concrete specimens (Zerbino, Giaccio and Marfil 2014, Rashed and Williamson 1991). Figure 25 shows

SEM images of a paste sample showing a micro-crack (Figure 25a). Upon further magnification, hydration products can also be visible (Figure 25b). Although some of these methods can be used to obtain a more detailed picture of concrete microstructure, they can be expensive and time consuming. Researchers have also used fluorescence microscopy and digital image processing (DIP) for detection of micro-cracks (Tekin et al. 2015). Typically, samples are epoxy impregnated under vacuum. Thin slices are then made followed by grinding and polishing for observation under a microscope. Yio et.al. used a method of serial sectioning of specimens and fluorescence microscopy for 3D reconstruction of defects inside paste, mortar, and concrete samples (Yio et al. 2015). Micro Computed Tomography (μ-CT) technique has been used as an alternative tool to characterize voids inside concrete (Tekin et al. 2015).

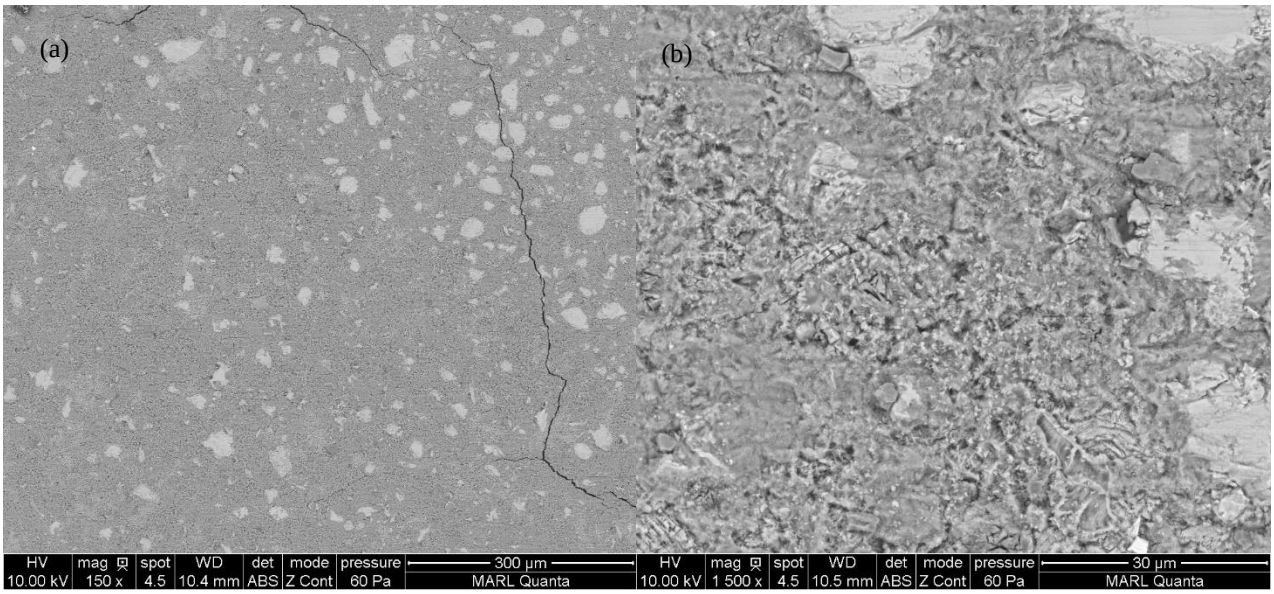

Figure 25. SEM image of a typical paste sample at (a) 150X magnification, and (b) 1500X magnification

Various factors affecting drying shrinkage in concrete including mixture proportions, aggregate properties and binder characteristics Drying shrinkage is significantly affected by the fineness of cement (Mehta and Burrows 2001) because finer cementitious systems require more water for workability compared to coarser cements (Bennett and Loat 1970); therefore more water

is available to evaporate from the surface (Deshpande 2007). Cement chemistry also influences shrinkage in concrete in that increasing tri-calcium aluminate (C_3A) and alkali contents may increase shrinkage (Roper 1974, Zayed et al. 2014) while decreasing sulfate content may increase shrinkage (Tsuruta et al. 2004). The use of limestone inter-ground with portland cement clinker may also slightly reduce shrinkage of concrete (Barrett et al. 2014). Additionally, the presence of supplementary cementitious materials like fly ash and microsilica can also influence shrinkage (Haruehansapong, Pulngern and Chucheepsakul 2017).

The use of randomly dispersed fibers may help in reducing the cracking tendency of concrete by reducing crack widths (Iyer, Kenno and Das 2016). (Branston et al. 2016, Suksawang, Mirmiran and Yohannes 2014).

In this study, potential relationships between micro-cracking of paste samples from different cementitious combinations and drying shrinkage strain of concrete were investigated. The study consists of two phases: in the first phase, three cementitious combinations (coarse ground cement CG-P, Type IL portland limestone cement TIL-P, and Type I portland cement and 5% replaced with nanosilica TI-NS) were used to investigate the effect of drying shrinkage on their micro-cracking tendency. A method was developed and tested for detection and quantification of micro-cracks in these paste samples. Porosity distribution in the paste samples was also investigated. In the second phase of this study, the analysis technique was modified to increase the likelihood of micro-crack formation at desired locations of paste samples for convenience of analysis.

Additionally, eight different cementitious combinations were investigated for micro-cracks:

- Coarse ground cement (CG-P),

- Type I portland cement (TI-P),
- Type I portland cement and 30% Class C fly ash (TI-FC),
- Type I portland cement and 20% Class F fly ash (TI-FF),
- Type I portland cement and 5% nanosilica (TI-NS),
- Type IL portland limestone cement (TIL-P),
- Type IL portland limestone cement and 30% Class C fly ash (TIL-FC),
- Type IL portland limestone cement and 30% Class C fly ash, and 0.25% (v/v) addition of chopped basalt fibers (TIL-FC (B)).

The goal of this study is detection and quantification of micro-cracks in paste samples and determination of relationships between crack density and restrained shrinkage.

4.3. Experimental Section

4.3.1. Materials

In this study, three cement types were used: Coarse Ground portland cement (CG), Type I portland cement (TI), and Type IL portland limestone cement (TIL). Additionally, Class C fly ash (FC), Class F fly ash (FF), and colloidal nanosilica (NS) were used as supplementary cementitious materials (SCM). The chemical and physical properties of the cementitious materials are presented in Table 2, Table 3 and Table 4, respectively. For concrete specimens, ½" (nominal aggregate size) limestone aggregates and locally available sand were used. A combined gradation chart for the aggregates is presented in Figure 26. The water-to-cementitious materials ratio and binder content were fixed at 0.42 and 580 lb/yd^3 respectively. Other ingredients in the mixtures included chopped basalt fibers 13μm in diameter, and 24 mm in length, treated with a silane-based coating (0.25% w/w), an acid-based air entraining agent, and a polycarboxylate based Type F high range water reducer.

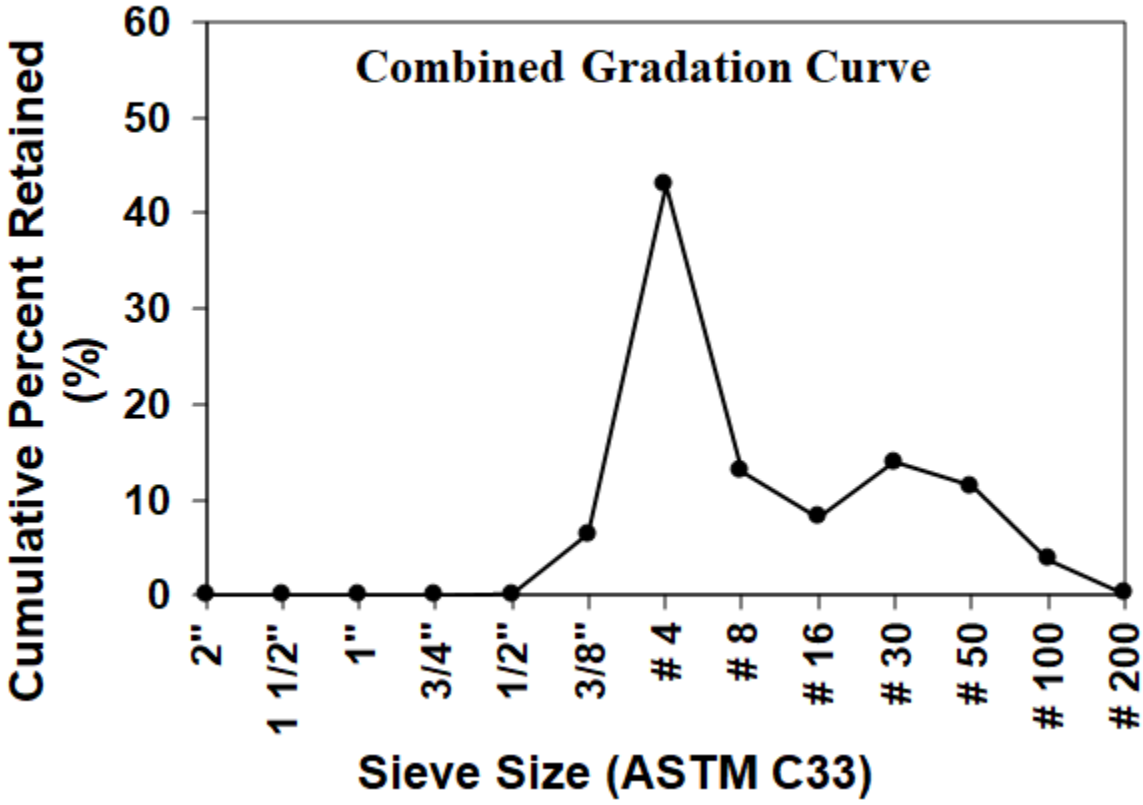

Figure 26. Combined particle size distribution curve for coarse and fine aggregates

4.3.2. Experimental Program I

4.3.2.1. Concrete Specimens

In this first phase, three cementitious combinations (coarse ground cement CG-P, Type IL portland limestone cement TIL-P, and Type I portland cement and 5% replaced with nanosilica TI-NS) were investigated. The mixture proportions for the concrete used are shown in Table 12. Ring tests were conducted to investigate drying shrinkage (ASTM C1581).

Table 12. Mixture proportions for Experimental Program I

Mix Code	Cement (pcy)	Class F Fly Ash (pcy)	Class C Fly Ash (pcy)	Nano Silica (pcy)	Water (pcy)	WR (oz/cwt)	AEA (oz/cwt)	Fine Aggregates. (pcy)	Coarse Aggregates (pcy)
CG-P	580	0	0	0	244	3.96	0.2	1789	1295
TIL-P	580	0	0	0	244	6.5	0.2	1789	1295
TI-NS	551	0	0	29	244	17.62	0.2	1789	1295

4.3.2.2. Paste Specimens

Cement paste samples were made for the three cementitious combinations mentioned in section 2.2.1. Water to cementitious materials ratio was fixed at 0.40. For microstructure studies, paste samples were cast in metal molds with internal dimensions 0.5”x0.5”x2” (Figure 27). Restraints were provided along the shorter edges of the molds by using US size #2 screws (0.08” diameter, ¼ long). Cement paste was prepared in accordance with ASTM C305 and poured into the metal molds. The exposed faces of the molds were covered with molten steel, and all the pieces are tied together by using rubber bands. These samples were then rotated at 10 rotations per minute (Figure 28) for approximately 12 hours to avoid bleeding. The four long edges were demolded after 24 hours and wet cured for up to seven days after mixing. Then the samples were completely demolded and allowed to dry under conditions compliant with ASTM C1581 for 28 days.

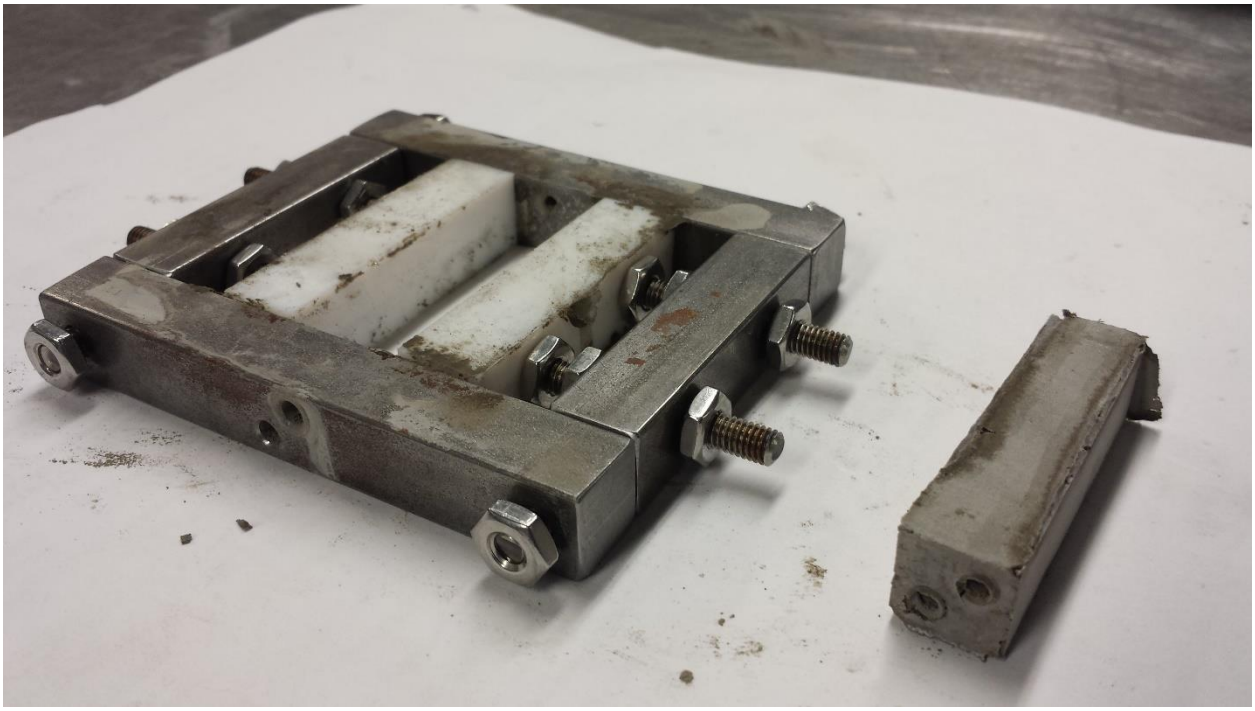

Figure 27. Metal mold for paste sample

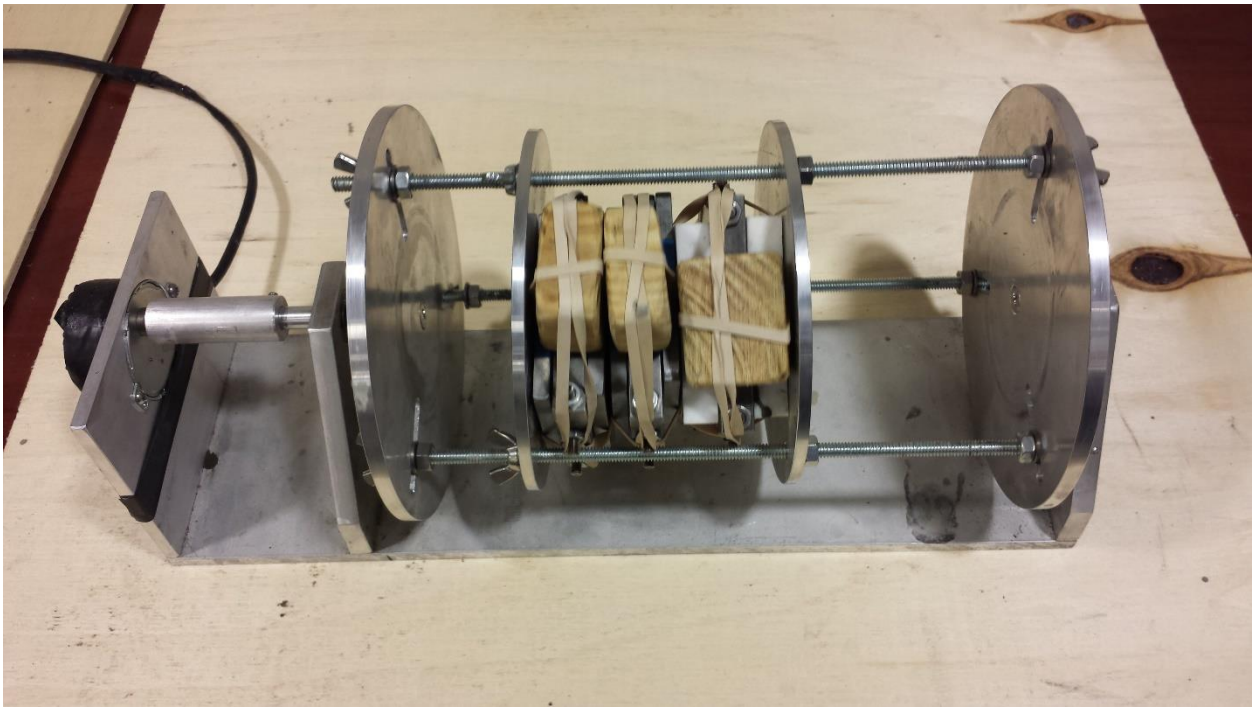

Figure 28. End-to-end rotator

4.3.3. Experimental program II

4.3.3.1. Concrete Specimens

In the second phase, eight different cementitious combinations were investigated for micro-cracks: coarse ground cement (CG-P), Type I portland cement with no SCMs (TI-P), 30% replaced with Class C fly ash (TI-FC), 20% replaced with Class F fly ash (TI-FF), 5% replaced with nanosilica (TI-NS), Type IL portland limestone cement (TIL-P), 30% replaced with Class C fly ash (TIL-FC), and 30% replaced with Class C fly ash, and 0.25% (v/v) addition of chopped basalt fibers (TIL-FC (B)). The mixture proportions for the concrete used are shown in Table 13. Ring test samples were made to investigate drying shrinkage under restrained conditions as per ASTM C1581. Standard 4”x8” cylinders were cast for measuring electrical resistivity (ASTM C1760).

Table 13. Mixture proportions for Experimental Program II

Mix Code	Cement (pcy)	Class F Fly Ash (pcy)	Class C Fly Ash (pcy)	Nano Silica (pcy)	Water (pcy)	WR (oz/cwt)	AEA (oz/cwt)	Fine Aggregates. (pcy)	Coarse Aggregates (pcy)	Chopped Basalt Fiber Addition (% v/v)
CG-P	580	0	0	0	244	3.9	0.2	1789	1295	-
TI-P	580	0	0	0	244	3.2	0.2	1789	1295	-
TIL-P	580	0	0	0	244	6.5	0.2	1789	1295	-
TI-FF	464	116	0	0	244	2.0	0.2	1789	1295	-
TI-FC	406	0	174	0	244	3.8	0.2	1789	1295	-
TIL-FC	406	0	174	0	244	4.3	0.2	1789	1295	-
TI-NS	551	0	0	29	244	17.6	0.2	1789	1295	-
TIL-FC (B)	406	0	174	0	244	4.3	0.2	1789	1295	0.25

4.3.3.2. Paste Specimens

Cement paste samples were cast for the eight cementitious combinations mentioned in section 2.3.1. Water to cementitious materials ratio was fixed at 0.40. For microstructure studies, paste samples were cast in hour glass shaped 3D printed molds with internal dimensions 0.5”x0.5”x2” (Figure 29). Additionally, another set of hour glass shaped PVC molds with the same internal dimensions as those of the 3D printed molds were used (Figure 29). The shape of these molds was selected so that stress due to drying shrinkage is a maximum along the middle section of the specimens. Sample preparation and curing was the same as that described in 2.2.2.

Figure 29. Paste samples in PVC molds (black), and 3D printed molds (white)

4.3.4. Test Methods

4.3.4.1. Concrete

Tests on fresh concrete included workability (ASTM C143), and air content/unit weight (ASTM C231, ASTM C138). Shrinkage in the concrete mixtures under restrained conditions was

measured by the standard ring test method specified in ASTM C1581 (Figure 30). Electrical resistivity test was also conducted (ASTM C1760).

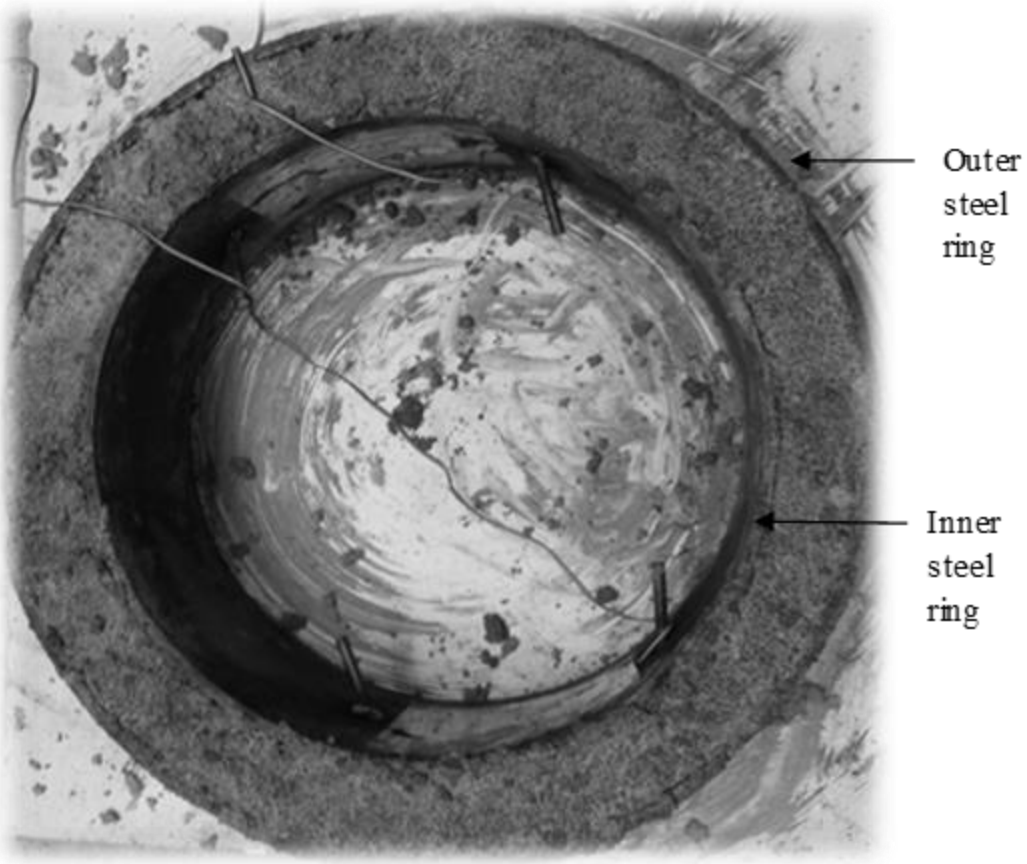

Figure 30. Restrained shrinkage test setup

4.3.4.2. Paste

4.3.4.2.1. Micro Computed Tomography

Dried paste samples inside their molds were subjected to X-ray µ-CT scans with a General Electric V|Tome|x s 240, at the NDSU Electron Microscopy Center Core facility. Scanning was done using the 180 kV x-ray tube running at 110 kV, 350 □A, exposure of 333 ms and a 1200 images collected per sample. Reconstructed volumes were analyzed with the commercial software package Volume Graphics Studio Max version 3.0. Initially, the Surface Determination mode of the software was used to distinguish between material and background (voids or pores in this case).

The surface fit function was applied using the threshold value as the central value between the peaks of material and background in the data histogram. Additionally, an iterative surface determination mode was applied for enhanced precision. This default histogram generated by the software can be used to have an approximate idea of defects within the system. Although the surface determination histogram can be manually fit for detailed detection and quantification of voids as small as 30 µ, for a quick comparison of porosity for voids of size 75 µ and larger, among different cementitious combinations the default method is deemed adequate (Du Plessis et al. 2016). Surface determination was followed by measurement of void sizes by the default Porosity/Inclusions/Defects determination mode of VG Studio Max 3.2. Minimum voxel size was maintained at 8 voxels, and minimum probability of voids was maintained at 0. Figures 31a, 31b show an example of the pore system as imaged through this procedure.

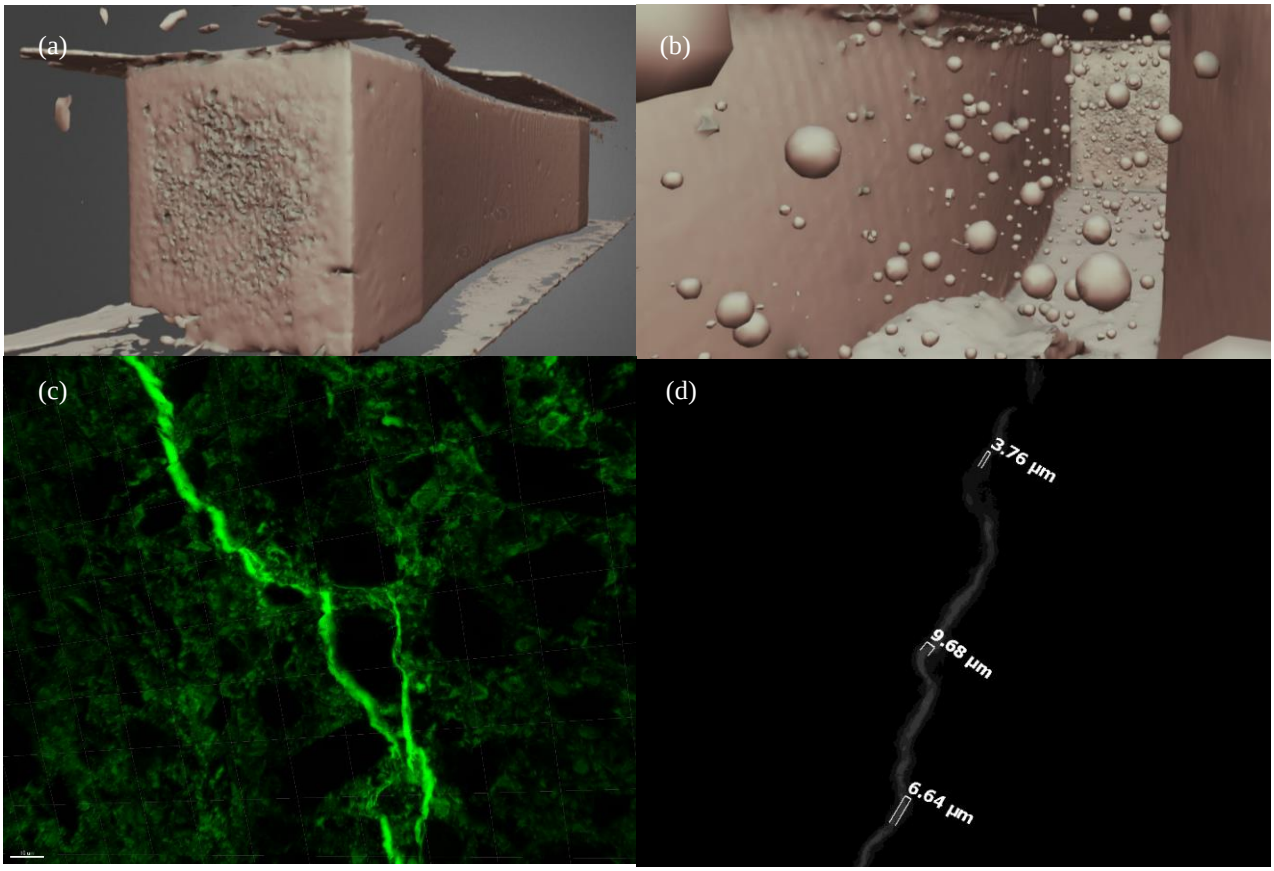

Figure 31. (a) 3D reconstruction of a paste sample (b) 3D reconstruction of pore distribution inside a paste sample (c) typical micro-crack observed through fluorescence microscopy (d) binary format of a micro-crack

4.3.4.2.2. Fluorescence Microscopy

Based on the mean porosity results from µ-CT analysis, critical areas of vulnerability to micro-cracking were identified and samples were made for micro-crack analysis. For Experimental Program I, paste specimens were impregnated with a two-part epoxy resin. A green fluorescent dye was mixed with the resin in a homogenizer and the paste specimens were introduced immediately. The epoxy resin and dye were impregnated into the paste samples under vacuum pressure of 7 kPa for an hour (Figure 32). Then the sample was air dried for 24 hours. The identified vulnerable regions were ground and polished using subsequently smaller grit sized grinding pads. An alcohol-based diamond polish was used for smoother finish. These samples were then observed

under a confocal microscope at 20X magnification. Fluorescence was detected at an excitation wavelength of 488 nm. Recorded images were then analyzed for micro-cracks by using a software ImageJ. Original images were converted into binary format (Figures 31c, 31d) and the crack area in terms of pixels^2 was calculated as a percentage over total area of the region of interest. For Experimental Program II, the specimens were epoxy impregnated with a blue dye and petrographic slides with thin sections (35 μ) and cover slips were created in the laboratories of Texas Petrographics, Inc. A diamond saw was used for making sections. These slides were then observed by using a slide analyzer at 40X magnification. Recorded images were analyzed by a method similar to that of Experimental Program I by using ImageJ.

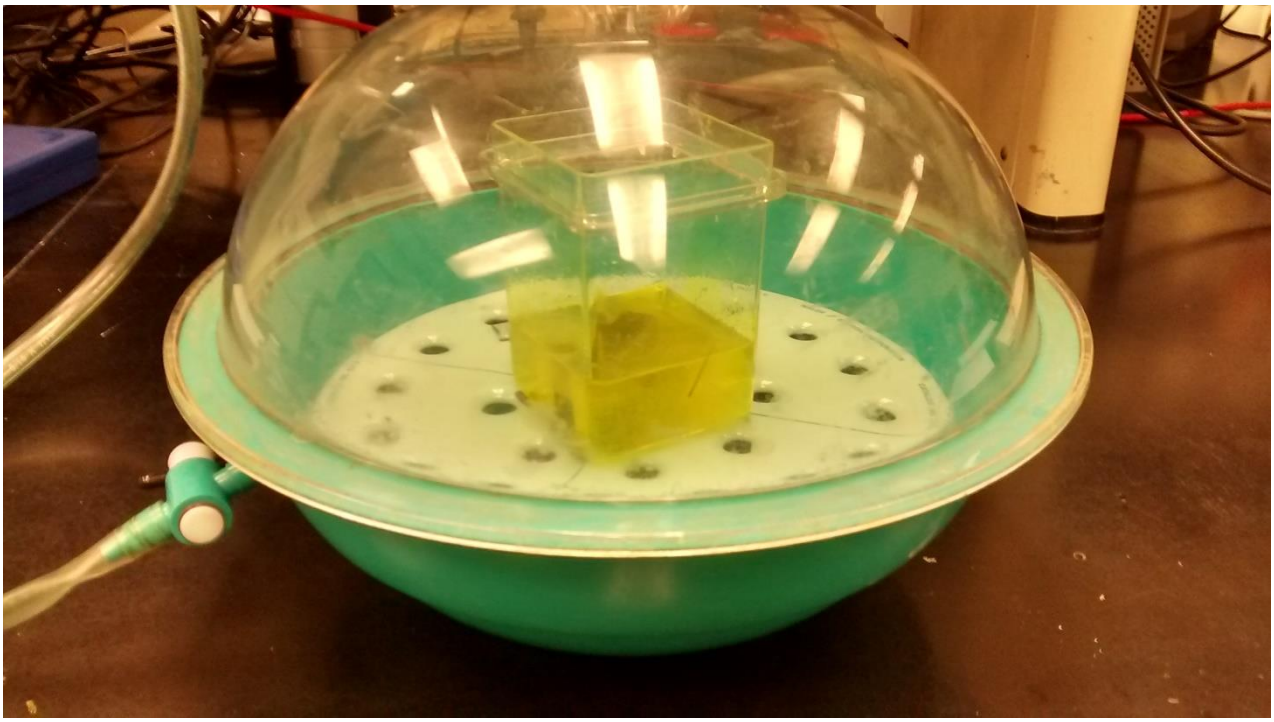

Figure 32. Test setup for epoxy impregnation

4.3.4.2.3. X-Ray Photoelectron Microscopy

The chemical composition of the dried cement paste samples was assessed through X-ray photoelectron spectroscopy (XPS) technique. Based on the compositions, the Ca/Si ratio of the specimens was calculated.

4.4. Results and Discussions

4.4.1. Experimental Program I

Figure 33 shows the restrained shrinkage results for the three mixtures mentioned in the section 4.3.2.1. Ring test results for TI-NS reveal cracks in about 5 days from mixing, as may be visible from the sudden spike in the strain curve.CG-P has the lowest shrinkage strain which is consistent with prior literature (Mehta and Burrows 2001, Bentz 2010). Coarser cementitious systems usually produce less heat during hydration leading to lower temperature gradients. TIL-P had higher shrinkage strain than CG-P but cracks were not observed.

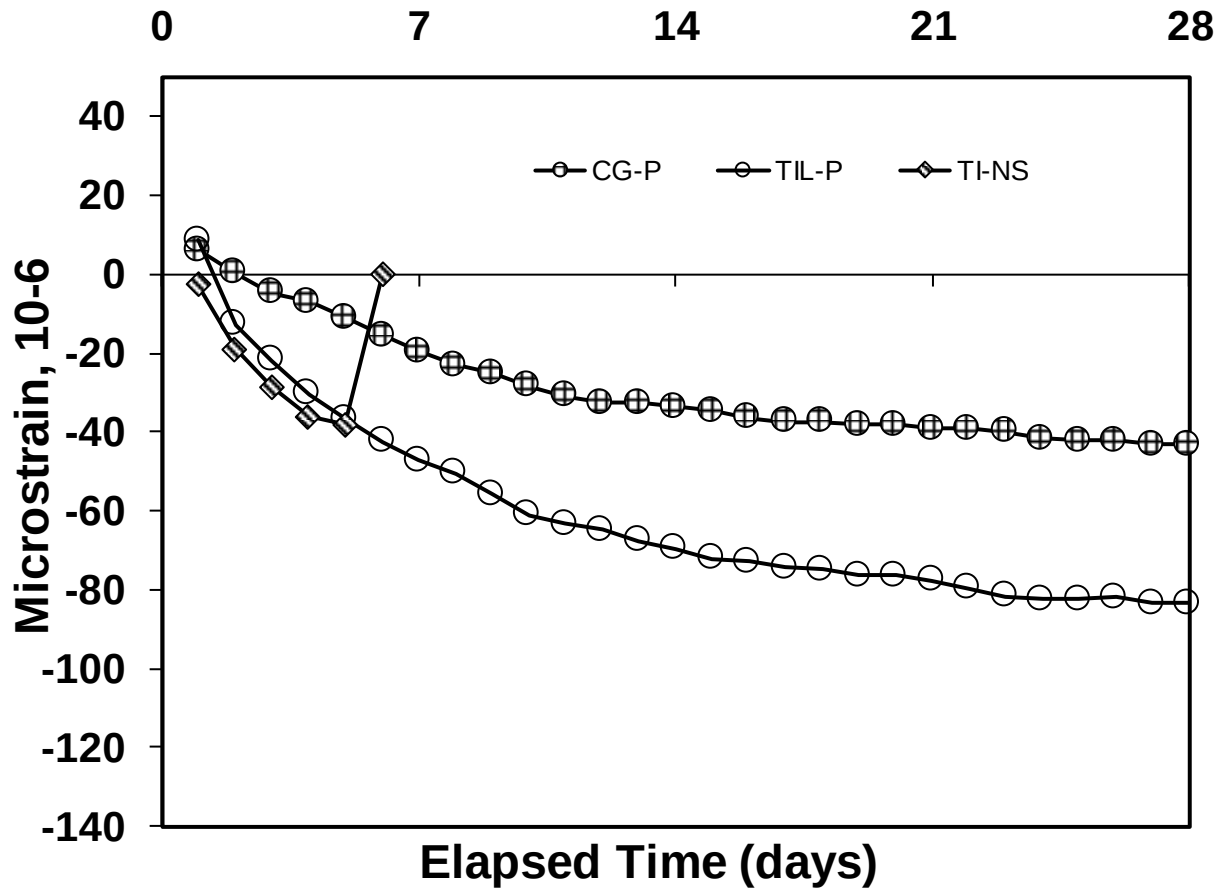

Figure 33. Restrained shrinkage strain for Experimental Program I

The cracking potential of the mixtures of the mixtures, calculated as per ASTM C1581, is presented in Table 14.

Table 14. Potential for Cracking: Experimental Program I (ASTM C1581)

Mix	α (in/in)/day$^{1/2}$	S (psi/day)	Cracking Potential
CG-P	-11.492	11	Low
TIL-P	-19.321	19	Moderate Low
TI-NS	-28.535	67	High

Figure 34 shows the porosity distribution along the width of the paste specimens as analyzed through µ-CT. It may be observed that regions of high mean porosity are located near the surface of the specimens. This is consistent with prior literature (de Sa et al. 2008).

Cracks were observed in the regions near the surface of the paste specimens. Figure 35 shows the relationship between crack density and average stress rate of the mixtures. There appears to be a relationship among the two quantities, but validation through further investigation is required.

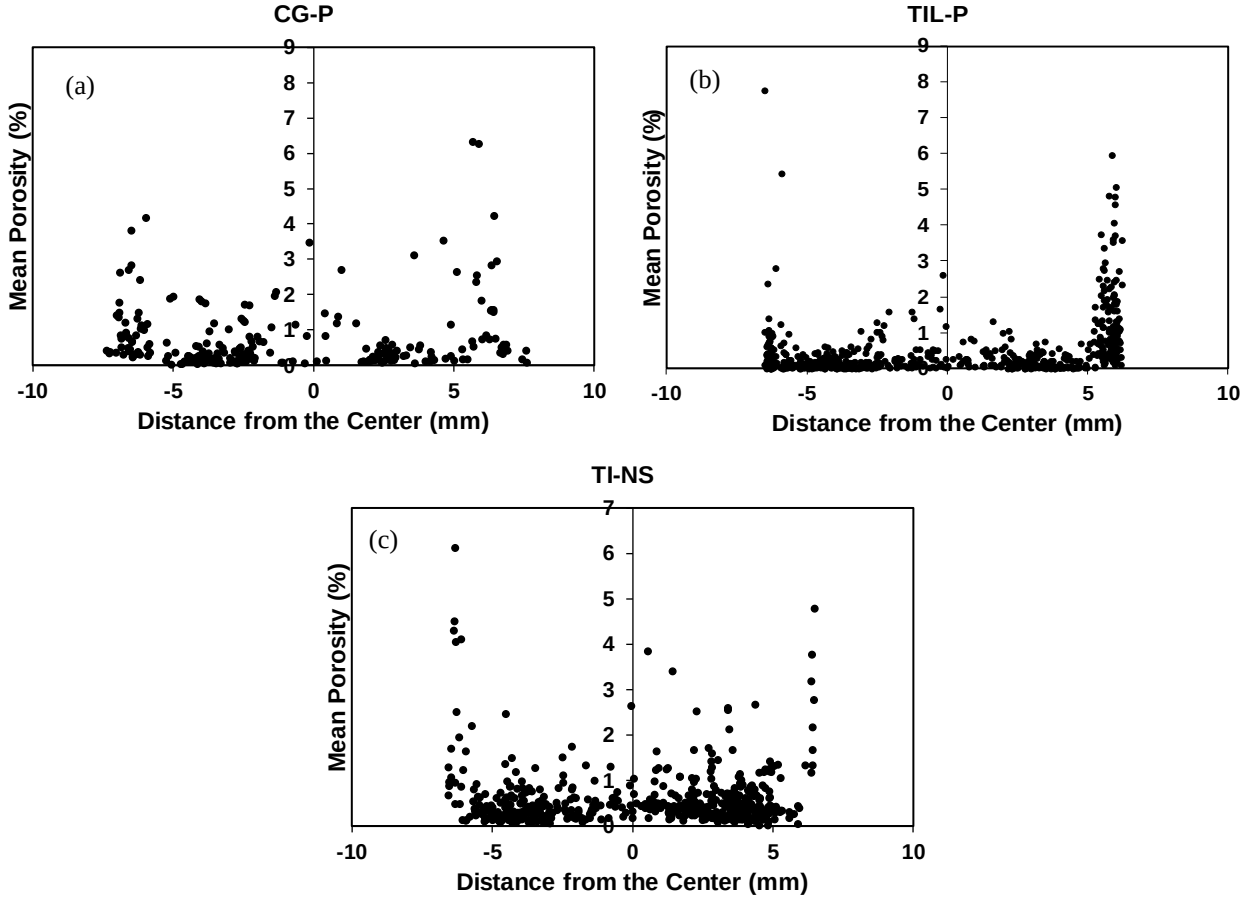

Figure 34. Porosity distribution along width axis for (a) CG-P, (b) TIL-P, and (c) TI-NS

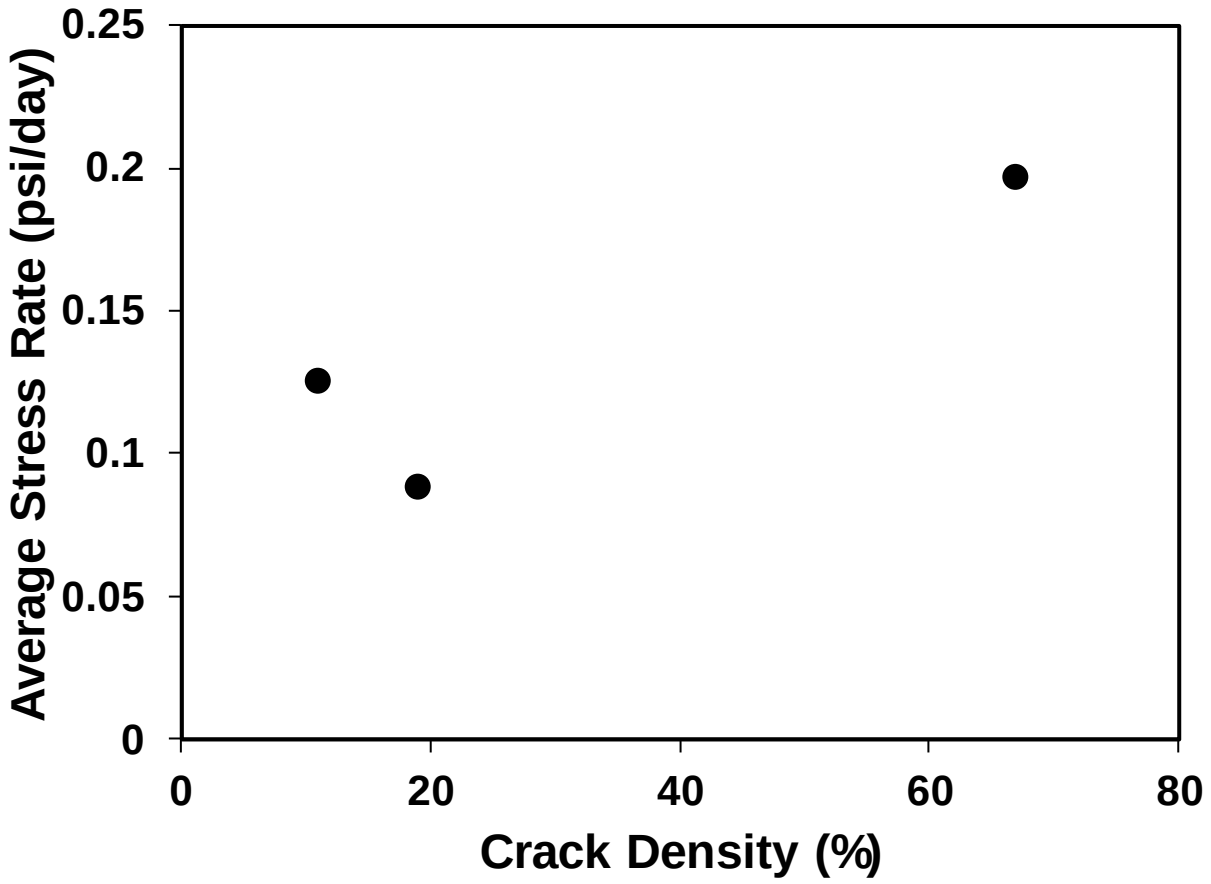

Figure 35. Crack density and stress rate relationship for Experimental Program I

4.4.2. Experimental Program II

Figure 36 shows the electrical resistivity results for the eight mixtures mentioned in section 4.3.4.1. In general, an improvement in resistivity may be due to a refinement in the microstructure of the concrete system. TIL-FC has the highest 28-day resistivity among the eight mixtures as expected. Limestone particles can facilitate accelerated cement hydration due to a nucleation effect (Kadri et al. 2010, De Weerdt et al. 2011). Additionally, carboaluminate hydrates may provide a physical filling effect of the interfacial transition zone (ITZ) between the aggregates and paste (Ramezanianpour and Hooton 2014).

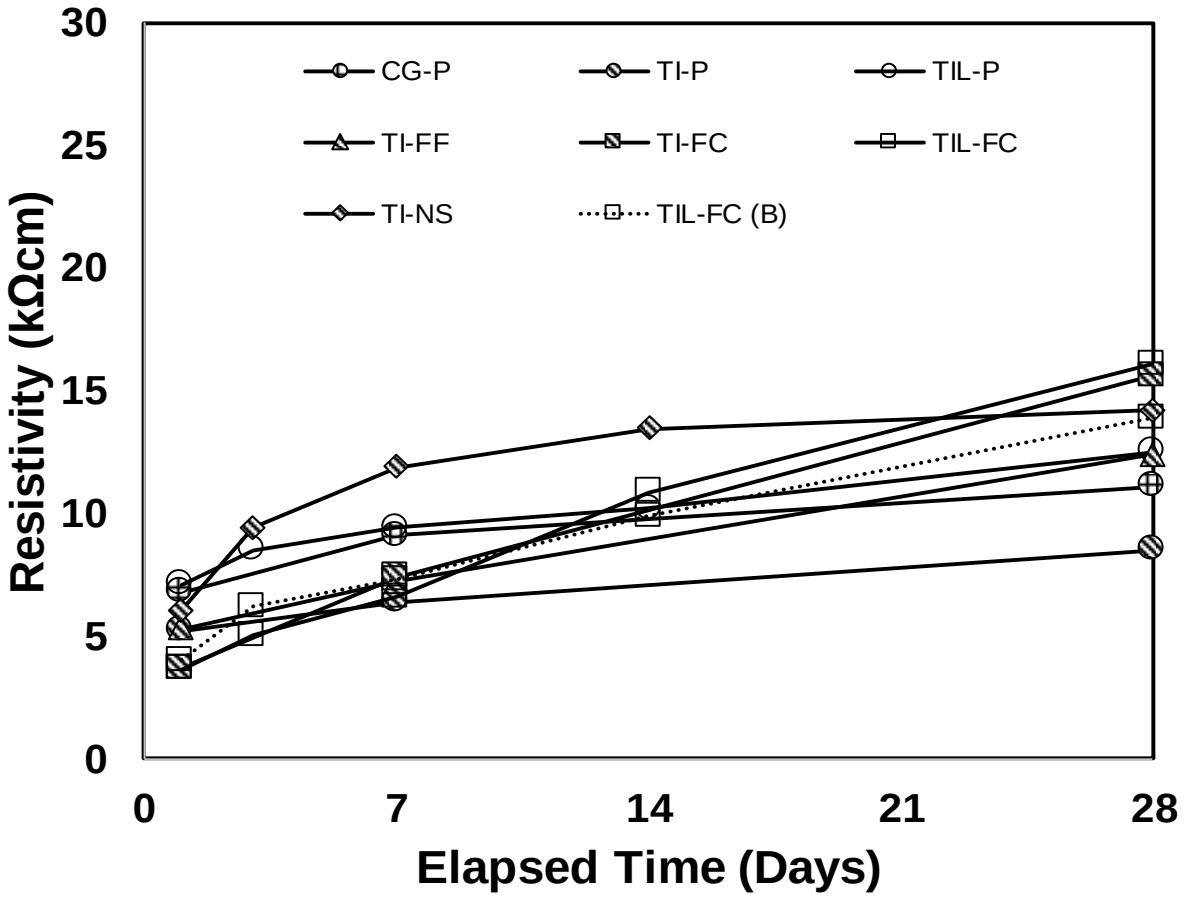

Figure 36. Resistivity for Experimental Program II

Figure 37 shows the drying shrinkage strain curves for the eight mixtures. Type I portland cement with 30% Class C fly ash has higher shrinkage strain than that without fly ash. This is consistent with previous literature (Munday et al.).

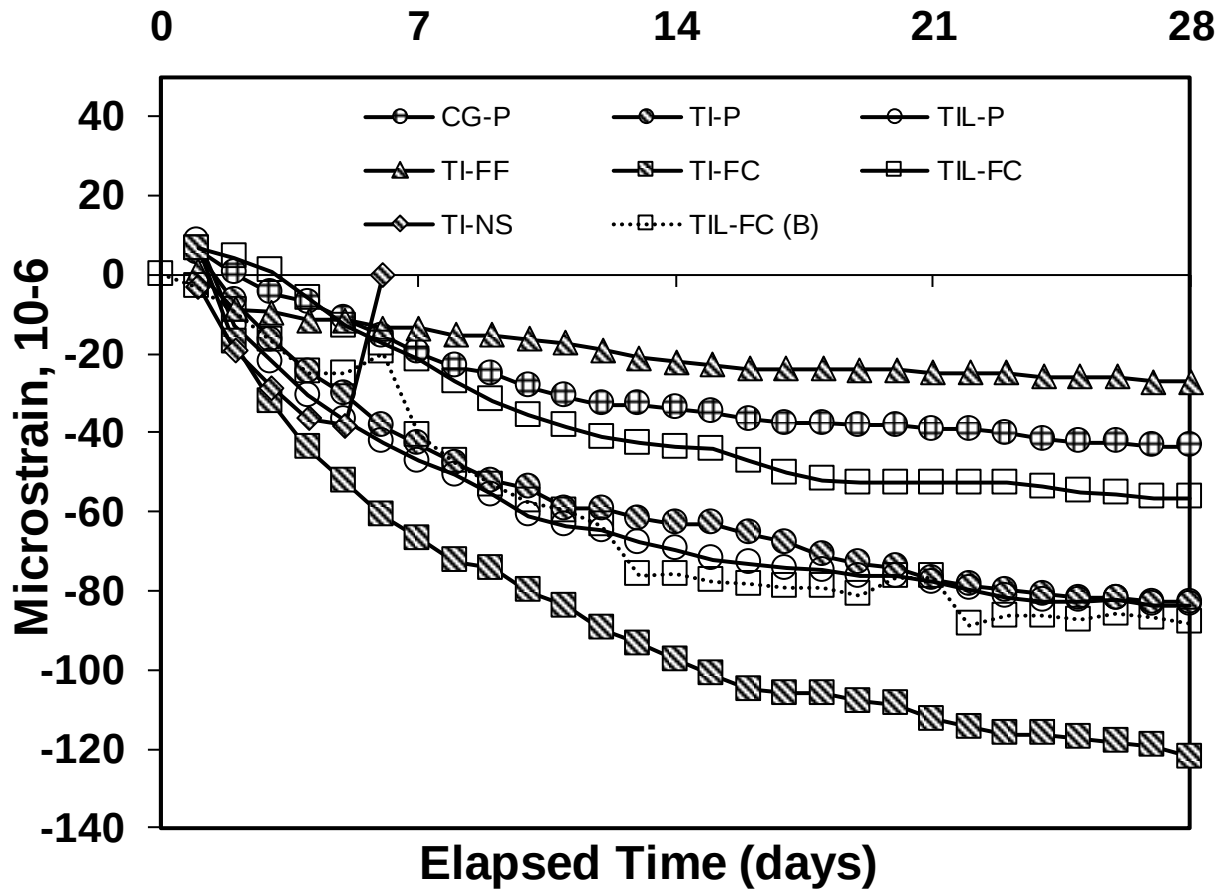

Figure 37. Restrained shrinkage strain for Experimental Program II

Cracks were observed in case of rings for TI-NS. This crack can also be inferred from the curve in Figure 37, where an abrupt change in the strain can be seen. However, such abrupt changes are not observed in case TIL-FC (B). Some residual strength is provided by the basalt fibers, likely by physically bridging cracks. Table 15 shows the stress rate of the mixtures as calculated from the shrinkage results.

Table 15. Potential for Cracking: Experimental Program II (ASTM C1581)

Mix	S (psi/day)	Cracking Potential
CG-P	11	Low
TI-P	20	Moderate Low
TIL-P	19	Moderate Low
TI-FF	6	Low
TI-FC	27	Moderate High
TIL-FC	16	Moderate Low
TI-NS	67	High
TIL-FC (B)	21	Moderate Low

Figure 38 shows the relationship between average porosity, as calculated through µ-CT and 28day resistivity. No clear trends are observed as may be expected because resistivity is dependent upon the permeability of concrete rather than porosity.

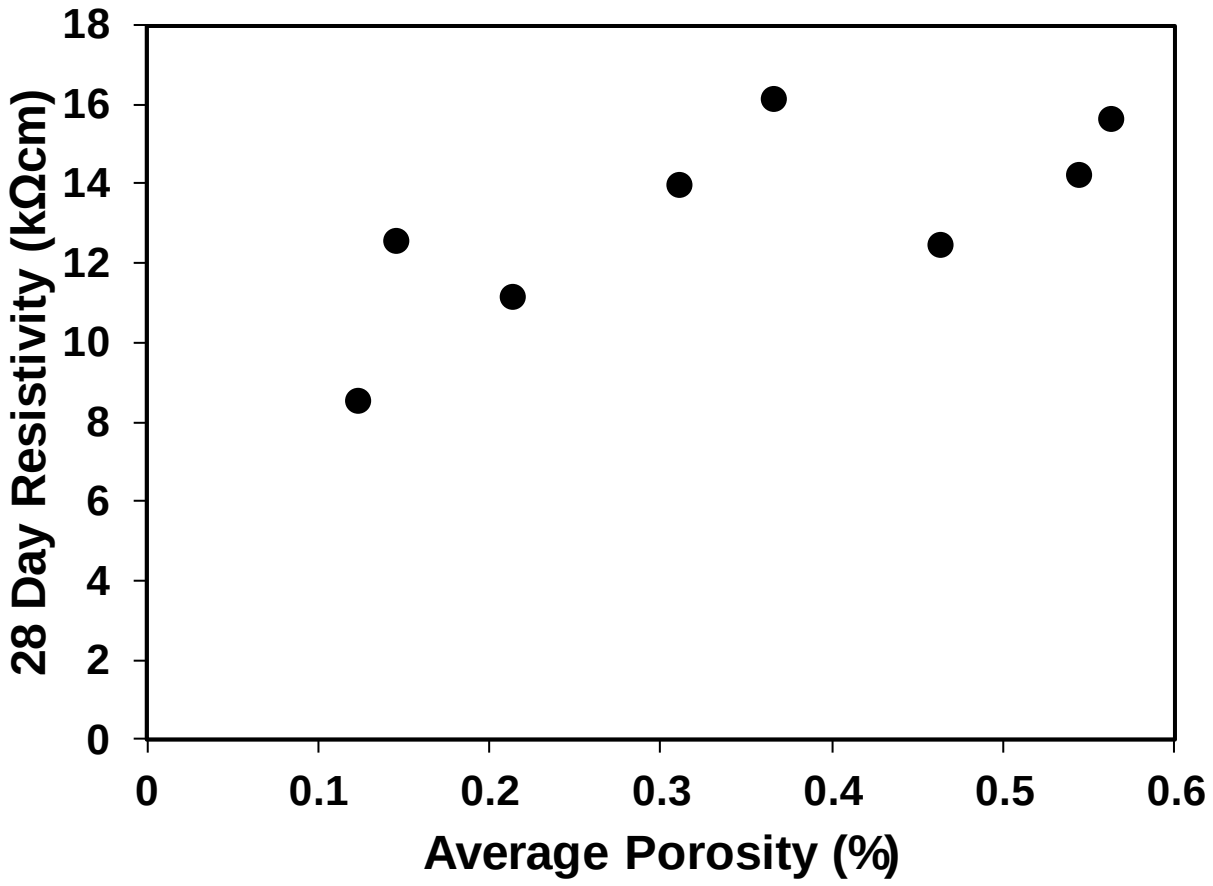

Figure 38. Average porosity and 28-day resistivity relationship

Figure 39 shows the crack density of the cementitious combinations. CG-P has the lowest crack density among all the mixtures. This is similar to Experimental Program I. It may be noticed that TIL-C (B) has a lower crack density than TIL-C. From Figure 40, it is also evident that micro-cracks are more concentrated near the center of the specimen. This is due to the hour glass shape of the mold maximizing stresses in the middle section of the specimen. It may be noticed that some cracks are stained with the blue dye, while others are not. This may be due to differences in depths of such cracks within the specimen. If allowed to dry further, shallower cracks would grow into deeper micro-cracks, and the propagation of a system of such cracks would ultimately lead to bigger cracks.

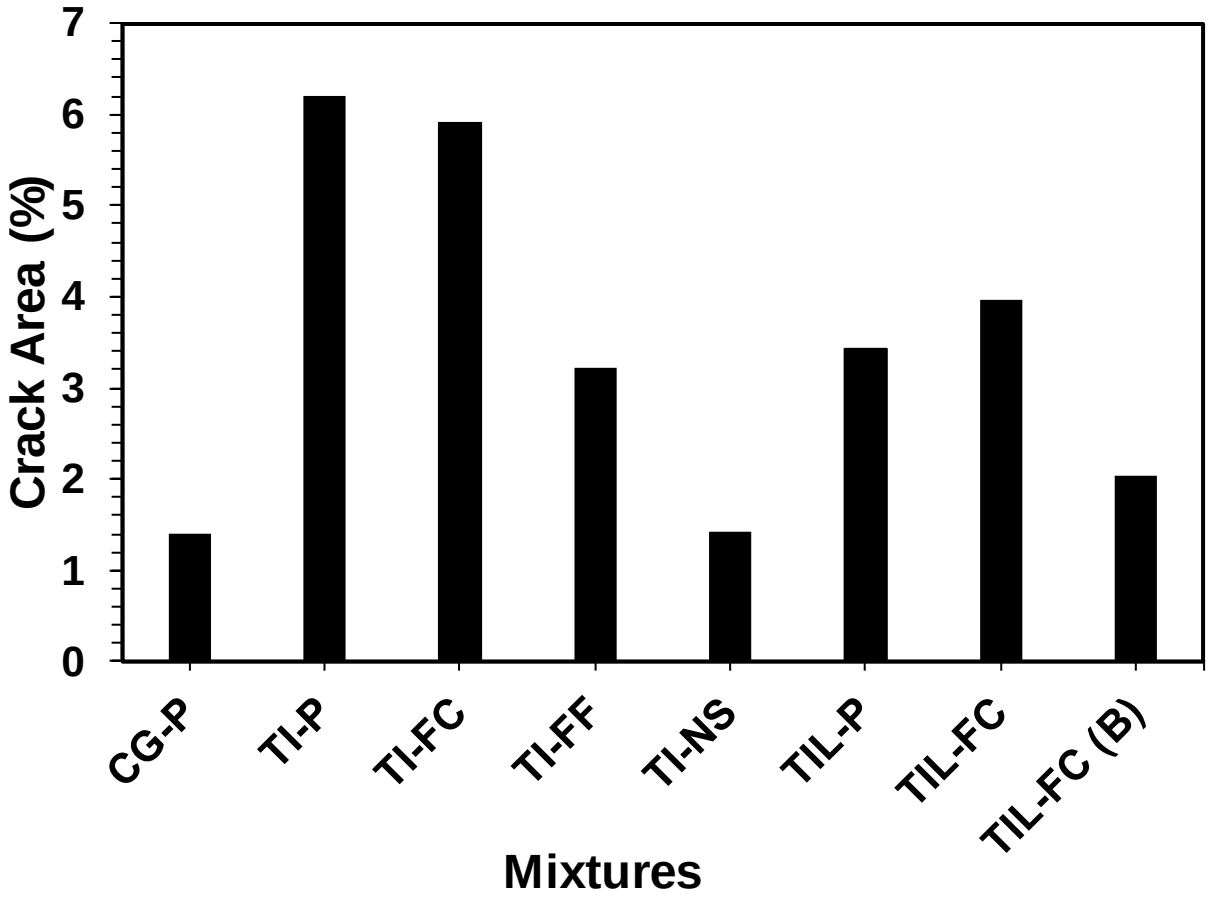

Figure 39. Crack density of mixtures from Experimental Program II

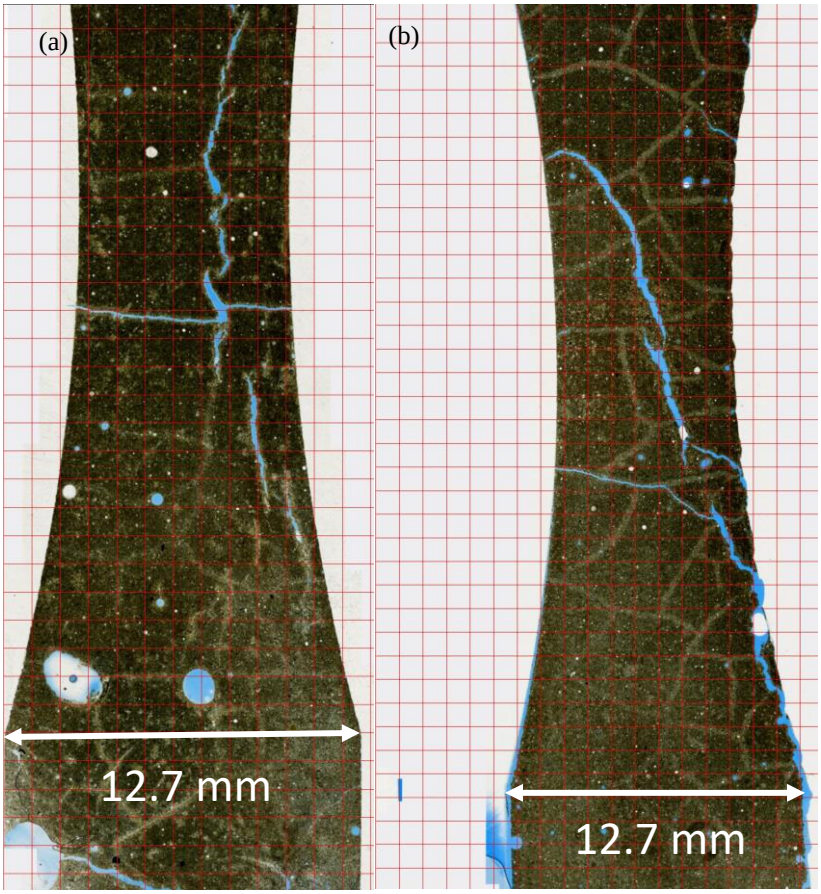

Figure 40. Micro-crack analysis of (a) TIL-FC (B), and (b) TIL-FC

Figure 41 shows the relationship between crack density and stress rate. As observed in Experimental Program I, in this case also there may be a relationship between the two parameters. There may be a possibility of substituting the conventional ring test by ASTM C1581 with this technique of micro-crack detection and quantification. This will be a cheaper and less labor-intensive method with disposable and easily reproducible molds. However, further quantitative investigation is required with a higher number of replicates to validate this hypothesis.

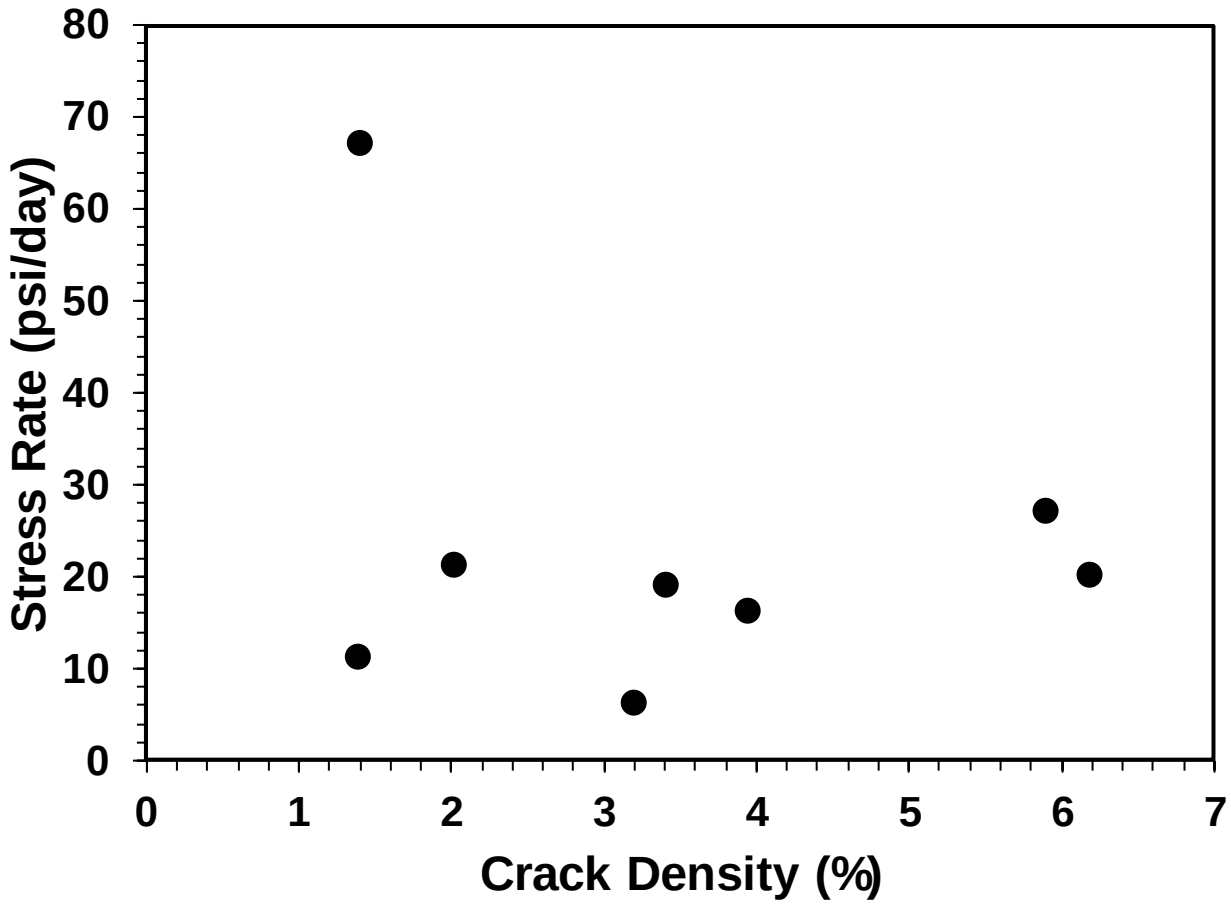

Figure 41. Crack density and stress rate relationship for Experimental Program II

Figure 42 shows the Ca/Si ratio results obtained through XPS. Lower Ca/Si ratio may indicate higher amounts of calcium silicate hydrate (C-S-H) (Wang 2011). That means, the degree of hydration is higher. This indicates a higher consumption of alite and belite to form C-S-H and calcium hydroxide (CH). CH further reacts with Silica from pozzolans like fly ash to form additional C-S-H (Escalante-Garcia, Mendoza and Sharp 1999). TIL-FC had the lowest Ca/Si ratio (Figure 42a). This can be expected as fly ash helps in prolonged hydration of concrete. From Figure 18b, it may be observed that shrinkage strain decreased with increasing Ca/Si ratio. A higher Ca/Si ratio may lead to reduced size and volume of gel pores in C-S-H. As a result, the removal of interlayer water will be more difficult and the risk of shrinkage may be reduced (Selvam et al. 2009, Wang 2011).

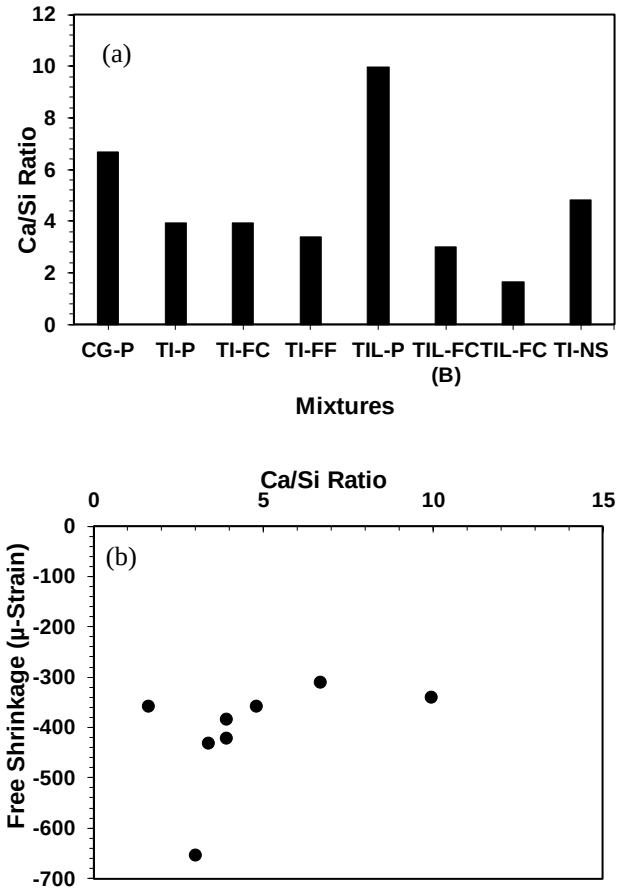

Figure 42. Ca/Si ratio

4.5. Conclusions

In this study, potential relationships between micro-cracking of paste samples from different cementitious combinations and drying shrinkage strain of concrete were investigated. The following are the key conclusions from this study:

- Micro-cracks can be analyzed by identifying vulnerable regions of a paste sample by µ-CT, and epoxy impregnation and suitable sample preparation at such key regions followed by observation through a confocal microscope.
- Porosity distribution from Experimental Program I revealed that high porosity regions exist near the surface of the specimen.

- Type IL portland limestone cement with 30% Class C fly ash (TIL-FC) had high electrical resistivity likely due to an improved particle packing.
- Concrete containing coarse ground cement (CG-P) had low shrinkage; its corresponding cement paste sample had low crack density.
- Basalt fibers had likely provided post-cracking residual strength to concrete as observed from drying shrinkage strain under restraint.
- There may be a relationship between crack density and stress rate from drying shrinkage; such relationships need to be validated further with more investigations.
- Shrinkage strain decreased with increasing Ca/Si ratio. This may be due to a reduction of size and volume of gel pores with an increase in Ca/Si ratio and likely reduction in the removal of interlayer water.

4.6. Acknowledgement

This paper is based upon work supported by the U. S. Department of Energy under Award No.DE-EE0007246. The authors also acknowledge Mr. Robert Steffes for his constant support and insight.

4.7. Disclaimer

Any findings, opinions, and conclusions or recommendations expressed in this report are those of the author(s) and do not necessarily reflect the views of the Department of Energy.

4.8. References

ASTM. (2015). “Standard Specification for Blended Hydraulic Cements.” C595/C595M-15, West Conshohocken, PA

ASTM. (2016). “Standard Specification for Portland Cement.” C150/C150M-16e1, West Conshohocken, PA.

ASTM. (2012). “Standard Test Method for Bulk Electrical Conductivity of Hardened Concrete.” C1760-12, West Conshohocken, PA

ASTM. (2014). “Standard Test Method for Length Change of Hardened Hydraulic-Cement Mortar and Concrete.” C157/C157M-08, West Conshohocken, PA.

ASTM. (2018). “Standard Test Method for Determining Age at Cracking and Induced Tensile Stress Characteristics of Mortar and Concrete under Restrained Shrinkage.” C1581/C1581M-18, West Conshohocken, PA.

Barrett, T., H. Sun, C. Villani, L. Barcelo & J. Weiss (2014) Early-age shrinkage behavior of Portland limestone cement. *Concrete international,* 36.

Bennett, E. W. & D. R. Loat (1970) Shrinkage and creep of concrete as affected by the fineness of Portland cement. *Magazine of concrete research,* 22**,** 69-78.

Bentz, D. P. (2010) Blending different fineness cements to engineer the properties of cement-based materials. *Magazine of Concrete Research,* 62**,** 327-338.

Bisschop, J. & J. G. M. Van Mier (2002a) Drying shrinkage microcracking in cement-based materials. *Heron, 47 (3), 2002*.

Bisschop, J. & J. G. M. Van Mier (2002b) How to study drying shrinkage microcracking in cement-based materials using optical and scanning electron microscopy? *Cement and concrete research,* 32**,** 279-287.

Bisschop, J. & J. G. M. van Mier (2008) Effect of aggregates and microcracks on the drying rate of cementitious composites. *Cement and Concrete Research,* 38**,** 1190-1196.

Branston, J., S. Das, S. Y. Kenno & C. Taylor (2016) Influence of basalt fibres on free and restrained plastic shrinkage. *Cement and Concrete Composites,* 74**,** 182-190.

de Sa, C., F. Benboudjema, M. Thiery & J. Sicard (2008) Analysis of microcracking induced by differential drying shrinkage. *Cement and Concrete Composites,* 30**,** 947-956.

Deshpande, S. S. (2007). *Evaluating free shrinkage of concrete for control of cracking in bridge decks*. University of Kansas.

Du Plessis, A., B. J. Olawuyi, W. P. Boshoff & S. G. Le Roux (2016) Simple and fast porosity analysis of concrete using X-ray computed tomography. *Materials and Structures,* 49**,** 553-562.

Gesoğlu, M., E. Güneyisi & E. Özbay (2009) Properties of self-compacting concretes made with binary, ternary, and quaternary cementitious blends of fly ash, blast furnace slag, and silica fume. *Construction and Building Materials,* 23**,** 1847-1854.

Haruehansapong, S., T. Pulngern & S. Chucheepsakul (2017) Effect of Nanosilica Particle Size on the Water Permeability, Abrasion Resistance, Drying Shrinkage, and Repair Work Properties of Cement Mortar Containing Nano-SiO2. *Advances in Materials Science and Engineering,* 2017.

Iyer, P., S. Y. Kenno & S. Das (2016) Performance of Fiber-Reinforced Concrete Made With Basalt-Bundled Fibers. *Advances in Civil Engineering Materials,* 5**,** 107-123.

Jiang, L. H. & V. M. Malhotra (2000) Reduction in water demand of non-air-entrained concrete incorporating large volumes of fly ash. *Cement and Concrete Research,* 30**,** 1785-1789.

Lomboy, G., K. Wang & C. Ouyang (2010) Shrinkage and fracture properties of semiflowable self-consolidating concrete. *Journal of Materials in Civil Engineering,* 23**,** 1514-1524.

Mehta, P. K. & R. W. Burrows (2001) Building durable structures in the 21 st century. *Indian Concrete Journal,* 75**,** 437-443.

Munday, J. G. L., L. T. Ong, L. B. Wong & R. K. Dhir. (1982). Load independent movements in opc/pfa concrete. 243-246.

Nath, P. & P. K. Sarker (2013) Effect of mixture proportions on the drying shrinkage and permeation properties of high strength concrete containing class F fly ash. *KSCE Journal of Civil Engineering,* 17**,** 1437-1445.

Quercia, G., P. Spiesz, G. Hüsken & H. J. H. Brouwers (2014) SCC modification by use of amorphous nano-silica. *Cement and Concrete Composites,* 45**,** 69-81.

Ramezanianpour, A. M. & R. D. Hooton (2014) A study on hydration, compressive strength, and porosity of Portland-limestone cement mixes containing SCMs. *Cement and Concrete Composites,* 51**,** 1-13.

Rashed, A. I. & R. B. Williamson (1991) Microstructure of entrained air voids in concrete, Part I. *Journal of materials research,* 6**,** 2004-2012.

Roper, H. (1974) Shrinkage, tensile creep and cracking tendency of concretes. *Australian Road Research,* 5.

Suksawang, N., A. Mirmiran & D. Yohannes (2014) Use of Fiber Reinforced Concrete for Concrete Pavement Slab Replacement. Transportation Research Board.

Taylor, P. & X. Wang (2014) Concrete Pavement Mixture Design and Analysis (MDA): Factors Influencing Drying Shrinkage.Iowa State University.

Tekin, I., R. Birgul, I. O. Yaman, O. Gencel & H. Y. Aruntas (2015) Monitoring macro voids in mortars by computerized tomography method. *Measurement,* 63**,** 299-308.

Tritsch, N., D. Darwin & J. Browning. (2005). Evaluating Shrinkage and Cracking Behavior of Concrete Using Restrained Ring and Free Shrinkage Tests. University of Kansas Center for Research, Inc.

Tsivilis, S., E. Chaniotakis, G. Batis, C. Meletiou, V. Kasselouri, G. Kakali, A. Sakellariou, G. Pavlakis & C. Psimadas (1999) The effect of clinker and limestone quality on the gas permeability, water absorption and pore structure of limestone cement concrete. *Cement and Concrete Composites,* 21**,** 139-146.

Tsuruta, H., H. Matsushita, K. Harada & T. Goto (2004) Effect of gypsum content in cement on autogenous shrinkage of portland blast-furnace slag cement concrete. *Special Publication,* 221**,** 683-702.

Wang, X. (2011). *Drying shrinkage of ternary blends in mortar and concrete*. Iowa State University.

Yio, M. H. N., M. J. Mac, H. S. Wong & N. R. Buenfeld (2015) 3D imaging of cement-based materials at submicron resolution by combining laser scanning confocal microscopy with serial sectioning. *Journal of microscopy,* 258**,** 151-169.

Zayed, A., A. Sedaghat, A. Bien-Aime & N. Shanahan (2014) Effects of portland cement particle size on heat of hydration. Florida Department of Transportation

Zerbino, R., G. Giaccio & S. Marfil (2014) Evaluation of alkali–silica reaction in concretes with natural rice husk ash using optical microscopy. *Construction and Building Materials,* 71**,** 132-140.

CHAPTER 5: CEMENT CHANGES TO PREVENT CONCRETE SHRINKAGE: LIFE CYCLE ANALYSIS AND LIFE CYCLE COST ANALYSIS

5.1. Abstract

In this paper, a life cycle assessment (LCA) and life cycle cost analysis (LCCA) have been performed on selected cementitious combinations. For LCA, the goal of this study is to estimate the emission of carbon dioxide (CO_2) into the environment from the production of a metric ton of cement by investigating these five different cementitious combinations. This is represented by the global warming potential (GWP) in CO_2 equivalent. The LCCA has been performed on an imaginary concrete bridge in Minnesota with the five different types of cementitious combinations for the concrete deck. A method of calculation of CO_2 emissions per unit weight of pure compounds produced during cement manufacture is adopted. Results obtained indicate that Type IL portland limestone cement with 30% Class C fly ash (TIL-FC) has the lowest emissions of CO_2 into the atmosphere. The comparison between total present worth of the five cementitious systems during the life cycle of the bridge reveals Type I portland cement with 30% Class C fly ash (TI-FC) has the lowest life cycle costs among the five scenarios. This work was supported by the US Department of Energy.

5.2. Introduction

One of the primary driving factors of climate change and global warming is emission of greenhouse gases (Montzka et al. 2011). Recent reports have indicated higher anthropogenic emissions of greenhouse gases globally than those from the past decades (Pachauri et al. 2014). The most critical greenhouse gas is carbon dioxide (CO_2) (Ramanathan and Feng 2009). CO_2 emissions from man-made sources, such as combustion of fossil fuel, industrial processes, and agriculture amounts up to 76% of the total greenhouse gases (Mikulčić et al. 2016). One of the

major anthropogenic sources of CO_2 emission is the manufacture of cement (Ali et al. 2011). Some parties have posited that cement industry contributes between 5 and 8 % (approximately) of global CO_2 emissions (Mikulčić et al. 2016). There are various mechanisms encompassing cement manufacturing which lead to emission of CO_2. The main contributing factors include calcination of limestone into calcium oxide, and combustion of fossil fuels (Ali et al. 2011). Therefore, if the amount of portland cement produced can be reduced, then significant reductions in CO_2 can be accomplished. To accomplish this goal of emission reduction, the cement industry may be inclined towards using products such as portland limestone cement (Type IL, ASTM C595), and/or partial replacement of portland cement with supplementary cementitious materials such as fly ash or slag to effectively reduce the amount of portland cement produced. Additionally, the use of pozzolanic materials, such as nanosilica can also be a good way to slightly reduce the use of portland cement. Use of such cementitious combinations may provide improvements in properties of concrete such as shrinkage (drying shrinkage, and plastic shrinkage). Other engineering properties of concrete such as compressive strength, and electrical resistivity may also be improved by appropriate changes in the cementitious system. One of the ways of assessing the reduction of carbon footprint is environmental life cycle assessment (LCA) (Huntzinger and Eatmon 2009). Life cycle assessment (LCA) is defined as the process of analyzing the life cycle of a particular product under purview from its inception to its disposal, from cradle to grave (Huntzinger and Eatmon 2009).

Portland cement concrete is one of the most widely used materials for the construction of structures because of the strength and durability and its maintenance costs (Mehta 1999). Concrete although strong in compression, is weak in tension and is prone to attack from chemicals. This can lead to loss of serviceability of concrete structures. Hundreds of billions of taxpayer dollars are spent every year to repair poor roads and bridge decks (Kendall et al. 2008). If longer lasting

concrete materials can be developed, the overall cost of maintenance might be reduced. Based on previous work by this research group, some alternatives have been identified.

One way of investigating the cost associated with a product is Life Cycle Cost Analysis (LCCA). Unlike LCA described earlier, Life cycle cost analysis (LCCA) is a technique used to analyze the efficiency of cost during the life cycle of a product. LCCA can be used to compare between total life cycle costs of alternative products (ACPA 2012). In this process, potential costs of a product, such as installation costs, and repair and maintenance costs are taken into consideration. In the case of construction projects, an LCCA typically consists of some or all of the following self-explanatory steps (ACPA 2012; Walls and Smith 1998):

- Selection of analysis period
- Selection of a discount rate
- Estimation of initial agency costs
- Estimation of user costs
- Estimation of future agency costs
- Estimation of residual value
- Comparison of net present value of alternatives

In this work, LCA and LCCA have been performed on five cementitious combinations: coarse ground cement, Type I/II cement with 20% Class F fly ash replacement, Type I cement with 30% Class C fly ash replacement, Type IL cement (portland limestone cement) with 30% Class C fly ash replacement, and Type I cement with 5% nanosilica replacement. For LCA, the goal of this study is to estimate the emission of CO_2 into the environment from the production of a metric ton of cement by investigating these five different cementitious combinations. This is represented by the global warming potential (GWP) in CO_2 equivalent. The LCCA has been

performed on an imaginary concrete bridge in Minnesota with the five different types of cementitious combinations for the concrete deck.

5.3. Background

5.3.1. Shrinkage

Volume changes or shrinkage in concrete can be a significant contributor to cracking, and therefore loss of serviceability of concrete (Deshpande 2007). Shrinkage may be defined as the volume changes resulting from loss of water from capillary pores within the concrete system. This loss can be typically due to various environmental factors and desiccation associated with hydration (Taylor and Wang 2014). Shrinkage may also occur as a result of differential heat due to hydration between the surface and interior of massive concrete structures. When concrete is restrained, volume changes are restricted, therefore, tensile stresses are developed that may lead to fracture (Deshpande 2007). Concrete shrinkage may be of different forms (autogenous, chemical, thermal, plastic, and drying). For concrete with a water to cementitious materials ratio above 0.42, the predominant type of shrinkage is drying shrinkage (Tritsch et al. 2005).

A means of limiting shrinkage is to adjust the composition of the mixture. Concrete consists of cement paste (cementitious materials, water and chemical admixtures), aggregates and air. Paste is more prone to volume changes than aggregates. Factors such as fineness of cement, and chemical composition influence shrinkage of cement paste (Bentz 2010). Coarser cements are reported to shrink less, while increasing tri-calcium aluminate (C_3A), and alkali content can lead to greater shrinkage (Zayed et al. 2014). As the concrete industry has moved towards faster reacting cementitious systems, the risk of shrinkage cracking has arguably increased (Mehta and Burrows 2001). Although the solution may seem to be to use coarser cementitious systems with lower C_3A and alkali contents, this might adversely affect the speed of construction. This research

group has sought to investigate reducing shrinkage and associated cracking with by including blended cementitious systems. Engineering performance of these mixtures has been reported elsewhere (Sirotiak 2016).

5.3.2. Greenhouse Emissions

Some of the key compounds identified as greenhouse gases are carbon dioxide (CO_2), methane (CH_4), and nitrous oxide (N_2O), contributing towards global warming at 60%, 15%, and 5% respectively (Ipc 1996). The impact of these gases upon the environment can be assessed by a parameter called Global Warming Potential (GWP). According to US EPA, GWP can be defined as the amount of energy absorbed due to the emission of a ton of a substance (typically gas), relative to the emission of a ton of CO_2. From a perspective of agriculture, the following relation has been presented for by a research group (Bhatia et al. 2007):

$$GWP = CO_2 \text{ emission} + CH_4 \text{ emission} \times 21 + N_2O \text{ emission} \times 310 \quad (5.1)$$

Anthropogenic CO_2 is the major component of global warming which may ultimately lead to a rise in mean sea level (Solomon et al. 2009). One of the major anthropogenic sources of CO_2 is the process of cement manufacture (Ali et al. 2011). This CO_2 emission is mainly from the process of calcination and burning of fuel for electrical and thermal use.

5.3.3. Portland Cement

Portland cement is a grey colored fine powder comprising of a mixture of the compounds tricalcium silicate (alite), dicalcium silicate (belite), tricalcium aluminate, and tetracalcium aluminoferrite. These elements typically have calcium sulfate (gypsum) to make cement. Portland cement, consisting primarily of hydraulic calcium silicates hardens by reacting chemically with water. Silicates in portland cement hydrate to form calcium silicate hydrates which constitutes the glue called paste. This paste binds coarse and fine aggregates together to form concrete. Cement

normally constitutes 7% to 15% of the concrete's total mass by weight (Marceau et al. 2006). Cement is the main contributor of anthropogenic carbon dioxide into the environment in among all the ingredients of concrete.

5.3.3.1. Cement Manufacture

The process of cement manufacture can be divided into multiple steps: quarry and crush, raw meal preparation, pyro-process, and finish grind (Marceau et al. 2006). The first step is raw material acquisition by quarrying and crushing. Calcium is the element of highest concentration in portland cement. The most common source of calcium is limestone. According to ASTM C150, limestone in cement should consist of at least 70% of $CaCO_3$. Other major raw materials like clay, sand, and iron ore are acquired in this step. These raw materials are quarried or mined and transferred to the manufacturing facility for crushing and grinding (Huntzinger and Eatmon 2009). The next step is to send the crushed and milled powder to a rotary kiln where materials reach temperatures greater than 1400 °C (Huntzinger and Eatmon 2009).

There are wet and dry process portland cement plants. In the wet process, a pumpable slurry is formed by suspending the ground raw materials in water. These plants contain rotary kilns. On the other hand, in the dry process, the crushed and milled powder from raw materials is dried to a flowable powder. Dry processes employ simple rotary kilns and have higher thermal efficiency (Marceau et al. 2006).

The rotary kiln is an inclined steel tube lined with refractory materials, which rotates slowly. The raw meal prepared from the wet or dry process is converted into clinker in the rotary kiln at a very high temperature (1400 °C). This process is called pyro-process. The enormous heat in the kiln is generated by burning predominantly coal in the United States. The output from this step is clinker. It is allowed to cool through a clinker cooling device and the cooled clinker is

mixed with the previously described gypsum (calcium sulfate). The mixture is then ground in ball or tube mills to produce portland cement. This step is called finish grinding (Marceau et al. 2006).

5.3.3.2. Carbon dioxide Emissions from Portland Cement

As mentioned earlier, CO_2 emissions from the process of portland cement manufacture can be divided into two categories: CO_2 converted from carbon rich compounds in the raw materials (e.g. calcination of limestone), and CO_2 emitted due to combustion of fossil fuels necessary to drive the manufacturing process (Gartner 2004). Calcination can be defined as the process of conversion of calcium carbonate ($CaCO_3$) to lime (CaO) and emitting carbon dioxide (CO_2). This can be represented stoichiometrically by the following equation (Hendriks et al.):

$$CaCO_3 \rightarrow CaO + CO_2 \quad (5.2)$$

In this process, 1 kg of $CaCO_3$ converts into 0.56 kg of CaO and 0.44 kg of CO_2. The bulk of the CO_2 produced in the process of cement manufacture is from the process of calcination (Marceau et al. 2006). The emissions from burning of fossil fuels differ from process to process. A small proportion of CO_2 is also contributed by the movement of mobile equipment and associated fuel burning (Mikulčić et al. 2016). In this paper, this component has been assimilated into the overall category of burning of fossil fuels.

5.3.4. Sustainability

According to World Commission on Environment and Development (Wced 1987), sustainability may be defined as “development that meets the needs of the present without compromising the ability of future generations to meet their own needs”. It means that new developments to technology need to be focused towards imposing the least possible adverse impacts on future needs, and at the same time fulfilling the goals and needs of the present. Sustainability can be made of three components: environmental, social, and economic (Harvey et

al. 2016). Traditionally, economic sustainability of processes and products were mainly focused upon. However, the importance of environmental and social sustainability has been identified in the recent years (Van Dam et al. 2015). The ill effects of CO_2 emissions into the environment due to concrete, predominantly by the portland cement used, have been well documented (Gartner 2004; Huntzinger and Eatmon 2009; Mikulčić et al. 2016; Monteiro et al. 2017).

5.3.4.1. Life Cycle Assessment (LCA)

One way of measuring environmental sustainability of a product is life cycle assessment (LCA). Life cycle assessment (LCA) may be defined as a tool to assess and quantify the impact of a product or process on the environment (Harvey et al. 2016). In this process, all potential inputs and outputs are taken into consideration and emissions are calculated. An approach of analysis of a product from acquisition of raw materials to end of life is called *cradle to grave*. Alternately, analysis can be made from acquisition of raw materials to the end of a process, which may not mark the end of life of the product under consideration. Such an approach is called *cradle to gate*. For example, the life cycle assessment (LCA) of portland cement during manufacture can be considered as a cradle to gate process.

LCA is conducted according to the specifications of ISO (International Organization for Standardization) 14040 (International Standard 1997). According to ISO 14040, an LCA consists of a life cycle inventory analysis (LCI) phase, and a life cycle impact assessment (LCIA) phase. An LCI is defined as a compilation of material and energy inputs, and emissions to the environment associated with a process or a step in the manufacture of a product (Marceau et al. 2006). LCIA is the assessment of potential impacts of the various processes involved during the life cycle of the product.

5.4. Methods

5.4.1. Life Cycle Assessment (LCA)

The LCA methodology followed in this study is according to the following predefined stages by ISO 14040 (International Standard 1997).

1. Determination of scope and boundaries
2. Selection of inventory for inputs and outputs (LCI)
3. Life cycle inventory assessment (LCIA)
4. Interpretation of Results

5.4.1.1. Scope and Boundaries

The scope of this study focusses on the raw material acquisition through quarrying and crushing, raw meal preparation, pyroprocess, and finish grind (Figure 43). In other words, this analysis is limited to the manufacture of portland cement. Therefore, this is termed as a cradle-to-gate analysis. The functional unit of this LCA has been considered to be 1 metric ton (Huntzinger and Eatmon 2009).

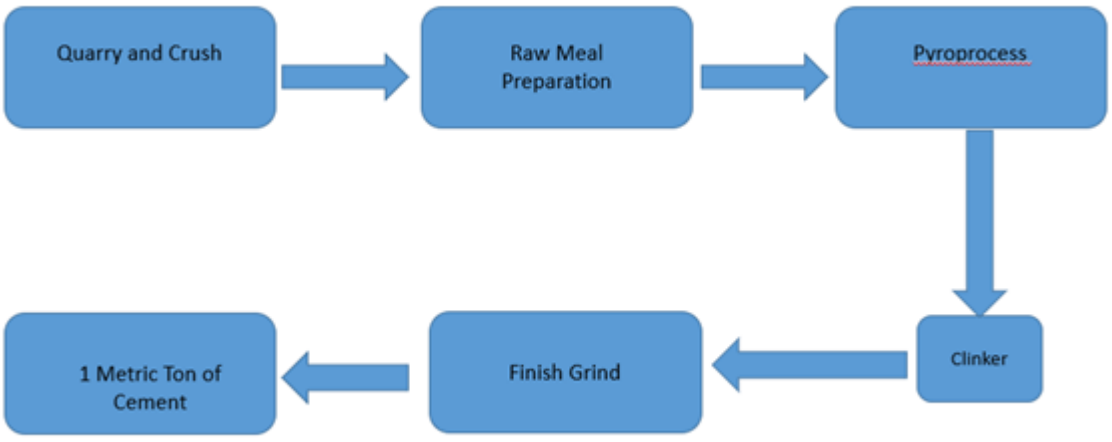

Figure 43. Manufacture of Portland Cement

5.4.1.2. Life Cycle Inventory

In this study, an LCA has been performed on five cementitious systems: coarse ground cement (CG-P), Type I/II cement with a 20% replacement with Class F fly ash (TI/II-FF), Type I cement with a 30% replacement with Class C fly ash (TI-FC), Type IL cement with a 30% replacement with Class C fly ash (TIL-FC), and Type I cement with a 5% replacement with colloidal nanosilica (TI-NS). Input quantities have been acquired from previous literature (Huntzinger and Eatmon 2009; Keller et al. 2013; Marceau et al. 2006; Santero et al. 2011). Additionally, some of the information was also acquired from mill certificates of the four different cement types used. Fly ash has been assumed to have no impact on CO_2 emissions.

Some of the major raw materials considered for this study are limestone, clay, sand, and iron ore. Other raw materials such as shale, slate, and blast furnace slag have not been considered due to their relatively low percentages, as preferred by previous studies (Huntzinger and Eatmon 2009). The CO_2 emissions in the pyroprocess step have been calculated by a methodology recommended by Greenhouse Gas Protocol. Clinker too cement ratio has been adjusted based on the percentage of blend with other materials. For example, the clinker to cement ratio for CG-P would be 0.951, while that for TI/II-FF has been calculated as 0.76.

It may be noted that this cementitious combination is a commonly used standard mix for pavements in the states of North Dakota and Minnesota, as confirmed by industry collaborators. LCA calculations have been made by using a software GaBi for TI-FC. This is followed by a spreadsheet based method of calculating life cycle CO_2 emissions. Comparisons have been made at the end between emissions by all the five cementitious combinations.

5.4.2. Life Cycle Cost Analysis

For comparison purposes, a life cycle cost analysis (LCCA) was conducted on an imaginary bridge in Minnesota. The bridge comprises two lanes, each lane 12 feet wide, and 12 inches deep. The length of the bridge is 528 feet. Pile foundations 120 feet in depth have been used for the bridge project. Two pairs of 45 feet tall piers support the span of the bridge. This is an extradosed bridge, in lines with the St. Croix river bridge in Minnesota (DOT). The loads on the bridge deck are also supported by 8 HDPE (High Density Poly Ethylene) steel stay cables spanning on either side of each pier. The stay cables are attached at a slope of 1/15 (1 part vertical : 15 part horizontal) (Stroh 2014). This framework is used to perform cost calculations with five different deck concrete scenarios described above The life cycle cost analysis performed on these five alternatives was based on the following steps (ACPA 2012):

5.4.2.1. Step 1: Selection of Analysis Period

The analysis period is the timeframe over which costs are calculated. The recommended analysis period for highways in the state Minnesota is 50 years or more, respectively (ACPA 2012; Rangaraju et al. 2008), therefore, an analysis period of 60 years was chosen.

5.4.2.2. Step 2: Selection of a Discount Rate

Real discount rate is the rate of change of true value of money over time. This rate takes into account fluctuations in both investment interest rates and the rates of inflation (ACPA 2012). In the absence of a recommended discount rate, it is recommended that the values should be chosen based on the United States Office of Management and Budget's (OMB) recommendations (Kendall et al. 2008). In this study, a real discount rate of 0.93% has been chosen. This value reflects the average real discount rate for the past three years.

5.4.2.3. Step 3: Estimation of Initial Agency Costs

Initial costs incurred by the agency may include initial design, construction and inspection costs (ACPA 2012). Other costs such as, maintenance and rehabilitation costs will be considered in latter steps. The initial agency costs have been estimated based on cost estimates of a bridge over St. Croix River in Minnesota, built in 2006. The cost of concrete has been considered to be the same for four of the five cementitious systems, except the mix with nanosilica, based on industry recommendations. Nanosilica has a higher cost of purchase which makes the mix containing nanosilica more expensive, as shown later.

5.4.2.4. Step 4: Estimation of User Costs

User costs typically consist of three types: traffic delay, increased risk of traffic crashes, and increased vehicle operating costs due to construction (Kendall et al. 2008). Since, the impacts of user costs can be expected to be similar for all scenarios, user costs were not considered in this study.

5.4.2.5. Step 5: Estimation of Future Agency Costs

During the analysis period, periodic maintenance and rehabilitation work will be required. For this analysis, maintenance work was patching, and rehabilitation was a 6" overlay, or deck replacement. Potential costs have been based on estimated unit costs by industry collaborators. The period from initial construction completion to deck replacement has been calculated based on the following relation

$$N_{DR} = 0.53(0.3A + 0.3B + 0.1C + 0.3D) \tag{5.3}$$

$$N_{DO} = {}^{N_{DR}}/_{2} \tag{5.4}$$

$$N_{P} = {}^{N_{DR}}/_{6} \tag{5.5}$$

Where,

N_{DR} = Number of years before deck replacement

N_{DO} = Number of years before deck overlay

N_P = Number of years before patching

A = Percent improvement of 28 day resistivity over a threshold value of 10 kΩcm

B = Percent improvement of stress rate (S) of restrained shrinkage over a threshold value of 70 psi/day

C = Percent improvement of maximum plastic shrinkage strain over a threshold of $8.5x10^{-4}$ strain

D = Percent improvement of 28 day compressive strength over a threshold of 4000 psi.

The timelines for the five different scenarios have been selected based on practicable schedules over the analysis period of 60 years.

5.4.2.6. Step 6: Residual Value

Typically, residual value calculations are made to account for the remaining functionality of the product at the end of its life. Residual value may be defined as the net value of a product at the end of its life, if it is recycled or salvaged (Rangaraju et al. 2008). In this analysis, it was assumed that there was no residual life of the structure after the analysis period of 60 years.

5.4.2.7. Step 7: Comparison of Net Present Value of Alternatives

The five alternatives in this study have been compared with a common measure of economic worth. Net present worth is the discounted equivalent of future maintenance and rehabilitation costs calculated on the basis of the real discount rate (ACPA 2012). This method is

used by many states across the United States, including the state of Minnesota. Present worth is calculated by the following equation:

$$\$P = \$F \times \frac{1}{(1+d)^t} \qquad \text{(ACPA 2012)} \qquad (5.6)$$

Where,

$P = Present value or worth

$F = One-time future cost

d = Real discount rate

t = the year in which one-time future cost occurs.

5.5. Results and Discussions

5.5.1. Life Cycle Assessment

5.5.1.1. Life Cycle Impact Assessment

Impacts of portland cement during the life cycle of production can be regional or global. Environmental impacts may include noise, and air pollution. Air pollution is brought about by greenhouse gas emissions. Such gases include sulfur dioxide (SO_2), nitrogen oxides (NO_X), and carbon dioxide (CO_2). This study is focused only on CO_2 as it is the predominant greenhouse gas in the production of cement. Figure 44 shows the CO_2 equivalent emitted in different stages of portland cement production for TI-FC. Noticeably, more than half of the emissions are in the pyroprocess stage where CO_2 is produced from $CaCO_3$ by the process of calcination. CO_2 emission from raw meal preparation, and minor emissions in quarrying and crushing stages, are mainly due to direct and indirect (electricity consumption) burning of fossil fuels.

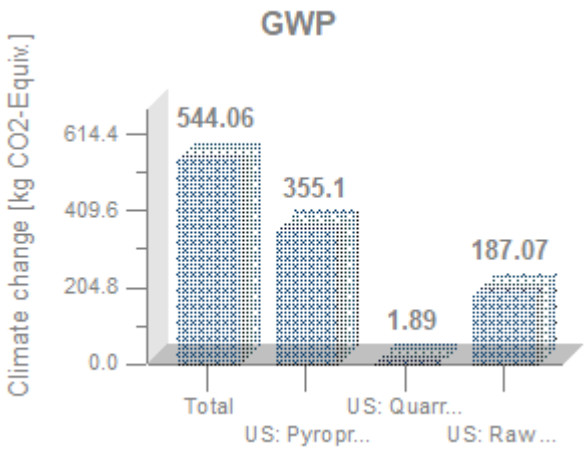

Figure 44. CO_2 Emissions Per Metric Ton of TI-FC

For the sake of comparison between the five cementitious combinations, calculations were made through linked spreadsheets to find CO_2 emissions from calcination, and those from burning fuel.

Table 16 shows the CO_2 emissions due to calcination during pyroprocess. It is evident that the clinker to cement ratio has significant impact on the emission of CO_2.

Table 16. CO_2 Emissions due to Calcination

Mix	CG-P	TI/II-FF	TI-FC	TIL-FC	TI-NS
Clinker to Cement Ratio (%) **A**	0.95	0.76	0.67	0.60	0.90
Ton of Raw Material per Ton of Clinker **B**	1.62	1.62	1.62	1.62	1.62
$CaCO_3$ Equivalent Raw Material Ratio (%) **C**	0.66	0.66	0.68	0.70	0.68
CO_2 to $CaCO_3$ Stoichiometric Ratio **D**	0.44	0.44	0.44	0.44	0.44
CO_2 Emitted per 1000 kg of Cement (kg) **(AxBxCxD)1000**	**446.57**	**356.88**	**321.12**	**298.93**	**435.79**

Figure 45 shows the comparison between emissions from the five mixes. CG-P has been shown to emit the highest amount of CO_2, while TIL-FC has the lowest. It may be noted that although coarse ground cement requires less grinding energy in the finish grind stage, total emissions in this stage are less than 1 kg per metric ton of cement produced. Therefore, such reductions have been ignored in this study. Additionally, it is assumed that there will be a contribution of about 1 kg of CO_2 per metric ton of cement in case of TI-NS, due to manufacturing cost of nanosilica (Keller et al. 2013).

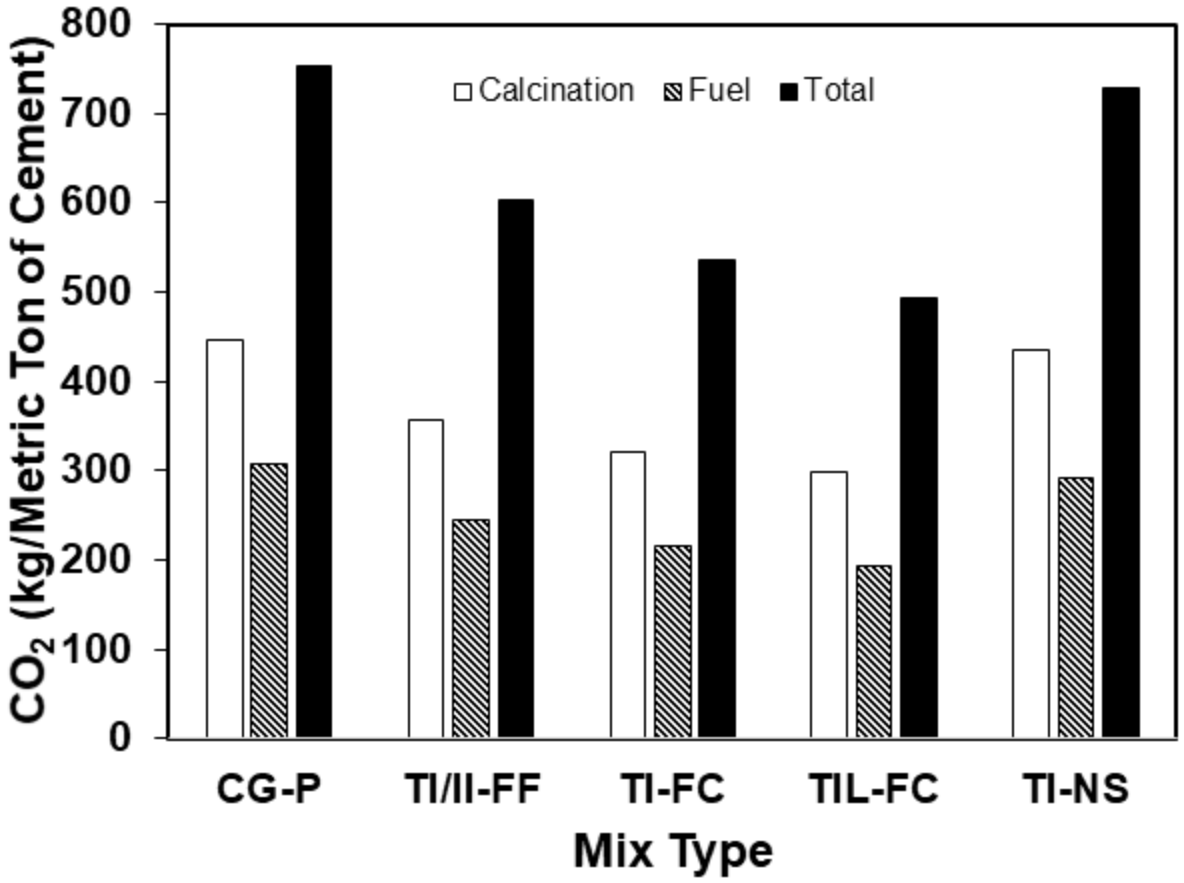

Figure 45. Comparison Between CO_2 Emissions from All Five Mixes

It has been reported in the past that it is very difficult to estimate the emissions due to burning of fossil fuels during the process of cement manufacture (Loijos, Santero and Ochsendorf 2013, Huntzinger and Eatmon 2009, Gartner 2004). Therefore, the reliability of such number is

sometimes questionable. Therefore, an alternative way to estimate CO_2 emissions due to burning of fuels was proposed by Gartner et.al. (Gartner 2004). In this method, the CO_2 produced during the production of a unit mass of pure cement compounds ($RMCO_2$) can be considered. $RMCO_2$ stands for raw mass of carbon dioxide. These quantities can be found from the mill certificates of the cement type used.

Table 17 shows the calculations for $RMCO_2$ of TI-FC. Noticeably, the total of 344.90 kg is higher than that calculated by the previous mentioned method (214.90 kg). Figure 46 consists of the comparison made by this method for all the mixes. It is evident that in four out of five cases, the $RMCO_2$ content is higher than CO_2 due to calcination.

Table 17. CO_2 Emissions from the Manufacture of Pure Cement Compounds for TI-FC

Cement Compounds	% in Cement	Mass in a ton of Cement (kg)	$RMCO_2$ (kg)
MgO	2.80	28.00	30.58
C_3S	60.00	600.00	346.80
C_2S	9.00	90.00	45.99
C_3A	9.00	90.00	44.01
C_4AF	7.00	70.00	25.34
Total	87.80	878.00	492.72
% Replacement with Fly Ash C			RMCO2 (kg)
30			**344.90**

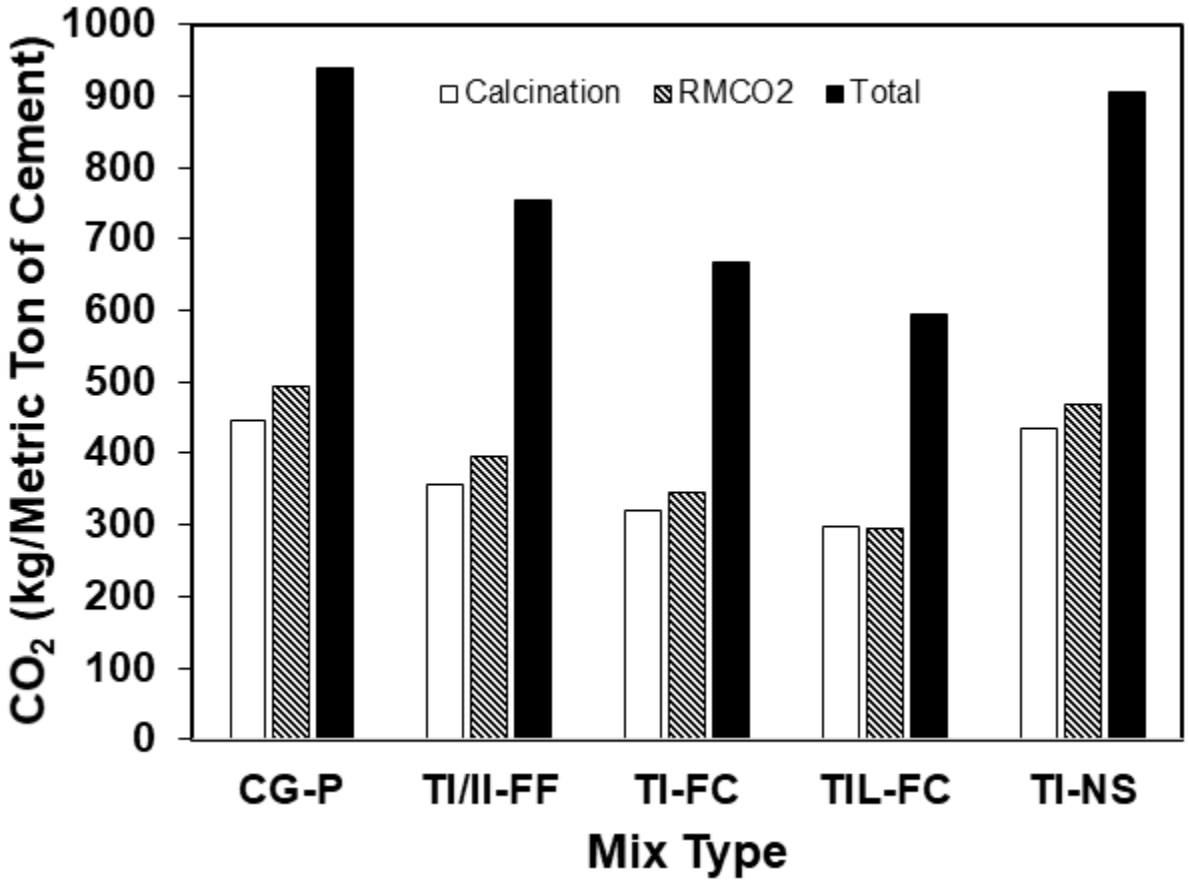

Figure 46. Comparison with Compounds Method

5.5.1.2. Interpretation and Recommendations

The comparisons between life cycle CO_2 emissions by both the reported methods reveal that TIL-FC has the lowest emissions among the five mixes. This is mainly because of a higher partial replacement percentage of portland cement by interground limestone and blended fly ash. These five mixes were chosen for analysis based on similar engineering properties. Based on the results from this study, it is recommended that blending of portland cement with supplementary cementitious materials is encouraged.

5.5.2. Life Cycle Cost Analysis

Based on the methodology followed in the above section, the total present worth calculations have been made and the comparison between the five scenarios containing five

cementitious mixes have been presented in Figure 47. TI-NS evidently is the most expensive alternative among the five. This is mainly due to the high initial cost of using nanosilica in concrete. The life cycle cost of TI-FC has been estimated to be the lowest. TIL-FC and TI/II-FF have shown similar results for life cycle cost equated to total present worth. CG-P costs are higher than TI-FC, TIL-FC, and TI/II-FF. Individual cases are discussed in greater detail below:

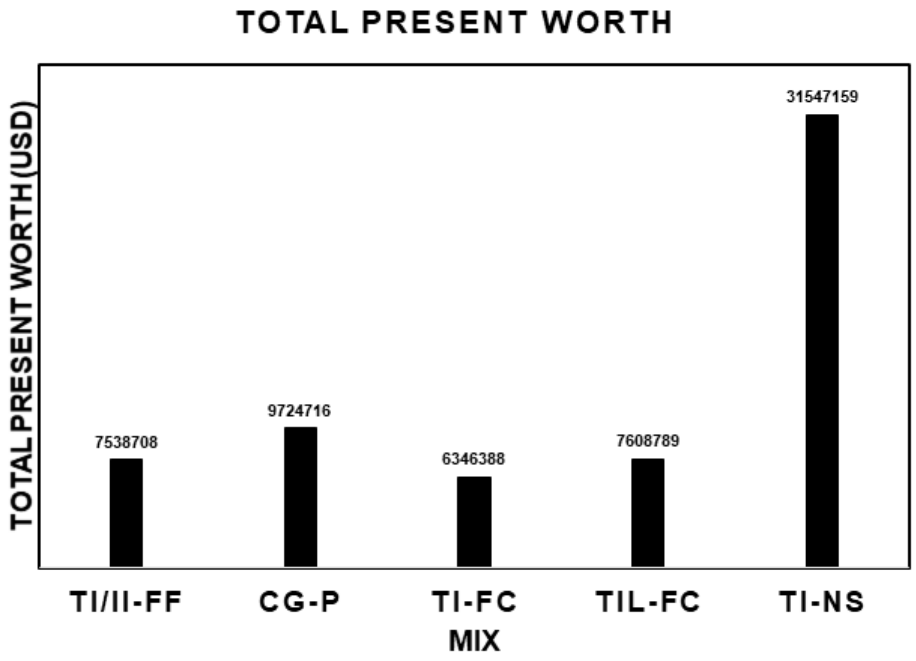

Figure 47. Comparison of Total Present Worth

5.5.2.1. Type I/II Cement with 20% Replacement with Class F Fly Ash (TI/II-FF)

Considering an analysis period of 60 years, and a discount rate of 7%, and neglecting user costs, approximate number of years before deck replacement (N_{DR}) was calculated to be 30 years. Based on this calculation, number of years before shallow deck overlay was estimated at (N_{DO}) 15 years, and frequency of patching (N_P) was found to be 5 years, according to equations 5.3 through 5.5. These calculations are shown in Table 18.

Table 18. Mix Performance for TI/II-FF

	% Improvement of 28 Day Resistivity (Over Base of 10 kΩcm) **A**	% Improvement of Stress Rate (S) (Over Base of 70 psi/day) **B**	% Improvement of Maximum Plastic Shrinkage Strain (Over Base of $8.5x10^{-4}$ Strain) **C**	% Improvement of 28 Day Compressive Strength (Over Base of 4000 psi) **D**
Quantities	15.4	18	3.5	5695
%	54.00	74.29	58.82	42.38
Number of years before deck replacement = 0.53(0.3A+0.3B+0.1C+0.3D) =				30
Number of years before shallow deck overlay or resurfacing =				15
Number of years before patching =				5

Table 19 shows the cost estimates for present worth for TI/II-FF. Present worth calculations have been based on equation 5.6. Figure 48 shows the cash flow diagram for TI/II-FF. It may be noticed that initial construction costs are the highest when compared among the others cost throughout the life cycle of the bridge.

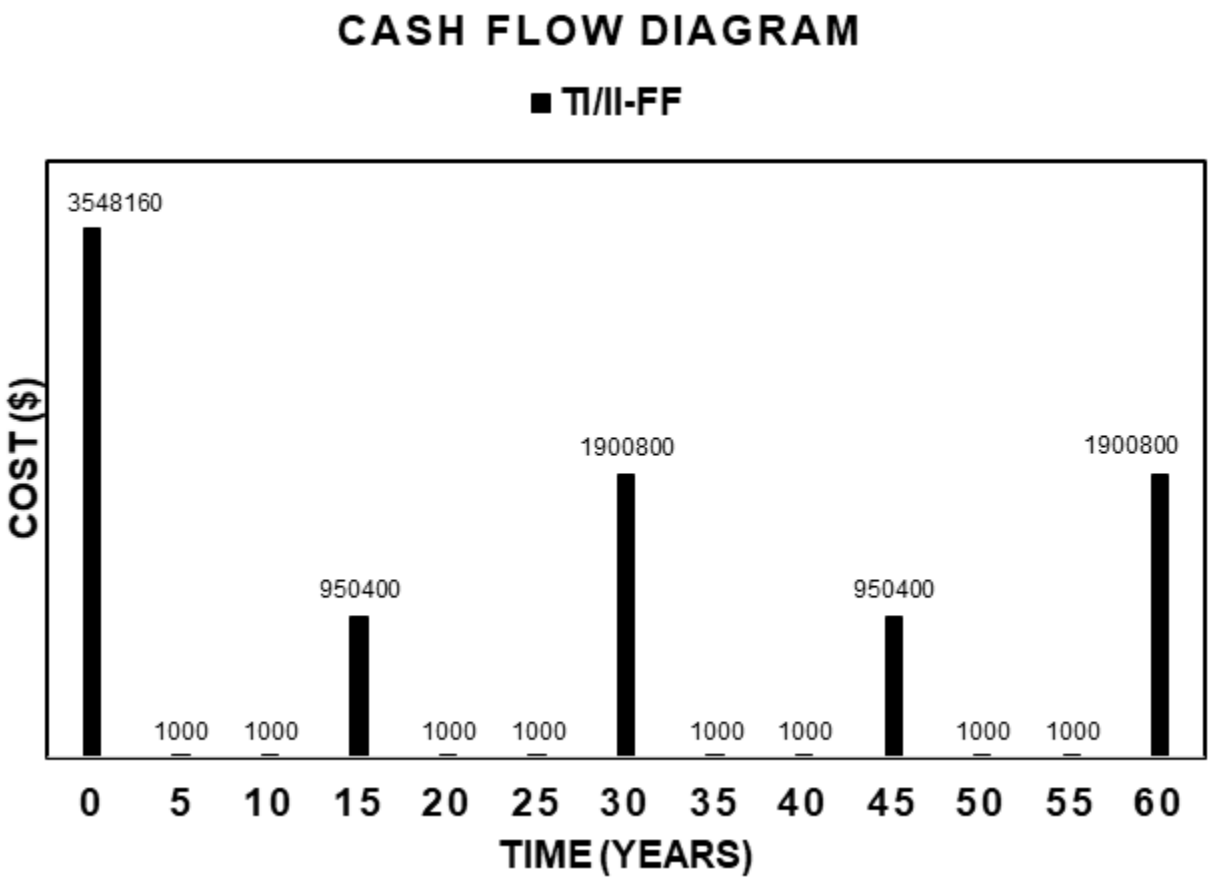

Figure 48. Cash Flow Diagram for TI/II-FF

Table 19. Present Worth Calculations for TI/II-FF

Year	Type of Work	Description	Total Cost ($)	Present Worth ($)
0	Initial Construction	Construction	3548160	3548160
5	Maintenance	Patching 1	1000	955
10	Maintenance	Patching 2	1000	912
15	Rehabilitation	Shallow overlay 1	950400	827184
20	Maintenance	Patching 3	1000	831
25	Maintenance	Patching 4	1000	793
30	Rehabilitation	Deck Replacement 1	1900800	1439886
35	Maintenance	Patching 5	1000	723
40	Maintenance	Patching 6	1000	691
45	Rehabilitation	Shallow overlay 2	950400	626605
50	Maintenance	Patching 7	1000	629
55	Maintenance	Patching 8	1000	601
60	Rehabilitation	Deck Replacement 2	1900800	1090737
Total Present Worth ($)				**7538708**

5.5.2.2. Coarse Ground Cement (CG-P)

Considering an analysis period of 60 years, and a discount rate of 7%, and neglecting user costs, approximate number of years before deck replacement (N_{DR}) was calculated to be 21 years. Based on this calculation, number of years before shallow deck overlay (N_{DO}) was estimated at 11 years, and frequency of patching (N_P) was found to be 4 years, according to equations 5.3 through 5.5. These calculations are shown in Table 20. For convenience of estimation and practicality issues, N_{DR}, N_{DO}, and N_P have been assumed to be 20 years, 10 years, and 4 years respectively.

Table 20. Mix Performance for CG-P

	% Improvement of 28 Day Resistivity (Over Base of 10 kΩcm) **A**	% Improvement of Stress Rate (S) (Over Base of 70 psi/day) **B**	% Improvement of Maximum Plastic Shrinkage Strain (Over Base of $8.5x10^{-4}$ Strain) **C**	% Improvement of 28 Day Compressive Strength (Over Base of 4000 psi) **D**
Quantities	11.1	27	4.3	5845
%	11.00	61.43	49.41	46.13
Number of years before deck replacement = 0.53(0.3A+0.3B+0.1C+0.3D) =				21
Number of years before shallow deck overlay or resurfacing =				11
Number of years before patching =				4

Table 21. Present Worth Calculations for CG-P shows the cost estimates for present worth for CG-P. Present worth calculations have been based on equation 5.6. Figure 49 shows the cash flow diagram for CG-P. It may be noticed that like TI/II-FF, initial construction costs are the highest when compared among the other costs throughout the life cycle of the bridge.

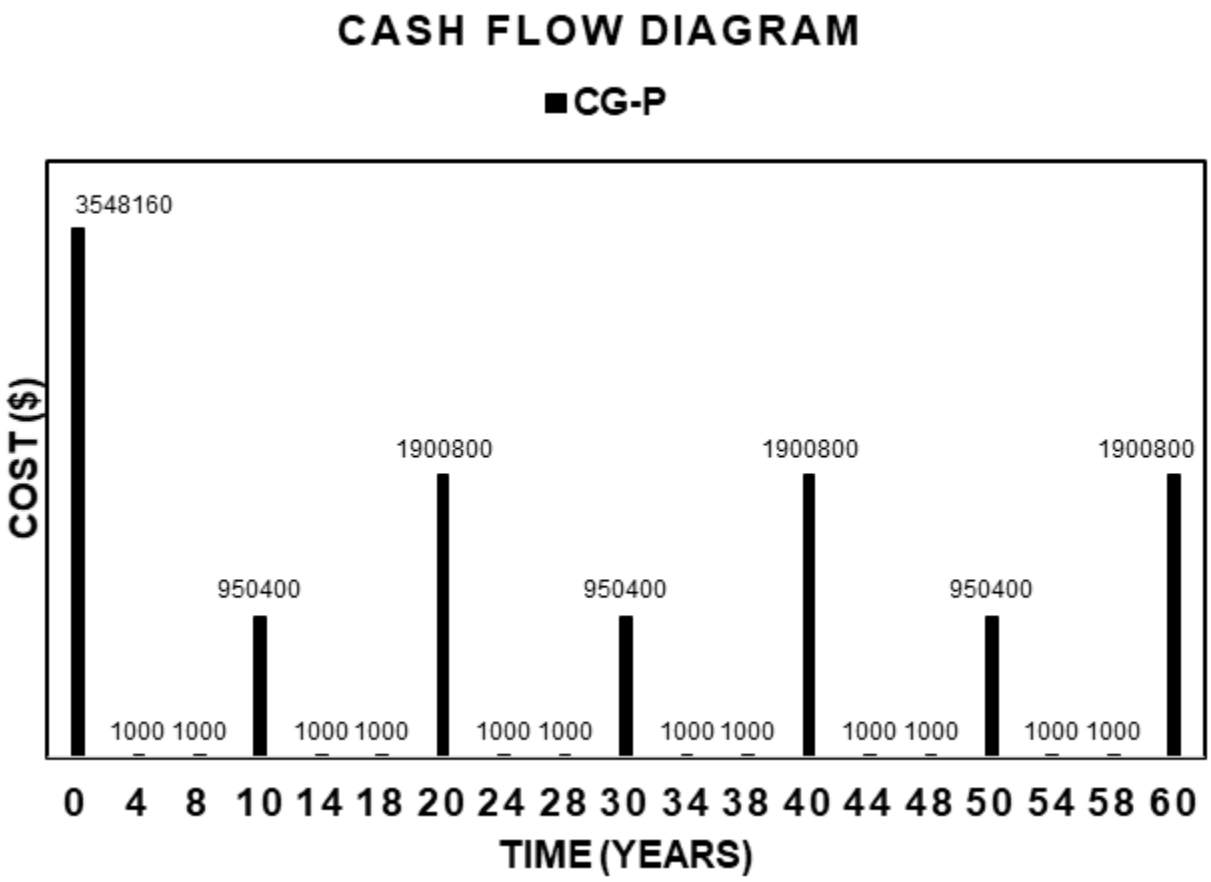

Figure 49. Cash Flow Diagram for CG-P

Table 21. Present Worth Calculations for CG-P

Year	Type of Work	Description	Total Cost ($)	Present Worth ($)
0	Initial Construction	Construction	3548160	3548160
4	Maintenance	Patching 1	1000	964
8	Maintenance	Patching 2	1000	929
10	Rehabilitation	Shallow overlay 1	950400	866371
14	Maintenance	Patching 3	1000	878
18	Maintenance	Patching 4	1000	847
20	Rehabilitation	Deck Replacement 1	1900800	1579541
24	Maintenance	Patching 5	1000	801
28	Maintenance	Patching 6	1000	772
30	Rehabilitation	Shallow overlay 2	950400	719943
34	Maintenance	Patching 7	1000	730
38	Maintenance	Patching 8	1000	703
40	Rehabilitation	Deck Replacement 2	1900800	1312579
44	Maintenance	Patching 9	1000	665
48	Maintenance	Patching 10	1000	641
50	Rehabilitation	Shallow overlay 3	950400	598264
54	Maintenance	Patching 11	1000	607
58	Maintenance	Patching 12	1000	585
60	Rehabilitation	Deck Replacement 3	1900800	1090737
Total Present Worth ($)				**9724716**

5.5.2.3. Type I Cement with 30% Replacement with Class C Fly Ash (TI-FC)

Considering an analysis period of 60 years, and a discount rate of 7%, and neglecting user costs, approximate number of years before deck replacement (N_{DR}) was calculated to be 34 years. Based on this calculation, number of years before shallow deck overlay (N_{DO}) was estimated at 17 years, and frequency of patching (N_P) was found to be 6 years, according to equations 5.3 through 5.5. These calculations are shown in Table 22.

Table 22. Mix Performance for TI-FC

	% Improvement of 28 Day Resistivity (Over Base of 10 kΩcm)	% Improvement of Stress Rate (S) (Over Base of 70 psi/day)	% Improvement of Maximum Plastic Shrinkage Strain (Over Base of $8.5x10^{-4}$ Strain)	% Improvement of 28 Day Compressive Strength (Over Base of 4000 psi)
Quantities	15.6	11	7	6738
%	56.00	84.29	17.65	68.45
Number of years before deck replacement = 0.53(0.3A+0.3B+0.1C+0.3D) =				34
Number of years before shallow deck overlay or resurfacing =				17
Number of years before patching =				6

Table 23 shows the cost estimates for present worth for TI-FC. Present worth calculations have been based on equation 5.6. Figure 50 shows the cash flow diagram for TI-FC. It may be noticed that like the previous scenarios, initial construction costs are the highest when compared among the other costs throughout the life cycle of the bridge.

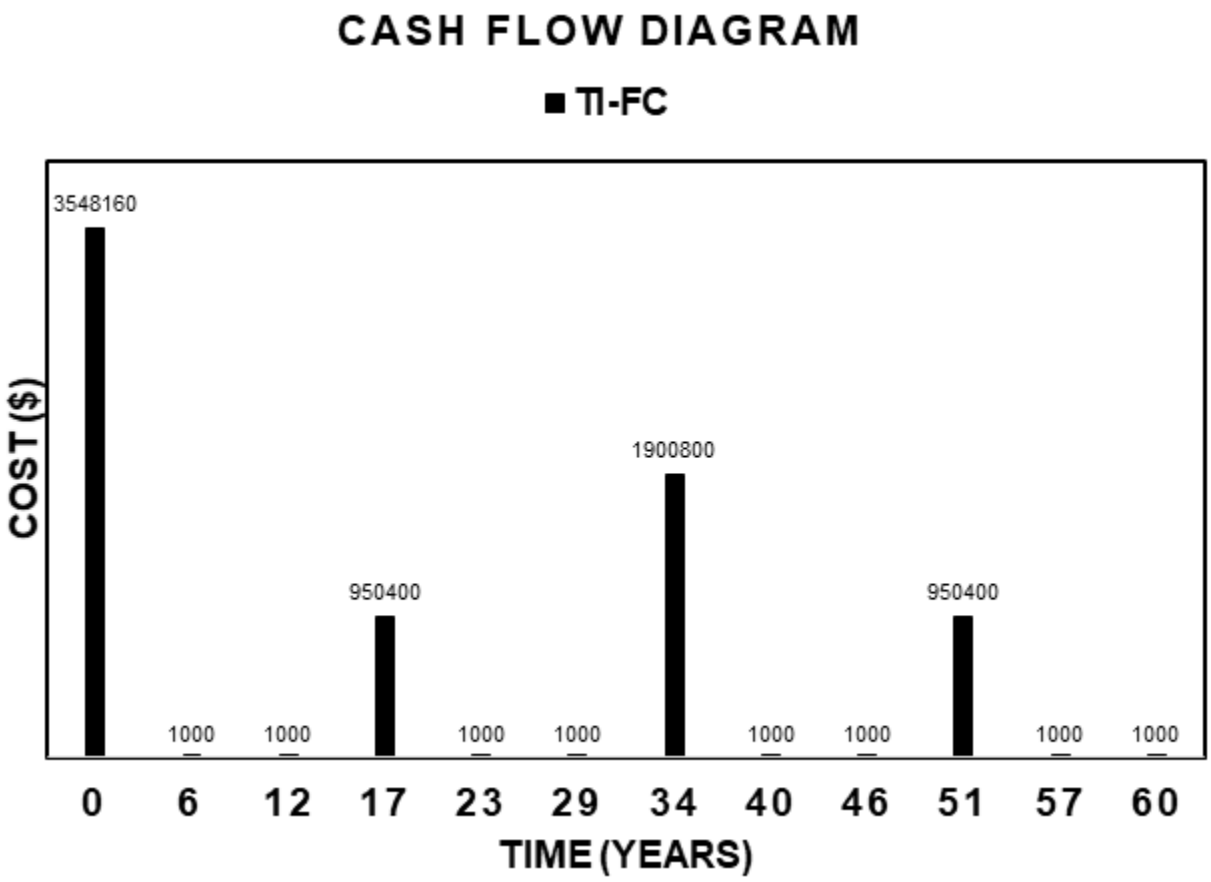

Figure 50. Cash Flow Diagram for TI-FC

Table 23. Present Worth Calculations for TI-FC

Year	Type of Work	Description	Total Cost ($)	Present Worth ($)
0	Initial Construction	Construction	3548160	3548160
6	Maintenance	Patching 1	1000	946
12	Maintenance	Patching 2	1000	895
17	Rehabilitation	Shallow overlay 1	950400	812011
23	Maintenance	Patching 3	1000	808
29	Maintenance	Patching 4	1000	765
34	Rehabilitation	Deck Replacement 1	1900800	1387545
40	Maintenance	Patching 5	1000	691
46	Maintenance	Patching 6	1000	653
51	Rehabilitation	Shallow overlay 2	950400	592751
57	Maintenance	Patching 7	1000	590
60	Maintenance	Patching 8	1000	574
Total Present Worth ($)				**6346388**

5.5.2.4. Type IL Cement with 30% Replacement with Class C Fly Ash (TIL-FC)

Considering an analysis period of 60 years, and a discount rate of 7%, and neglecting user costs, approximate number of years before deck replacement (N_{DR}) was calculated to be 29 years. Based on this calculation, number of years before shallow deck overlay (N_{DO}) was estimated at 14 years, and frequency of patching (N_P) was found to be 5 years, according to equations 5.3 through 5.5. These calculations are shown in Table 24.

Table 24. Mix Performance for TIL-FC

	% Improvement of 28 Day Resistivity (Over Base of 10 kΩcm) **A**	% Improvement of Stress Rate (S) (Over Base of 70 psi/day) **B**	% Improvement of Maximum Plastic Shrinkage Strain (Over Base of $8.5x10^{-4}$ **C**	% Improvement of 28 Day Compressive Strength (Over Base of 4000 psi) **D**
Quantities	16.1	32	4.4	6084
%	61.00	54.29	48.24	52.10
Number of years before deck replacement = 0.53(0.3A+0.3B+0.1C+0.3D) =				29
Number of years before shallow deck overlay or resurfacing =				14
Number of years before patching =				5

Table 25 shows the cost estimates for present worth for TIL-FC. Present worth calculations have been based on equation 5.6. Figure 51 shows the cash flow diagram for TIL-FC. Like the previous scenarios, initial construction costs are the highest when compared among the other costs throughout the life cycle of the bridge.

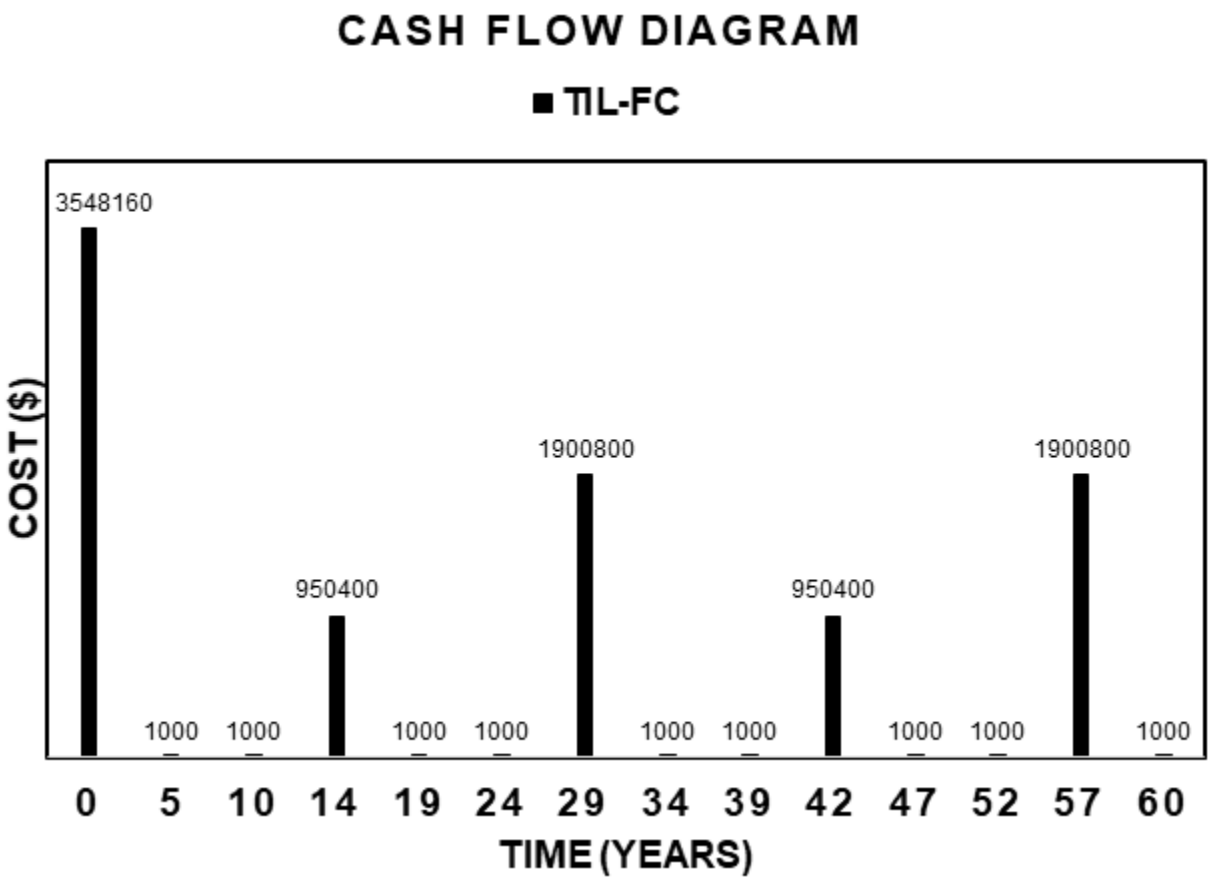

Figure 51. Cash Flow Diagram for TIL-FC

Table 25. Present Worth Calculations for TIL-FC

Year	Type of Work	Description	Total Cost ($)	Present Worth ($)
0	Initial Construction	Construction	3548160	3548160
5	Maintenance	Patching 1	1000	955
10	Maintenance	Patching 2	1000	912
14	Rehabilitation	Shallow overlay 1	950400	834877
19	Maintenance	Patching 3	1000	839
24	Maintenance	Patching 4	1000	801
29	Rehabilitation	Deck Replacement 1	1900800	1453277
34	Maintenance	Patching 5	1000	730
39	Maintenance	Patching 6	1000	697
42	Rehabilitation	Shallow overlay 2	950400	644251
47	Maintenance	Patching 7	1000	647
52	Maintenance	Patching 8	1000	618
57	Rehabilitation	Deck Replacement 2	1900800	1121452
60	Maintenance	Patching 9	1000	574
Total Present Worth ($)				**7608789**

5.5.2.5. Type I Cement with 5% Replacement with Nanosilica (TI-NS)

Considering an analysis period of 60 years, and a discount rate of 7%, and neglecting user costs, approximate number of years before deck replacement (N_{DR}) was calculated to be 28 years. Based on this calculation, number of years before shallow deck overlay (N_{DO}) was estimated at 14 years, and frequency of patching (N_P) was found to be 5 years, according to equations 5.3 through 5.5. These calculations are shown in Table 26.

Table 26. Mix Performance for TI-NS

	% Improvement of 28 Day Resistivity (Over Base of 10 kωcm) **A**	% Improvement of Stress Rate (S) (Over Base of 70 psi/day) **B**	% Improvement of Maximum Plastic Shrinkage Strain (Over Base of $8.5x10^{-4}$ Strain) **C**	% Improvement of 28 Day Compressive Strength (Over Base of 4000 psi) **D**
Quantities	14.2	67	3.4	8432
%	42.00	4.29	60.00	110.80
Number of years before deck replacement = 0.53(0.3A+0.3B+0.1C+0.3D) =				28
Number of years before shallow deck overlay or resurfacing =				14
Number of years before patching =				5

Table 27 shows the cost estimates for present worth for TI-NS. Present worth calculations have been based on equation 5.6. Figure 52 shows the cash flow diagram for TI-NS. Like the previous scenarios, initial construction costs are the highest when compared among the other costs throughout the life cycle of the bridge. In this case, the initial construction costs, and other activities throughout the life cycle of the bridge are significantly higher than the other scenarios due to high cost of colloidal nanosilica.

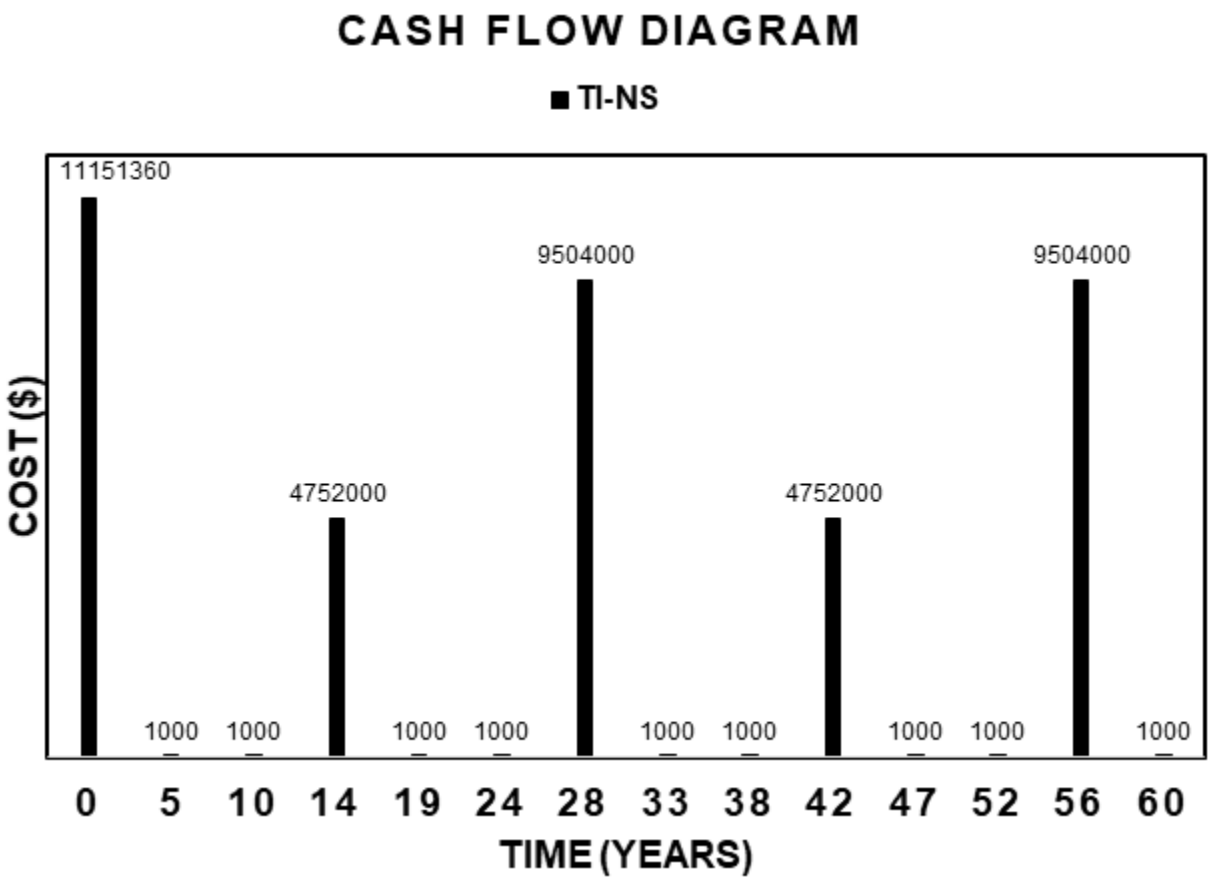

Figure 52. Cash Flow Diagram for TI-NS

Table 27. Present Worth Calculations for TI-NS

Year	Type of Work	Description	Total Cost ($)	Present Worth ($)
0	Initial Construction	Construction	11151360	11151360
5	Maintenance	Patching 1	1000	955
10	Maintenance	Patching 2	1000	912
14	Rehabilitation	Shallow overlay 1	4752000	4174386
19	Maintenance	Patching 3	1000	839
24	Maintenance	Patching 4	1000	801
28	Rehabilitation	Deck Replacement 1	9504000	7333964
33	Maintenance	Patching 5	1000	737
38	Maintenance	Patching 6	1000	703
42	Rehabilitation	Shallow overlay 2	4752000	3221254
47	Maintenance	Patching 7	1000	647
52	Maintenance	Patching 8	1000	618
56	Rehabilitation	Deck Replacement 2	9504000	5659410
60	Maintenance	Patching 9	1000	574
Total Present Worth ($)				**31547159**

5.5.2.6. Deterministic Results from RealCost 2.5

Table 28 and Figure 53 show the deterministic results derived from RealCost. It may be observed that the present worth amounts for the five mixes are slightly lower than those derived from the spreadsheet calculations presented above. Figure 54 shows the cash flow diagram as generated by RealCost.

Table 28. RealCost Deterministic Results for the Five Alternatives, d = 0.7% (Alternative 1 = TI/II-FF, Alternative 2 = CG-P, Alternative 3 = TI-FC, Alternative 4 = TIL-FC, Alternative 5 = TI-NS)

Total Cost	Alternative 1 ($1000)		Alternative 2 ($1000)		Alternative 3 ($1000)		Alternative 4 ($1000)		Alternative 5 ($1000)	
	Agency Cost	User Cost	Agency Cost	User Cost	Agency Cost	User Cost	Agency Cost	User Cost	Agency Cost	User Cost
Undiscounted Sum	$7,357	$0	$10,212	$0	$6,909	$0	$7,619	$0	$32,882	$0
Present Value	$6,447	$0	$8,633	$0	$6,089	$0	$6,691	$0	$27,651	$0
EUAC	$140	$0	$188	$0	$132	$0	$146	$0	$603	$0

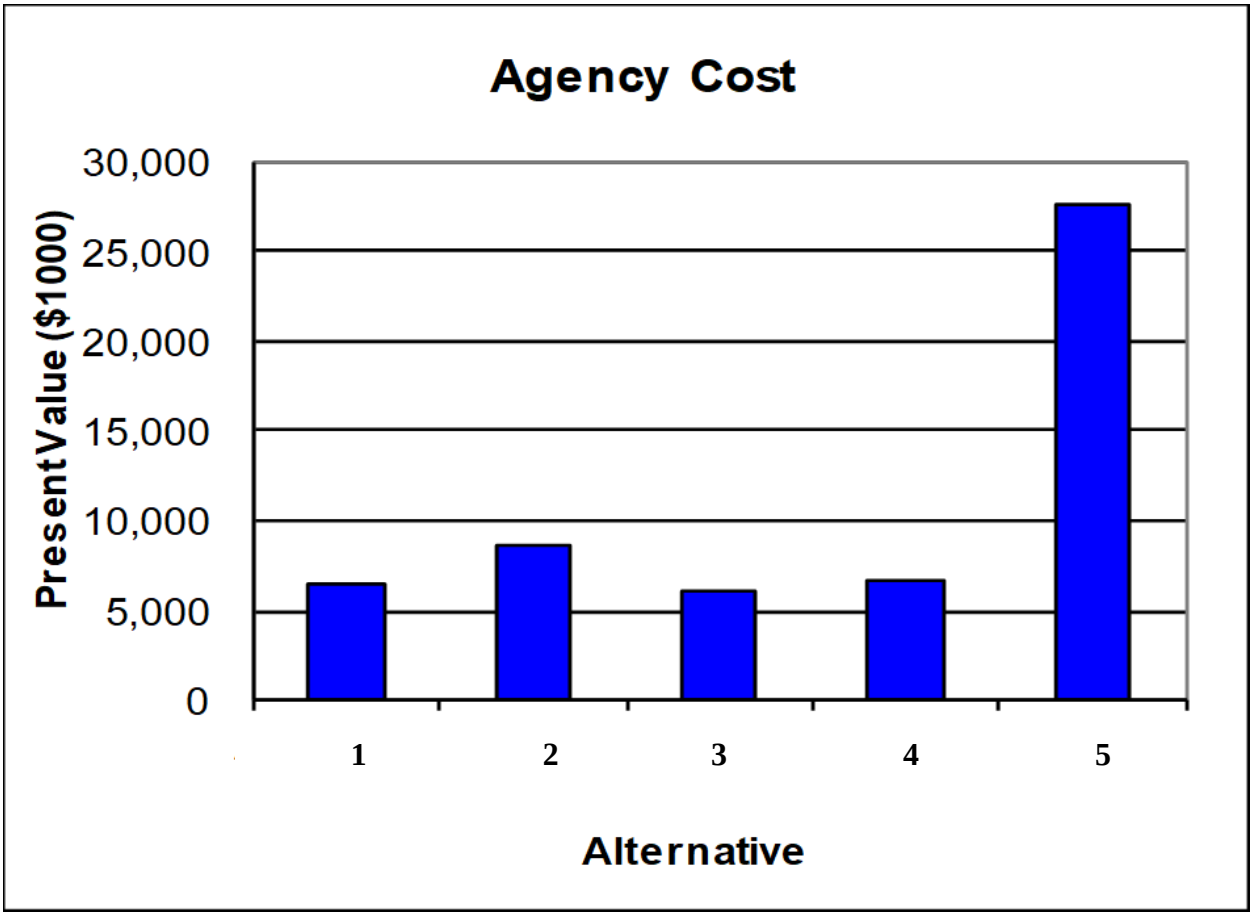

Figure 53. Comparison of Present Value by RealCost (Alternative 1 = TI/II-FF, Alternative 2 = CG-P, Alternative 3 = TI-FC, Alternative 4 = TIL-FC, Alternative 5 = TI-NS)

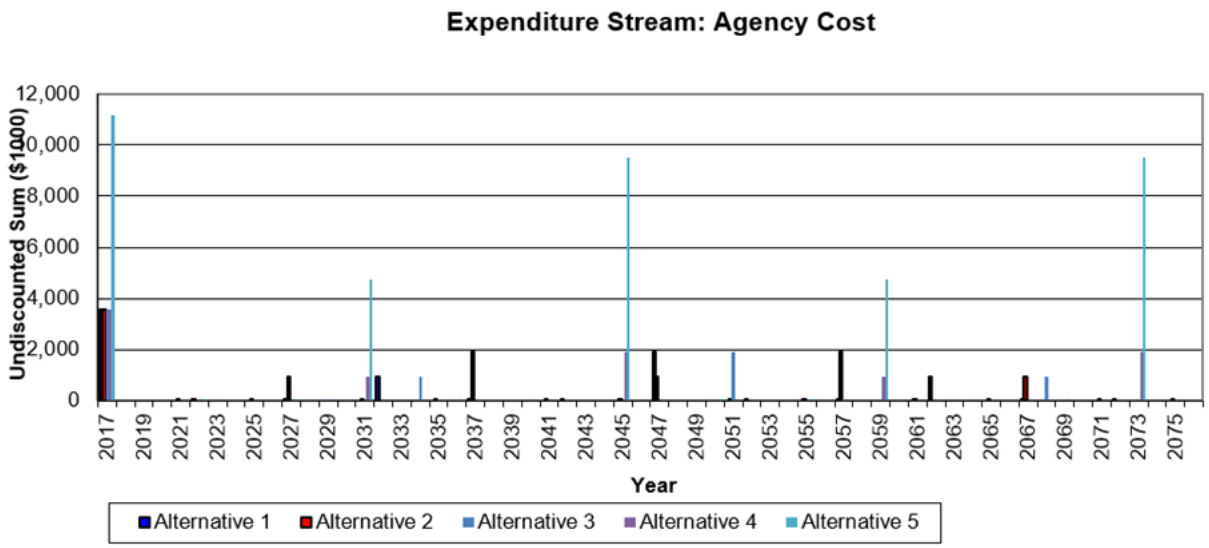

Figure 54. Cash Flow Diagram by RealCost (Alternative 1 = TI/II-FF, Alternative 2 = CG-P, Alternative 3 = TI-FC, Alternative 4 = TIL-FC, Alternative 5 = TI-NS)

5.6. Conclusion

In this study, a life cycle assessment (LCA) and life cycle cost analysis (LCCA) are performed on five cementitious systems: coarse ground cement (CG-P), Type I/II cement with a 20% replacement with Class F fly ash (TI/II-FF), Type I cement with a 30% replacement with Class C fly ash (TI-FC), Type IL cement with a 30% replacement with Class C fly ash (TIL-FC), and Type I cement with a 5% replacement with colloidal nanosilica (TI-NS). LCA results show that TIL-FC has the lowest emissions of CO_2 into the atmosphere. The comparison between total present worth of the five cementitious systems during the life cycle of the bridge reveals that TI-NS has the highest total life cycle cost. This is primarily because of current high expenses of colloidal nanosilica. TI-FC has the lowest life cycle costs among the five scenarios. This is mainly because of a higher N_{DR} value based on equation 5.3. Therefore, such blending of portland cement with supplementary cementitious materials, interground or blended, are encouraged.

5.7. Acknowledgement

This paper is based upon work supported by the U. S. Department of Energy under Award No.DE-EE0007246. The authors also acknowledge Mr. Robert Steffes for his constant support and insight.

5.8. Disclaimer

Any findings, opinions, and conclusions or recommendations expressed in this report are those of the author(s) and do not necessarily reflect the views of the Department of Energy.

5.9. References

ACPA. (2012). Life-Cycle Cost Analysis: A Tool for Better Pavement Investment and Engineering Decisions. Rosemont, IL.

Ali, M. B., R. Saidur & M. S. Hossain (2011) A review on emission analysis in cement industries. *Renewable and Sustainable Energy Reviews,* 15**,** 2252-2261.

Bentz, D. P. (2010) Blending different fineness cements to engineer the properties of cement-based materials. *Magazine of Concrete Research,* 62**,** 327-338.

Bhatia, A., P. K. Aggarwal & H. Pathak (2007) Simulating greenhouse gas emissions from Indian rice fields using the InfoCrop Model. *International Rice Research Notes,* 32**,** 38.

Deshpande, S. S. (2007). *Evaluating free shrinkage of concrete for control of cracking in bridge decks*. University of Kansas.

MNDOT. (2018) St. Croix Crossing. Minnesota Department of Transportation. (https://www.dot.state.mn.us/stcroixcrossing/)

Gartner, E. (2004) Industrially interesting approaches to "low-CO_2" cements. *Cement and Concrete research,* 34**,** 1489-1498.

Harvey, J. T., J. Meijer, H. Ozer, I. L. Al-Qadi, A. Saboori & A. Kendall. (2016). Pavement Life-Cycle Assessment Framework.

Hendriks, C. A., E. Worrell, D. De Jager, K. Blok & P. Riemer. (1998). Emission reduction of greenhouse gases from the cement industry. 939-944.

Huntzinger, D. N. & T. D. Eatmon (2009) A life-cycle assessment of Portland cement manufacturing: comparing the traditional process with alternative technologies. *Journal of Cleaner Production,* 17**,** 668-675.

International Standard, O. (1997). *ISO 14040: Environmental Management-Life Cycle Assessment-Principles and Framework*.

Ipc, C. (1996) Climate Change 1995: Impacts, Adaptations, and Mitigation of Climate Change: Scientific-Technical Analyses.

Keller, A. A., S. McFerran, A. Lazareva & S. Suh (2013) Global life cycle releases of engineered nanomaterials. *Journal of Nanoparticle Research,* 15**,** 1692.

Kendall, A., G. A. Keoleian & G. E. Helfand (2008) Integrated life-cycle assessment and life-cycle cost analysis model for concrete bridge deck applications. *Journal of Infrastructure Systems,* 14**,** 214-222.

Loijos, A., N. Santero & J. Ochsendorf (2013) Life cycle climate impacts of the US concrete pavement network. *Resources, Conservation and Recycling,* 72**,** 76-83.

Marceau, M., M. A. Nisbet & M. G. Van Geem. (2006). Life cycle inventory of portland cement manufacture. Portland Cement Association IL.

Mehta, P. K. (1999) Advancements in concrete technology. *Concrete International,* 21**,** 69-76.

Mehta, P. K. & R. W. Burrows (2001) Building durable structures in the 21 st century. *Indian Concrete Journal,* 75**,** 437-443.

Mikulčić, H., J. J. Klemeš, M. Vujanović, K. Urbaniec & N. Duić (2016) Reducing greenhouse gasses emissions by fostering the deployment of alternative raw materials and energy sources in the cleaner cement manufacturing process. *Journal of cleaner production,* 136**,** 119-132.

Monteiro, P. J. M., S. A. Miller & A. Horvath (2017) Towards sustainable concrete. *Nature Materials,* 16**,** 698-699.

Montzka, S. A., E. J. Dlugokencky & J. H. Butler (2011) Non-CO2 greenhouse gases and climate change. *Nature,* 476**,** 43.

Pachauri, R. K., M. R. Allen, V. R. Barros, J. Broome, W. Cramer, R. Christ, J. A. Church, L. Clarke, Q. Dahe & P. Dasgupta. (2014). *Climate change 2014: synthesis report. Contribution of Working Groups I, II and III to the fifth assessment report of the Intergovernmental Panel on Climate Change*. IPCC.

Ramanathan, V. & Y. Feng (2009) Air pollution, greenhouse gases and climate change: Global and regional perspectives. *Atmospheric Environment,* 43**,** 37-50.

Rangaraju, P. R., S. N. Amirkhanian & Z. Guven. (2008). Life cycle cost analysis for pavement type selection. South Carolina Department of Transportation Clemson, SC.

Santero, N., A. Loijos, M. Akbarian & J. Ochsendorf. (2011). Methods, impacts, and opportunities in the concrete pavement life cycle. MIT Concrete Sustainability Hub.

Sirotiak, T., Sharma, A. S., Taylor, P. C. (2016). Cement Changes and Solutions to the Industry: Phase I Final Report. North Dakota State University.

Solomon, S., G.-K. Plattner, R. Knutti & P. Friedlingstein (2009) Irreversible climate change due to carbon dioxide emissions. *Proceedings of the national academy of sciences,* 106**,** 1704-1709.

Stroh, S. L. (2014). Extradosed Prestressed Bridges. Florida Department of Transportation.

Taylor, P. & X. Wang (2014) Concrete Pavement Mixture Design and Analysis (MDA): Factors Influencing Drying Shrinkage. Iowa State University

Tritsch, N., D. Darwin & J. Browning. (2005). Evaluating Shrinkage and Cracking Behavior of Concrete Using Restrained Ring and Free Shrinkage Tests. University of Kansas Center for Research, Inc.

Van Dam, T. J., J. T. Harvey, S. T. Muench, K. D. Smith, M. B. Snyder, I. L. Al-Qadi, H. Ozer, J. Meijer, P. V. Ram & J. R. Roesler. (2015). *Towards sustainable pavement systems: a reference document*. US Department of Transportation, Federal Highway Administration.

Walls, J. & M. R. Smith (1998) Life-cycle cost analysis in pavement design: in search of better investment decisions.

Wced, U. (1987) Our common future. *World Commission on Environment and DevelopmentOxford University Press*.

Zayed, A., A. Sedaghat, A. Bien-Aime & N. Shanahan (2014) Effects of portland cement particle size on heat of hydration. Florida Department of Transportation.

CHAPTER 6: OVERALL CONCLUSIONS AND RECOMMENDATIONS

This overall goal of this work is to investigate the effects of different cementitious systems on shrinkage and durability of concrete. The crux of this research work is based on the recommendations of prior researchers about the commercial use of coarser portland cement which have low shrinkage due to drying, and subsequent cracking. Additionally, some chemical constituents of portland cement such as, tri-calcium silicate (C_3S) and tri-calcium aluminate (C_3A) also affect shrinkage of concrete due to which their presence in portland cement need to be controlled. However, finer cementitious systems are used according to current industry standards in the interest of time. The time required for strength gain of concrete is critical to meeting of deadlines by contractors and state agencies. A coarser ground cement typically takes longer to gain adequate strength and therefore, changing the current industry model to a slower system will be challenging. Additionally, the cement manufacturers will also have to make huge changes to their infrastructure in order to go back to a system used decades ago. Therefore, this research is focused on developing concrete with existing cementitious materials to achieve similar or lower resistance to shrinkage cracking, as compared to coarse ground cement, without adversely affecting other engineering properties of concrete. Key engineering properties include workability, degree of hydration, compressive and splitting tensile strengths, electrical resistivity, setting time, and bleeding.

Another aspect of the use of portland cement in concrete is its carbon footprint. The process of manufacture of portland cement results in the generation of about 8% of carbon dioxide (CO_2) into the atmosphere. Therefore, it will be of interest to find ways of partial replacement of portland cement with supplementary cementitious materials (SCMs) such as, fly ash. The emphasis of this research is laid on investigating the feasibility of portland limestone at replacement rates higher

than current industry standards in the United States. Typically, in the states of North Dakota, Minnesota, Montana, and Iowa up to 5% of portland is replaced with limestone. The limestone is blended with clinker of portland cement and ground together to form Type IL portland limestone cement. According to ASTM C595 of 2009, Type IL portland limestone cement can be used with partial replacement levels of up to 15%. However, industry professionals are concerned about loss of required properties of concrete such as, adequate workability and compressive strength at higher replacement levels of portland limestone cement. Therefore, lower replacement levels of limestone are used, if at all. Higher replacement levels of portland cement with limestone will reduce the emission of CO_2 into the atmosphere per unit weight of cement used in concrete. Therefore, in this study, the use of Type IL (10) portland limestone cement to achieve desired shrinkage properties of concrete is investigated.

The benefits of engineered nanoparticles are implemented in various disciplines. The use of silica nanoparticles in concrete have been investigated by prior researchers. As these engineered nanoparticles are thousand times smaller than typical cementitious materials, the surface area available for reactivity is much higher. Therefore, hydration reactions are driven much faster leading to the formation of a refined microstructure of concrete, with reduced volume of gel pores. This provided higher water tightness and the ingress of deleterious ions is minimized. There are however, very few published studies on the effects of nanosilica on shrinkage of concrete. Therefore, in this study such effects of nanosilica on shrinkage and durability of concrete is investigated.

The advantages of internal curing are also investigated in this study. In case of internal curing, fine aggregates are partially replaced with light weight aggregates pre-soaked in water. These aggregates release water inside the concrete system over time, thereby helping in continued

hydration. This process may have advantages of reduced shrinkage strain and a more refined microstructure.

In Chapter 2, mechanical properties of fifteen different cementitious combinations are investigated. These mixtures are formed from four different cement types: coarse ground portland cement (CG), Type I portland cement (TI), Type I/II portland cement (TI/II), and Type IL portland limestone cement (TIL). In addition to investigating the four cement types with no partial replacement, the latter three cement types are partially replaced with 20% Class F fly ash (FF), 30% Class C fly ash (FC), and 5% nanosilica (NS). For two of the mixtures, Type I/II cement and 20% replaced with Class F fly ash, and 30% of fine aggregates replaced with light weight aggregates (TI/II-FF (LWA)), and Type I cement with no SCMs, and 30% of fine aggregates replaced with light weight aggregates (TI-P(LWA)) the effects of internal curing is investigated. In this study, it has been observed that concrete containing Type IL portland limestone cement has low slump. The is consistent with prior literature. Partial replacement of portland cement with limestone reduces the capability of the cement to react with water to form the binder, as initially limestone acts as in inert filler. The workability is improved when fly ash is included. Fly ash consists of glassy spherical particles which improve workability and reduce the water demand. Concrete mixtures containing nanosilica have faster rates of hydration, higher temperature change peaks (as measured through semi-adiabatic calorimetry), and faster setting times as compared to their corresponding control mixtures. Concrete mixtures containing Class C fly ash have very long setting times. This is caused because of a depletion of sulfate in the system, due to the presence of high amounts of aluminates in the Class C fly ash used. Sulfate which is otherwise used to prevent the concreter from flash set, gets depleted, as indicated by isothermal calorimetry results. Mixtures containing Type IL portland limestone cement have not cracked due to plastic shrinkage. These

mixtures also have improved compressive strength and resistivity due to better particle size distribution, more nucleation sites for precipitation of hydration products, and physical filling of interfacial transition zone (ITZ) between aggregates and paste by carboaluminate hydrates. These mixtures also have shown similar or slightly higher drying shrinkage strain as compared to coarse ground cement. Drying shrinkage strain is higher for mixtures containing fly ash due to an unaltered water-binder ratio, allowing more available free water. Strain due to drying shrinkage under externally restrained conditions is investigated by the ASTM ring test. Rings of two of the mixtures have cracked due to restrained shrinkage: Type I cement with 5% nanosilica (TI-NS) and Type I/II cement with 30% Class C fly ash (TI/II-FC). Incorporation of larger agggregates and higher volume of aggregates has led to a reduction of drying shrinkage strain of two mixtures:Type IL cement with 30% Class C fly ash (TIL-FC) and Type I cement with 5% nanosilica (TI-NS). The results also indicate that internal curing can be beneficial for shrinkage and other engineering properties due to continued hydration. Based on key performance characteristics, two mixtures are considered to have superior properties over others: Type I/II cement with 20% Class F fly ash, and Type IL cement with 30% Class C fly ash.

Based on the results from Chapter 2, five cementitious combinations are selected for further investigations, as described in Chapter 3. Cementitious combinations investigated in this study include coarse ground cement with no SCMs (CG-P), Type I/II cement and 20% replaced with Class F fly ash (TI/II-FF), Type IL cement and 30% replaced with Class C fly ash (TIL-FC), Type I cement and 30% replaced with Class C fly ash (TI-FC), and Type I cement and 5% replaced with colloidal nanosilica (TI-NS). Additionally, chopped basalt fibers (B) are added to concrete containing the above cementitious combinations at a loading rate of 0.25% (v/v). It is hypothesized that the incorporation of chopped basalt fibers will help merge micro-cracks due to shrinkage, and

thereby restrict the propagation of such micro-cracks into bulk cracks. For the sake of comparison, the results obtained from this study are compared with the corresponding mixtures without basalt fibers. It is observed that the addition of basalt fibers in concrete reduces workability, resulting in low slump. Type F high range water reducers are added in high dosages to enhance the workability. High superplasticizer dosage has retarded the hydration of concrete as observed through semi-adiabatic calorimetry. Moreover, the peak temperature indicating hydration of the silicates has also reduced. Basalt fibers have lowered the setting time of concrete. On the other hand, superplasticizers have a tendency to increase the setting time. The setting times calculated from the calorimetry curves by the 20% and 50% fraction method are longer than those measured by the penetrometer method. Predictability is better for the mixtures without basalt fibers. Air content is increased because the addition of basalt fibers increased the amount of entrapped air. In order to control the total air content, the dosage of air entraining agent has to be controlled. There is not much improvement in compressive strength and splitting tensile strength due to fiber addition. This can be due to an increase in air content and high dosages of superplasticizers. Resistivity is also lower for the mixtures containing basalt fibers, due to a high dosage of high range water reducers and resulting increase in porosity. Plastic shrinkage and drying shrinkage strain is higher on account of high dosage of superplasticizers. However, due to a binding mechanism of basalt microfibers, there may be a reduced propagation of micro-cracks into macro-cracks and loss of serviceability. Based on a performance matrix, Type I/II cement with 20% Class F fly ash (TI/II-FF) is selected as the best mixture among those containing basalt fibers and recommended for further studies and field implementations. Mix proportions can be appropriately modified to prevent the use of high dosages of high range water reducers and resulting negative effects on mechanical properties.

Chapter 4 describes the microstructure studies conducted on select cementitious combinations. In this study, the effects of different cementitious combinations on micro-cracking due to drying shrinkage are investigated. The study consists of two phases: in the first phase, three cementitious combinations (coarse ground cement CG-P, Type IL portland limestone cement TIL-P, and Type I portland cement and 5% replaced with nanosilica TI-NS) are used to investigate the effect of drying shrinkage on their micro-cracking tendency. A convenient method is developed and tested for detection and quantification of micro-cracks in these paste samples. Porosity distribution in the paste samples is also investigated. In the second phase of this study, the analysis technique is suitably modified to increase the likelihood of micro-crack formation at desired locations of paste samples for convenience of analysis. Additionally, eight different cementitious combinations are investigated for micro-cracks: coarse ground cement (CG-P), Type I portland cement (TI-P), Type I portland cement and 30% replaced with Class C fly ash (TI-FC), Type I portland cement and 20% replaced with Class F fly ash (TI-FF), Type I portland cement and 5% replaced with nanosilica (TI-NS), Type IL portland limestone cement (TIL-P), Type IL portland limestone cement and 30% replaced with Class C fly ash (TIL-FC), and Type IL portland limestone cement and 30% replaced with Class C fly ash, and 0.25% (v/v) addition of chopped basalt fibers (TIL-FC (B)). The goal of this study is detection and quantification of micro-cracks in paste samples and determination of relationships between crack density and restrained shrinkage. It is concluded from this study that micro-cracks can be analyzed by identifying vulnerable regions of a paste sample by μ-CT, and epoxy impregnation and suitable sample preparation at such key regions followed by observation through a confocal microscope. Porosity distribution from the first phase reveals that high porosity regions exist near the surface of the specimen, thereby making such regions vulnerable to micro-cracking. Type IL portland limestone cement with 30% Class C

fly ash (TIL-FC) has high electrical resistivity due to an improved particle size distribution. Higher crack area has been observed for TI-NS in the first phase. This is due to a higher water demand by virtue of a high surface area of nanosilica and subsequently higher availability of free water for evaporation. This results in higher shrinkage and subsequent cracking. Concrete containing coarse ground cement (CG-P) has low shrinkage; its corresponding cement paste sample has low crack density. Type I portland cement (TI-FC) has higher shrinkage strain than that of its control (TI-P) due to an unaltered water-binder ratio. Basalt fibers have provided post-cracking residual strength to concrete as observed from drying shrinkage strain under restraint. There may be a relationship between crack density and stress rate from drying shrinkage; such relationships need to be validated further with more investigations. Based on X-ray photoelectron spectroscopy (XPS) results, it is observed that shrinkage strain decreases with increasing Ca/Si ratio.

In Chapter 5, a life cycle assessment (LCA) and life cycle cost analysis (LCCA) have been performed on selected cementitious combinations. LCA and LCCA have been performed on five cementitious combinations: coarse ground cement, Type I/II cement with 20% Class F fly ash replacement, Type I cement with 30% Class C fly ash replacement, Type IL cement (portland limestone cement) with 30% Class C fly ash replacement, and Type I cement with 5% nanosilica replacement. For LCA, the goal of this study is to estimate the emission of CO_2 into the environment from the production of a metric ton of cement by investigating these five different cementitious combinations. This is represented by the global warming potential (GWP) in CO_2 equivalent. The LCCA has been performed on an imaginary concrete bridge in Minnesota with the five different types of cementitious combinations for the concrete deck. During the process of cement manufacture, CO_2 is emitted into the atmosphere primarily during the process of calcination or clinker formation ($CaCO_3$ is converted into CaO and CO_2), and due to burning of

fossil fuels. Prior researchers have indicated that CO_2 formed during calcination is roughly 50% of the total emissions due to the cement. It is however, difficult to accurately assess the emissions from fossil fuels used. Therefore, a method of calculation of CO_2 emissions per unit weight of pure compounds produced during cement manufacture is adopted. Results obtained align well with the 50% emission rule, as mentioned above. LCA results indicate that Type IL cement with 30% Class C fly ash (TIL-FC) has the lowest emissions of CO_2 into the atmosphere. The comparison between total present worth of the five cementitious systems during the life cycle of the bridge reveals that Type I cement with 5% nanosilica (TI-NS) has the highest total life cycle cost. This is primarily because of high expenses of colloidal nanosilica. Type I cement with 30% Class C fly ash (TI-FC) has the lowest life cycle costs among the five scenarios.

Therefore, it may be concluded that Type IL portland limestone cement can be an effective alternative for reduced shrinkage strain and enhanced durability properties. Such properties can also be enhanced due to fly ash. Nanosilica may have advantages of enhanced microstructure, however, it is not feasible as of now in terms of cost. For future work, the freeze thaw durability of these concrete mixtures may be investigated. In order to explore the benefits of basalt fibers of imparting post-cracking residual strength to concrete, appropriate changes to the mixed proportions may be investigated. Finally, the water-binder ratio of mixtures containing fly ash may be optimized to reduce the availability of free water and better shrinkage performance.